Université de Liège
Département d'Electricité, Informatique et Electronique
(Institut Montefiore)

Preventive Assessment and Enhancement of Power System Voltage Stability

An Integrated Approach of Voltage and Thermal Security

Dissertation présentée en vue
de l'obtention du grade de
Docteur en Sciences Appliquées

par

Florin CAPITANESCU

Ingénieur en énergétique (orientation électroénergétique)

Année académique 2003-2004

To my parents,
Doina Maria and Vladimir

Acknowledgments

First of all I would like to thank my supervisor, Dr. Thierry Van Cutsem, for his constant human, technical and financial support. These five years spent together will certainly remain as an unforgettable experience of my career. My deepest thanks to him.

I wish to thank Dr. Sorin Patrascoiu: without his help I would have never come to Liège. He definitely contributed to a very happy change in my life and career.

A special thanks to my “grandfather” Dr. Constantin Bulac, the person who contaminated me with the virus of voltage stability. I will never forget his advices since we met.

A lot of thanks to my colleagues Cédric, Gaëtan, Christophe, Cristina, Philippe, Stefano, Daniel, Giorgos and the others for the excellent work environment they created.

I gratefully acknowledge RTE and Hydro-Québec companies for allowing me to work with their data.

Last but not least I thank my family as well as my lovely wife Katarzyna for their invaluable support and comprehension throughout these years.

Abstract

This thesis is devoted to the preventive assessment and enhancement of voltage stability and security in electric power systems. However, in the course of deriving all the proposed methods we have paid attention to keeping them compatible with the (more traditional) handling of thermal overloads, thereby providing a unified treatment of voltage and thermal security.

The approaches presented in this work apply to both deregulated environments and classical, vertically integrated ones.

The heart of most methods developed in this thesis is : (i) the derivation of sensitivities indicating the relative efficiency of the various bus injections to restore voltage stability or increase an insufficient voltage security margin, and (ii) the use of these sensitivities in linearized security constraints that can be incorporated to various optimization problems.

Using this formulation, we deal with three different problems of interest in preventive security analysis:

1. *congestion management*. We propose two optimization-based approaches to manage congestions due to voltage instability and/or thermal overload. The control variables are either power injections (generation rescheduling and load curtailment) or power transactions;
2. *computation of Available Transfer Capabilities (ATCs)*. We determine the simultaneous ATCs of multiple transactions by means of a single optimization-based computation;
3. *evaluation of security margins interval*. To face the uncertainty affecting power transfers, we present an optimization-based computation of the minimal and maximal margins under the assumption that individual injections vary within specified bounds.

Besides this main theme, the thesis offers additional reflections on the:

- *filtering of contingencies*. We propose a simple and reliable technique to filter out harmless contingencies when computing voltage security margins of a large set of contingencies;
- *evaluation of reactive reserves with respect to a contingency*, an important topic for voltage security reasons as well as within the context of a deregulated market where providing reactive reserves is an ancillary service which should be properly paid.

Most of the methods proposed in this thesis were successfully tested on realistic power system models.

From a practical viewpoint all the above computations have been coupled to the fast time-domain quasi steady-state simulation used in the ASTRE software developed at the University of Liège.

Contents

Notation

As a convenience to the reader, we have collected below some of the more frequently used abbreviations and symbols.

TSO	Transmission System Operator
BM	Balancing Market
MP	Marginal Price
VSA	Voltage Security Assessment
SOL	Secure Operation Limit
ATC	Available Transfer Capability
M	security Margin
S	system Stress
BS	Binary Search
SBS	Simultaneous Binary Search
IC	Injection Control
TC	Transaction Control
QSS	Quasi Steady-State
LT	Long-Term
SNB	Saddle-Node Bifurcation
OEL	OverExcitation Limiter
LTC	Load Tap Changer
m	total number of system buses
b	total number of system branches
g	total number of system generators in service
t	total number of transactions
c	total number of specified contingencies
α_i	the participation factor of the source of i-th bus to a power transfer
β_i	the participation factor of the sink of i-th bus to a power transfer
$\mathcal{S}_V$	Voltage Security region
$\mathcal{S}_T$	Thermal Security region
$\mathcal{B}_V$	Voltage security region Boundary
$\mathcal{B}_T$	Thermal security region Boundary
$\mathbf{n}$	Normal vector
$\mathbf{P}$	Power injections vector

Chapter 1

Introduction

1.1 The road towards deregulation: short history

The first distribution power system was built in the early 1880's based on the idea of Thomas Edison. It provided Direct Current (DC) electricity to some customers of Manhattan. However, the delivery of DC electricity over long distances, while keeping almost the same low voltage at all consumers, was impractical due to the high losses associated. This difficulty was overcome by using electric transformers within Alternating Current (AC) power systems. A first such system was built in 1886 by George Westinghouse and William Stanley. AC systems quickly prevailed over the DC ones, so that by the end of the 1890's the entire electricity supply was at AC.

Since their beginning power systems have operated monopolistically. One single company has provided the services of generation, transport and sometimes distribution of electricity. For a long time, every of these sectors was thought of as a natural monopoly.

As far as the combined transmission and distribution network is of concern it was argued that one network serving all customers had lower costs per customer than several duplicating networks each serving only some customers (network economies) [Hym98]. On the other hand, competing in these sectors would raise another problem related to the fact that, in a power system, power flows obey the physical (Kirchhoff's) laws ! Thus interconnecting networks belonging to different rival companies would affect their respective capacities to carry power [BB00]. Moreover, environmental constraints deterred the presence of wires (in amounts more than necessary) "covering the sky" or "digging up the streets".

As regards generation, the larger the power plant capacity, the lower the cost per unit of output [Hym98, BB00]. Therefore, in order to achieve the lowest price of electricity the largest generators have to operate at their maximum output (economies of scale). This gave no economic incentives for operating many competing smaller plants. Moreover, huge investments required for building large power plants were also discouraging for potential private investors.

The economies of scale attained the maximum efficiency in the 60's. From there on it started to be gradually undermined by a series of events such as: a significant technological improvement of turbine efficiency, the decline of gas price and the revocation of the prohibition on gas burning which had been imposed in some countries [HS96, Hym98]. Clearly, smaller gas turbine and combined cycle units have become cheaper than the old plants. This created the premises of the movement towards the liberalization of the generation segment. Besides, significant difference in prices between neighbouring power systems have brought a supplementary motivation for creating a free market where they can compete together.

Started in Chile in 1982, the process of unbundling the electricity services is nowadays widespread around the world. The deregulation of electricity markets has been driven by political decision and changes in ideology. It belongs to a large process of economy liberalization which encompassed the restructuring of different services, e.g. natural gas, telecommunications, airlines, etc. [Hym98, BB00, RV02]. The initial goal of deregulation was twofold: to lower prices and to improve reliability. To attain the former objective a free competition has been first allowed at generation level and in some countries also at the distribution level. The transmission system remains, however, a natural monopoly at least for three reasons. The first two concern the network economies and the physical laws, explained earlier. The third motivation is that splitting the existing transmission system between several private companies would lead to higher electricity prices (each company needs separate service of human resources, equipment maintenance, etc.) as well as security problems.

While in order to protect customers against abusive electricity prices governments introduced caps on the profit of monopolistic companies, in the deregulated environment the prices are freely established from the supply and demand offers. Electricity is no longer a public service but a product.

1.2 Deregulation models

1.2.1 Market players and transmission system operator

The advent of deregulation has brought many changes in the operation and control of power systems. Depending on the particular characteristics of every power system, various forms of electricity services unbundling were implemented. However, despite specific achievement differences, two conceptual models emerged: the *pool model* and the *bilateral contract model* [SHP98, WV99, Dav98]. Initially, power markets around the world have rather adopted one of these two models in its pure form. The need to bring more choice to customers while maintaining the advantages of centralized operation has progressively led to a hybrid pool-bilateral contract model. Thus, nowadays one encounters markets where the emphasis is put more on the pool model (e.g. Chile, UK, Sweden, Argentina, Spain), while others are based mostly on bilateral transactions (e.g. USA, Norway).

A common feature to all deregulated environments is the creation of two new basic institutions, namely an *electricity market* and a *transmission system operator*.

Electricity market is the place where market participants (generators, distributors, brokers, etc.) trade energy or sign financial contracts. One may broadly distinguish between three temporal electricity markets: long-, mid- and short-term. Since in this work we will mainly deal with on-line aspects of security, only the *short-term market* will be considered. There are two short-term markets: the *day-ahead* and the *balancing* market [1]. The role of the day-ahead market is to set up the schedule of power exchanges between market players for the each hour of the next day. This task is similar to the traditional unit commitment in a vertically integrated environment. The purpose of the balancing market is to correct in real-time the mismatch between generation and load, owing to the load deviation from the forecasted value.

The Transmission System Operator (TSO) must ensure nondiscriminatory access to the transmission network by all market participants and be independent of their financial interest. In some markets, the TSO is completely independent, not only of generating companies but also of the transmission company. This is known as an Independent System Operator (ISO), a non-profit entity regulated by the state. In other markets, the TSO is also the owner of the transmission grid, and may be a for-profit or a non-profit company.

The TSO is responsible for maintaining the security of the integrated generation and transmission system, even if it owns none of them. To this purpose, the TSO runs an "ancillary services" market (e.g. automatic generation control, spinning reserve, var support, etc.) in order to procure enough operating reserves to the system. An important task of the TSO is the *congestion management*. A power system is said to be "congested" when it operates beyond one or more transfer limits. Congestion management consists in controlling the transmission system such that no transfer limit is exceeded [CWW00]. Removing congestion is more challenging in a deregulated environment than in the former vertically integrated structure because the TSO does not have anymore the full control on generators. In order to provide more choice to control power system security the participation in both the day-ahead and the balancing market should be mandatory (as in UK) and not optional as is still the case in some countries (e.g. Argentina).

1.2.2 The pool model

In this model there is a neutral entity, namely the *Market Operator* (MO), who operates the wholesale day-ahead energy market (also called in this model *spot* market or power exchange). All trades are done only with the MO, who buys electricity from the competing generators and sells it to the distribution companies.

The salient features of the pool model are a bid-based auction dispatch to match generator supply with customer demand as well as a pricing scheme of electricity. There are generally two such pricing methods:

[1] known also as *regulating* or *hour-ahead* market

- the *uniform pricing* (e.g. Spain, Alberta, former system in UK, New England and Ontario schemes)
- the *locational (nodal) spot pricing* (e.g. New York, PJM, California)

A common feature of both pricing methods is that they start with an auction-based dispatch [CGA03]. The goal of the latter is to maximize the *social benefit* [2], i.e. the power producers should obtain the largest prices for their energy while the consumers should pay the lowest prices for the purchased energy.

Let us first describe this auction procedure for the operation of the day-ahead market in intervals of one hour of the next day. Generators and distributors submit bids to the MO. Each generator bid consists of the minimum price at which the generator is willing to sell power and the corresponding amount of power. Similarly, each distributor bid consists of the desired amount of power and the maximum price at which it is willing to pay for this power. The MO establishes a merit order of generators (by increasing order of their offer) and distributors (by decreasing order of their offer), and then aggregates the supply and demand curves (see Fig. 1.1). The crossing point of these curves defines the *Marginal Price* (MP), or *clearing price*, of the system and the quantity of traded power, or total cleared power. Note that in some systems there is an auction on the generators side only, and the demand curve is replaced by the forecasted load level in the concerned interval of time. In this case, the demand curve corresponds to a vertical line (inelastic load). This situation leads to a particular objective, which has been extensively used in vertically integrated systems, i.e. minimize the generation cost for a given consumption.

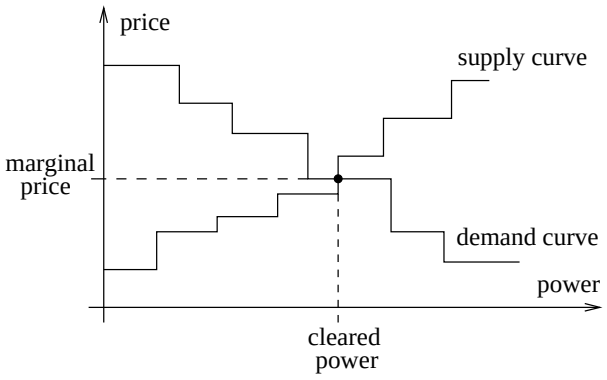

Figure 1.1: Supply-consumption bid curves

One can remark that this *unconstrained* least-cost dispatch computed by the MO is identical to the classical economic dispatch, with the distinction that generator cost curves are replaced by bid prices. However, unlike the cost curves which are known with certainty, the bid prices vary according to the strategy followed by the suppliers and may be different from the real costs.

Once the unconstrained dispatch is known, the uniform pricing method encompasses two successive steps [MGC02, CGA03]. One first checks whether this dispatch violates any

[2] or *social welfare*

transmission limit. If it is the case, a redispatch is carried out to remove congestion. The transmission losses are then computed and allocated to producers and consumers.

The TSO should relieve the congestion by redispatching at the least cost the generators whose bids were accepted (initially "constrained-on" or "in-merit" generators). If the congestion cannot be removed by redispatching the constrained-on units, one must envisage the commitment of generators with unsuccessful bids (initially "constrained-off", "out-of-merit", or "must-run" generators) taking into account their cost and their efficiency for congestion relief. This may require the withdrawal of the most expensive initially constrained-on generators.

According to the uniform pricing theory, in a lossless system, if there is no congestion the price of electricity is the same everywhere in the system and equal to the price bid by the most expensive generator scheduled to operate. In other words, each generator is paid at the MP and each customer pays this price.

The uniform pricing method is thus very simple and transparent. On the other hand, its main drawback stems from the separate handling of transmission congestions and losses. However, techniques to handle all three steps together were recently proposed in [MGC02, Mil03].

The spot pricing method [3] takes into account, for a given unconstrained dispatch, transmission limits and losses simultaneously. Simply stated, according to this theory, the price is adjusted for each market player in order to take into account its contribution to network losses and constraints. The nodal prices are usually obtained as dual variables (or Lagrange multipliers) of an *optimal power flow* computation performed to compute the optimal dispatch. The Lagrange multiplier associated with each power flow equation represents the variation of the overall generation cost for an increment of load at that bus. Thus, each generator is paid a price based on the marginal cost of serving an increment of load at its location. Generally, the nodal prices are higher at the consumer locations than at suppliers locations.

It is noteworthy that in an uncongested and lossless system, if one ignores reactive power, both the uniform and spot pricing methods provide the same results, i.e. the price of electricity is the same everywhere in the system, and equal to the MP. Both methods reflect, albeit differently, the contribution to congestion price.

There are two main advantages of nodal pricing over uniform pricing. Firstly, it reflects the contribution of each market player to network losses. Secondly, by considering location dependent prices, it gives incentive for building new power plants at the proper place. As any method, it has also weaknesses. It is more complex and much less transparent comparatively to the uniform pricing because the solution of a set of nonlinear equations is required. On the other hand, the main drawback of nodal pricing is *price volatility*, namely large variations of spot prices, under congested conditions, due to subtle changes in dispatch. These variations may stem from [FHR97]: (i) additional congestion constraints becoming active (or inactive) under changing load and generation; (ii) changes in bid price by suppliers and distributors; (iii) subtle load variation while bids and congestion

[3] whose theory was first proposed in [SCT88]

constraints remain unchanged. The first is the most significant cause of volatility.

We mentioned that when using uniform pricing, the last-in generator determines the clearing price paid to all other in-merit plants. This system of pricing is non-discriminatory because all winning generators are paid the same price, regardless of their individual bids. This kind of auction creates incentives for bidders to bid their true costs and avoid guessing the bids of others. In an ideal market it is each generator interest to bid its true marginal cost, otherwise it could be rejected from the market.

Significant decrease in prices were reported in some pool markets after deregulation, e.g. the Nordel pool. Nevertheless, it is not the case everywhere (e.g. UK system and California) because this type of auction is vulnerable to "gaming" [Bia02]. The latter refers to a strategic behaviour of generators aimed at artificially increasing the clearing price. This situation may occur in a market with a lower extent of competition in the generation sector (called *oligopoly* market), e.g. when few companies own all generators. In such an environment, the higher the load conditions, the greater the possibility for gaming. The reason is that under high load conditions few generators among the most expensive compete for establishing the clearing price. Conversely, under light load conditions generators which would be prone to increase their bid risk to be displaced by other, cheaper generators. Let us finally note that the simplest mechanism of gaming is by inflating the bid price whereas all in-merit plants benefit from any clearing price increase (tacit collusion) [Bia02].

1.2.3 The bilateral contract model

This paradigm relies on the conjecture that free market competition is the best way to achieve economic efficiency. In this model consumers have "direct access" to a supplier of their choice. Consumers and suppliers independently arrange trades, setting by themselves the amount of generation and consumption and the corresponding financial terms [SHP98, WV99]. Obviously, consumers seek for the cheapest generators while generators seek for the best-paying consumers.

It is noteworthy that, unlike the pool, this model has no centralized dispatch of generators. The brokers or scheduling coordinators take care of balancing each production with the corresponding consumption.

The underlying element of this model is the *transaction*. The latter is a bilateral exchange of power between a selling and a buying entity. The selling (resp. buying) entity is called *source* (resp. *sink*) and each one can encompass more than one generator (resp. one load). The transactions can be of two types: firm and non-firm. Firm transactions are not subject to curtailment and are willing to pay a cost in case of congestion. Conversely, non-firm transactions are unwilling to pay congestion cost and are subject to curtailment.

In this environment, a crucial information is the determination of the *Available Transfer Capability* (ATC) for all foreseen trade paths [ATC96, ESO01b]. Each ATC represents the maximum increment of power which can be transmitted from a supplier to a consumer without violating any security constraint. These values are typically computed for the next hour as well as for several hours ahead. They are put on a website known as OASIS (for

Open Access Same-time Information System), operated by the TSO. Each market player can use them in order to make reservation [CWW00]. Reservations can be made on the day-ahead market for each hour of the next day.

We briefly describe an auction mechanism to establish bilateral contracts [SLL02]. Generators submit bids to loads taking into account the posted ATC values. A load accepts electricity delivery from the generator with the lowest bid as long as this price is lower than what it is willing to pay. If the lowest price requested by generators is too high with respect to the load offer, the load either modifies its offer for a second auction or withdraws from the bilateral market. Note that generators are also responsible for paying system losses and transmission charge. Situations where a generator wins the auction of more than one load can occur. In this case the generator sells its available power, in decreasing order, to those loads that give it the highest profit. Once the auction is closed, the TSO has to check whether all desired bilateral trades are feasible or not. If there is no congestion, the schedules can be easily fulfilled by the TSO. Otherwise, the TSO has to either adjust transactions or redispatch at the least cost generators competing in the balancing market. In the latter case a challenging problem is to allocate in a fair way the extra cost due to congestion among transactions.

Two problems arise in this model. First, the lack of coordination among the independent trades may lead to a violation of transmission constraints because ATCs are usually computed for each transaction separately whereas they occur simultaneously. Second, it may be difficult to allocate losses to the various transactions.

In this model the role of the TSO is considerably reduced, one speaks of a minimum TSO model, as opposed to a maximum TSO model in the pool model [NN02]. Indeed, in this model the TSO does not control any energy market while in a pool it often manages the spot market and consequently replaces the market operator. However, in both paradigms, the TSO runs the balancing as well as the ancillary service market.

The strategic behaviour of market players still exists in this model [SLL02]. However it is significantly reduced in comparison with the pool model.

1.3 Motivation and objectives of this work

With the opening up of large electricity markets, in many countries, more and more power transactions have been established. Interconnections in particular have started to be more extensively used for trading (due to price differences on both sides of the border), increasing thus the size of the generation market. Besides, significant unidentified flows (stemming from trades between third countries) have been observed in some systems (e.g. Belgium in June 1999 [Bor01]). Obviously, system operation is pushed closer and closer to its limits. Moreover, power systems often operate in unforeseen conditions since transactions follow different patterns than those assumed at the planning stage. Accordingly, operation limits that were seldom met in the past could become more constraining in this new environment.

Actually, some power systems operated under rather stressed conditions even before deregulation. The last two decades especially were characterized by an important increase in electricity demand. At the same time transmission network expansion was slower and deterred by environmental, society and financial constraints. Besides, an increase of transmission capacity through FACTS devices was impractical in most cases due to their still prohibitive cost.

Voltage instability and *thermal overload* are two significant threats of power systems.

Thermal overload is the earliest cause of insecurity in power systems. It is related to the maximal allowable current which can be transferred through an equipment without damaging it irreversibly nor causing dangerous conductor sags. Some transmission lines may be equipped with overcurrent protections that disconnect them after some time. Their tripping by these devices or by operator may cause the overload to be "redirected" to other system elements thus leading to cascade trippings and eventually to a blackout (USA 1965 and 2003, New York 1977, Italy 2003 etc.).

The operation of power systems under the above mentioned stressed conditions has emphasized another danger to power system security, namely voltage instability. The latter stems from the attempt of load dynamics to restore power consumption beyond the amount that can be provided by the combined transmission and generation system [VCV98, VC00]. Many incidents around the world have resulted in severely depressed voltage profiles or even system collapse (France 1978 and 1987, Belgium 1982, Florida (USA) 1982, Sweden 1983, Japan 1987, etc.) [Tay94].

While already a major concern in vertically integrated companies, Voltage Security Assessment (VSA) becomes even more important in the open access environment. VSA should be performed in control centers for operating points forecasted on the each hour of the next day (by the day-ahead market) but also in real-time, in order to face unforeseen events. The TSO should evaluate security margins with respect to credible contingencies. For on-line applications an adequate contingency filtering is indispensable in order to quickly identify harmless contingencies and limit the analysis to the harmful ones. In case of congestion, i.e. when security margins are deemed insufficient or when the system has no margin with respect to a plausible contingency, the TSO should determine the best preventive actions to restore such margins. A particular case of security margin computation is the determination of non-simultaneous ATCs, a much needed information in an open access environment. Because the cumulative effects of transactions may lead to congestion, improved ATC values taking into account simultaneous power transfers should be considered.

Finally, because the system evolution assumed in the computation of security margins involves some uncertainty, the robustness of these margins with respect to parameter changes should be investigated, especially in a deregulated environment where the preventive actions taken should not be discriminatory.

Efficient computer methods are needed to carry out all these VSA tasks.

The main objective of this thesis was to derive such rigorous, although realistic procedures for the preventive analysis of voltage security in the day-ahead or real-time environments.

In the course of deriving such procedures we have paid attention to keeping them compatible with the (more traditional) handling of thermal overloads, thereby providing a unified treatment of voltage and thermal security constraints. Note that, very often, these two security aspects are analyzed separately, thermal overloads through linear techniques [WW96] and voltage instability through nonlinear ones [VCV98]. In some systems, the two aspects can be coupled.

1.4 Structure of the thesis

The remaining of this thesis encompasses seven chapters.

Chapter 2 recalls basic power system stability notions, with emphasis on voltage instability. In this respect, two mechanisms of long-term voltage instability are briefly reviewed through theoretical examples.

Chapter 3 deals with voltage (and thermal) security assessment. More precisely it concentrates on the computation of security limits (and margins). Two related problems of practical importance are also considered, namely the filtering of contingencies and the evaluation of reactive reserves.

Chapter 4 details the derivation of a sensitivity type of information, aimed at ranking candidate controls with respect to their efficiency in restoring or enhancing voltage and thermal security. After reviewing the available approaches, we propose a new sensitivity formulation. The linearized security constraints built on these sensitivities will be used to solve three distinct problems, discussed in the subsequent chapters.

Chapter 5 is devoted to the timely problem of congestion management in a deregulated environment. Two optimization approaches are proposed to cope with both voltage and thermal congestions. The first one considers power injections as control variables while the second one relies on power transactions.

The purpose of *Chapter 6* is to evaluate available transfer capabilities in the presence of several simultaneous transactions. Simultaneous ATCs are obtained as the solution of a voltage and thermal security constrained optimization problem. The fairness of allocating transmission capacity among multiple market players is discussed through the choice of the objective. We also compare the merit of this approach with that of non simultaneous ATCs.

The topic addressed in *Chapter 7* has to do with the uncertainty affecting the anticipated power transfers. More precisely, for given bounds on the individual injection variations, and for a given contingency, we determine the interval of variation of a security margin. To this purpose, we use once more an optimization formulation. We then pay attention to the sensitivity of the minimal margin with respect to the above bounds. We also discuss the extension to several contingencies.

General conclusions as well as directions for future work are presented in *Chapter 8*.

1.5 Publications

Most of ideas presented in this thesis can be found, albeit in a more compact form, on the following papers published during my PhD studies:

- T. Van Cutsem, F. Capitanescu, C. Moors, D. Lefebvre and V. Sermanson. An advanced tool for preventive voltage security assessment. In *Proc. of the VIIth SEPOPE conf.*, Paper IP-035, Curitiba (Brazil), 2000.

- F. Capitanescu and T. Van Cutsem. Evaluation of reactive power reserves with respect to contingencies. In *Proc. of Bulk Power System Dynamics and Control V*. Onomichi, Japan, August 2001, pp. 377-386.

- F. Capitanescu and T. Van Cutsem. Preventive control of voltage security margins: a multicontingency sensitivity-based approach. *IEEE Transactions on Power Systems*. Vol. 17, 2002, pp. 358-364.

- F. Capitanescu and T. Van Cutsem. Evaluating bounds on voltage and thermal security margins under power transfer uncertainty. In *Proc. of the 14th PSCC Conference*. Sevilla (Spain), June 2002.

- F. Capitanescu and T. Van Cutsem. Computation of simultaneous available transfer capability under voltage and thermal security constraints. In *Proc. of Modern Electric Power Systems Conference*. Wroclaw, Poland, September 2002, pp. 204-210.

- F. Capitanescu and T. Van Cutsem. Unified sensitivity analyisis of unstable or low voltages caused by load increases or contingencies. Paper submitted to IEEE Transactions on Power Systems, 2003.

Chapter 2

Voltage stability

This chapter contains a very brief introduction on the voltage instability phenomenon. We first give a short overview of the three forms of instability (angle, frequency and voltage) which a power system may exhibit. Then, we present the reference model for the time simulation of voltage stability phenomena, focusing especially on the Quasi-Steady State approximation which is at the heart of the software used throughout this whole research work. Finally, we present two typical examples of long-term voltage instability mechanisms.

2.1 Definition and classification

Power system stability is essentially a single problem. However, in order to properly understand and effectively deal with the various forms of power system instability, it is convenient to make simplifying assumptions which allow to analyze them using the right degree of detail of system representation and appropriate analytical techniques. The classification and the short description provided in this section are largely borrowed from [CTF02].

The instability forms that a power system may undergo are: *rotor angle*, *frequency* and *voltage* instability (see Fig. 2.1).

Rotor angle stability refers to the ability of synchronous machines of an interconnected power system to remain in synchronism after being subjected to a disturbance. It depends on the ability to maintain/restore equilibrium between electromagnetic torque and mechanical torque of each synchronous machine in the system. Angle instability occurs in the form of increasing angular swings of some generators leading to their loss of synchronism with other generators.

Small-disturbance (or small-signal) rotor angle stability is concerned with the ability of the power system to maintain synchronism under small disturbances. In practice, this form of instability is usually associated with insufficient damping of oscillations due to the lack of *damping torque*. *Large-disturbance rotor angle stability* or *transient stability*,

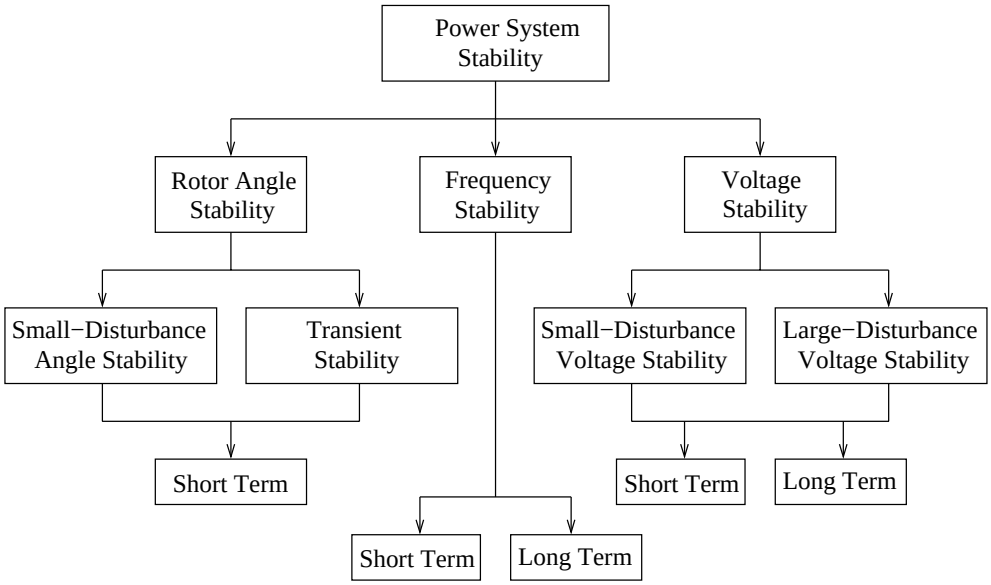

Figure 2.1: Classification of Power System Stability according to [CTF02]

on the other hand, is concerned with the ability of the power system to maintain synchronism when subjected to a severe disturbance, such as a short circuit. This kind of instability usually occurs in the form of aperiodic angular separation due to insufficient *synchronizing torque*.

Both forms of angle stability can be captured by simulating the system behaviour during 10-20 seconds following a disturbance.

Frequency stability concerns the ability to maintain/restore equilibrium between the total generation and the total load powers, with minimum unintentional loss of load. Frequency instability typically occurs in the form of frequency decay or rise leading to tripping of generating units and/or loads. In large interconnected power systems, this type of situation is most commonly associated with extreme conditions following splitting of systems into islands. Historically, improvements in protections and voltage regulators have reinforced considerably the system against angle instability. With the enhancement of the angle stability limit, in some systems, voltage instability has become more limiting.

Voltage stability refers to the ability of a power system to maintain steady voltages at all buses in the system after being subjected to a disturbance. Voltage instability generally occurs in the form of a progressive fall of voltages of some buses. Note that an overvoltage instability, manifesting as a progressive rise of voltages of some buses, also exists and has been experienced at least on one system [VCM97].

One term used in conjunction with voltage instability is *voltage collapse*. It refers to the process by which the sequence of events accompanying voltage instability leads to a blackout or abnormally low voltages in a significant part of the power system.

Loads are the driving force of voltage instability, and for this reason this phenomenon has also been called *load instability*. Note, however, that loads are not the only responsible for

instability. A transmission system has a limited transfer capability, as is well known from the Circuit Theory. This limit (also affected by the generation system) marks the onset of voltage instability. The cause of voltage instability is the attempt of load dynamics to restore power consumption beyond the capability of the combined transmission and generation systems [VCV98].

For convenience in analysis and for gaining useful insight into the nature of stability problems, it is useful to characterize voltage stability in terms of the following two categories:

- *small-disturbance voltage stability* which refers to the system ability to maintain steady voltages when subjected to small perturbations such as incremental changes in system load. This form of stability is influenced by the characteristics of loads, continuous controls, and discrete controls at a given instant of time. It can be studied with steady-state approaches that use linearization of system dynamic equations at a given operating point [GMK92, GMK96];
- *large-disturbance voltage stability* which concerns the system ability to maintain steady voltages following large disturbances such as system faults, loss of generation, or transmission line outages. This ability is determined by the system and load characteristics, and the interactions of both continuous and discrete controls and protections. It can be studied by using nonlinear time-domain simulations.

The time frame of interest for voltage stability problems may vary from a few seconds to tens of minutes, according to the speed of load restoration. Therefore, the analysis of voltage stability can be decomposed in two time scales:

- *short-term voltage stability* which corresponds to a time-frame of several seconds. It is motivated by loads with fast restoration, such as: induction motors, electronically controlled loads and HVDC interconnections. This is also the time scale of synchronous generators and their regulators (Automatic Voltage Regulator (AVR) and governor) and FACTS devices (e.g. static var compensators. Since this is also the time scale of angle stability, there is not always a clear separation between voltage and angle stability problems;
- *long-term voltage stability* which corresponds to a time-frame of several minutes. The main restoration mechanism comes from Load Tap Changers (LTC) and thermostatic loads. The most relevant system components to voltage stability in this time scale are: controllers (secondary voltage control, load-frequency control, shunt capacitor/reactor switching) and protecting devices (OverExcitation Limiters (OELs), armature current limiters).

Note, however, that small-disturbance and large-disturbance voltage instability manifests in the same way, that is as a progressive and uncontrollable fall of voltages. Therefore, this distinction is not as important as in the case of rotor angle stability, where transient and small-disturbance stabilities relate to distinct problems.

This work mainly focuses on long-term large-disturbance voltage instability.

2.2 Time simulation of voltage stability phenomena

Multi-time-scale simulation of voltage stability phenomena requires the numerical integration of a large set of differential-algebraic, continuous-discrete time equations [VCV98]. The reference model takes on the general form:

$$\dot{\mathbf{x}} = \mathbf{f}(\mathbf{x}, \mathbf{y}, \mathbf{z}_c, \mathbf{z}_d) \tag{2.1}$$

$$\mathbf{0} = \mathbf{g}(\mathbf{x}, \mathbf{y}, \mathbf{z}_c, \mathbf{z}_d) \tag{2.2}$$

$$\dot{\mathbf{z}}_c = \mathbf{h}_c(\mathbf{x}, \mathbf{y}, \mathbf{z}_c, \mathbf{z}_d) \tag{2.3}$$

$$\mathbf{z}_d(k+1) = \mathbf{h}_d(\mathbf{x}, \mathbf{y}, \mathbf{z}_c, \mathbf{z}_d(k)) \tag{2.4}$$

The differential equations (2.1) describe the behaviour of the short-term dynamics of generators, induction motors, HDVC and FACTS components, etc. $\mathbf{x}$ is their corresponding state vector.

The algebraic equations (2.2) represent the network equations, whose response is assumed *instantaneous*. $\mathbf{y}$ is the vector of bus voltage magnitudes and phase angles.

The equations (2.3) capture the continuous-time long-term dynamics, $\mathbf{z}_c$ being the corresponding state vector. For instance, such equations model the recovery of thermostatic and aggregate loads and also appear in the PI control laws of secondary frequency and voltage controllers.

Finally, the equations (2.4) capture the discrete-time long-term dynamics, $\mathbf{z}_d$ being the corresponding state vector. The latter includes, for instance, shunt susceptances or the ratio of transformers equipped with LTC.

When devising fast methods to analyze voltage stability it is convenient to exploit the time separation which exist between the short and the long-term phenomena. Thus two main approximations can be made [VCV98]:

- when short-term voltage stability is of concern, the slow variables ($\mathbf{z}_c$ and $\mathbf{z}_d$) are assumed as practically constant during the fast transients. Note that $\mathbf{z}_d$ is actually constant in the interval between discrete variable changes (e.g. in between tap changes). *Short-term voltage stability simulation* relies therefore only on (2.1, 2.2). Note that this is the model used in angle stability studies, with proper account of load behaviour. Thus, in principle, the numerical integration methods used for angle stability studies apply equally well to short-term voltage stability studies;
- when long-term voltage stability is of concern the short-term dynamics are considered infinitely fast. This leads to the *Quasi-Steady State (QSS)* approximation simulation of the long term dynamics [VCV98], which consists in replacing the fast dynamics (2.1) with their equilibrium equations:

  $$\mathbf{0} = \mathbf{f}(\mathbf{x}, \mathbf{y}, \mathbf{z}_c, \mathbf{z}_d) \tag{2.5}$$

  By neglecting the short-term dynamics (up to some point) the analysis of long-term voltage instability mechanisms is considerably speeded up.

The QSS approximation is at the heart of the ASTRE software, developed at the University of Liège and now used by four power companies. This software has been used throughout this whole research work.

This method, which has been validated with respect to detailed time simulation [VCM97], offers better accuracy and richer interpretations than those based on load flow equations. For instance, in unstable cases, the area in trouble is automatically pointed out, while complementary diagnosis tools, such as those developed in this thesis, can be run on the unstable system trajectory in order to identify appropriate remedial actions.

Thus, the method offers an interesting compromise between the computational efficiency of static methods, which is required for real-time applications, and the above advantages of time-domain based approaches.

While the equations (2.5) are formally obtained from the equilibrium conditions of (2.1), in practice, each synchronous generator, its governor and its AVR, are represented by three nonlinear algebraic equations which take into account the generator saturation, the AVR steady-state gain and the speed droop. The corresponding three variables $\mathbf{x}$ are the rotor angle, the electromotive force (e.m.f.) proportional to field current and the e.m.f. behind saturated synchronous reactances [VCV98]. These three nonlinear equations are solved at each time step, together with the network ones (2.2).

One of the typical load models used is represented in Fig. 2.2. Voltage dependent active and reactive powers are assumed at the MV bus behind the HV-MV distribution transformer, in parallel with a shunt compensation capacitor. Load power restoration mainly comes from the LTCs operating in such transformers.

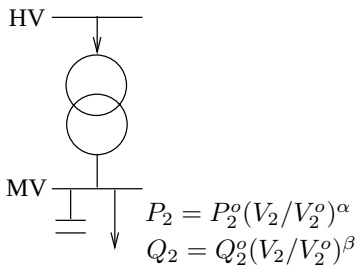

Figure 2.2: Exponential load model

QSS simulation reproduces the long-term dynamics of LTCs, OELs, automatically switched shunt compensation, secondary voltage control (if any), protecting devices, etc. This simulation takes into account the (initial and subsequent) delays in between transformer tap changes, the delays before a synchronous machine is switched under constant field current, etc. More details about the method as well as a discussion of its limitation can be found in [VCV98] and related publications.

2.3 Voltage instability mechanisms

From a system theoretical perspective, when a large disturbance causes a power system to be long-term voltage unstable, three main instability mechanisms can be thought of [VCV98]:

- LT1: loss of equilibrium of the long-term dynamics;
- LT2: lack of attraction towards the stable long-term equilibrium;
- LT3: growing voltage oscillations.

LT1 is the most typical instability mechanism, with the load trying either to recover their pre-disturbance powers through LTC actions or to reach their long-term characteristics through self-restoration. This scenario is further described in Section 2.3.1. Incidentally, in a system with no long-term load power restoration, LT1 voltage instability is not likely to be a concern.

A typical example of LT2 instability would be an LT1 scenario followed by a delayed corrective action which restores a stable equilibrium but not fast enough for the system to be attracted by the stable post-control equilibrium. This mechanism is further discussed in Section 2.3.2.

The LT3 instability mechanism, LT3 has apparently not been observed in a real power system.

Let us recall that similar instability mechanisms exist in the short-term time frame, leading to short-term voltage instability. They are out of scope of the present work. Moreover, a long-term instability may in turn trigger an instability of the short-term dynamics. The interested reader may refer to the Chapter 8 of [VCV98].

2.3.1 Example of LT1 instability

Let us consider the simple system of Fig. 2.3, in which a load is fed by a generator through a double circuit line and a transformer with LTC. The transformer is assumed ideal for simplicity.

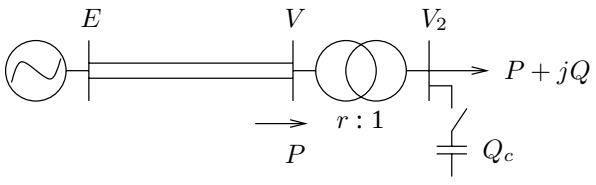

Figure 2.3: Two-bus LTC system

We assume an exponential *short-term load characteristic* :

$$P = P_o \left(\frac{V_2}{V_2^o} \right)^{\alpha} = P_o \left(\frac{V}{rV_2^o} \right)^{\alpha} \tag{2.6}$$

$$Q = Q_o \left(\frac{V_2}{V_2^o} \right)^{\beta} = Q_o \left(\frac{V}{rV_2^o} \right)^{\beta} \tag{2.7}$$

with $\alpha > 1$, $\beta > 1$ and we take the LTC setpoint V_2^o as reference for the exponential load.

In this system the long-term dynamics are due to the LTC. Neglecting the LTC deadband effects, the long-term equilibrium is such that $V_2 = V_2^o$ (or equivalently $P = P_o$) which means that the *long-term load characteristic* is constant power.

A large-disturbance long-term voltage instability scenario is sketched in Fig. 2.4 using the well-known PV curves, related to the primary side of the transformer. The solid curves represent the pre- and post-disturbance network characteristics, respectively. The dotted curves are the short-term load characteristics corresponding to equations (2.6), for various values of r. Finally, the dashed vertical line is the long-term load characteristic.

Let us consider that the system operates initially at the point A, the intersection between the pre-disturbance network characteristic and the long-term load characteristic $P = P_o$, see Fig. 2.4. Let us assume that a disturbance occurs, e.g. the loss of one circuit of the line. Consequently, the network characteristic shrinks and the short-term equilibrium point "jumps" in B, the intersection between the short-term characteristic and the post-disturbance network characteristic. As point B is characterized by a lower load power, and hence, a lower load voltage V_2, the LTC starts decreasing the transformer ratio r with the intention to restore the load voltage V_2. This causes the short-term characteristics to change as shown in the figure. The corresponding successive short-term equilibria are points D,E,F,G.

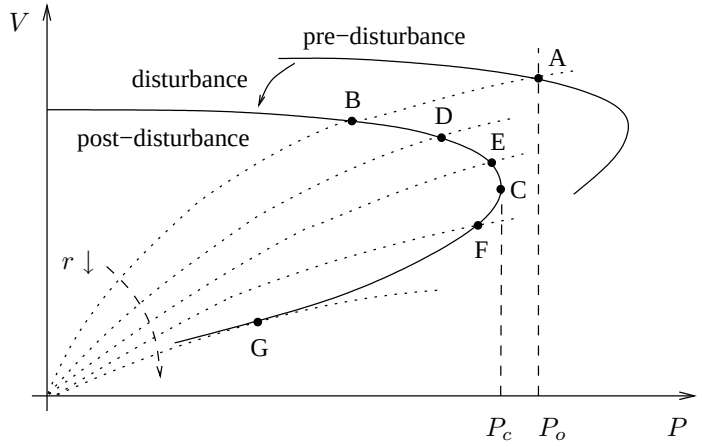

Figure 2.4: Loss of long-term equilibrium

Note that during this transition the system has crossed the point C which is the "nose" of the post-disturbance network characteristic. We call this point the *critical point* of the system evolution. The corresponding voltage is called the *critical voltage*. After this point both voltage and load power restoration by the LTC fail.

The nature of instability is revealed by observing that the long-term characteristic does not intersect the post-disturbance network characteristic (see Fig. 2.4). This is clearly a case of LT1 instability, for which the long-term equilibrium equations have no longer a solution. Any algorithm trying to solve them will diverge.

In this simple example and under the assumption $\alpha,\ \beta > 1$ there is always an intersection point between the short-term load characteristic and the post-disturbance network characteristic. However, in a more complex system, there may be a last point of intersection between the two characteristics as intentionally depicted by the point G in Fig. 2.4. Beyond this point, a further decrease of the ratio r will lead to a loss of short-term equilibrium. The short-term dynamics thus become unstable and the system collapses. Note that the final outcome of an LT1 instability may also be a pseudo-stabilization at low voltage due to LTC limitation. We mention that such a state should not be mistaken by declared it stable because other load recovery mechanisms, such as distribution regulating transformer, thermostatic loads, etc. may become active driving the voltage decline further towards a collapse. Thus it is more reasonable to consider the final operating condition as unstable, since any attempt to restore load will drive the system to further degradation.

We finally mention that, in a real-life system, the maximum power that can be delivered to loads, and hence the critical point, is strongly influenced by the reactive power limitation of generators (and compensators). The switching of generators from AVR control to field current limit by OELs causes the network PV characteristic seen by the loads to further shrink, in addition to the disturbance effect. This is shown graphically in Fig. 2.5. Since the limitation takes place after some delay, the operating point moves as indicated by the dotted arrows. The maximal power delivered to the load with the generator under OEL control, which corresponds to the point C (see Fig. 2.5), is significantly less than with the generator under AVR control.

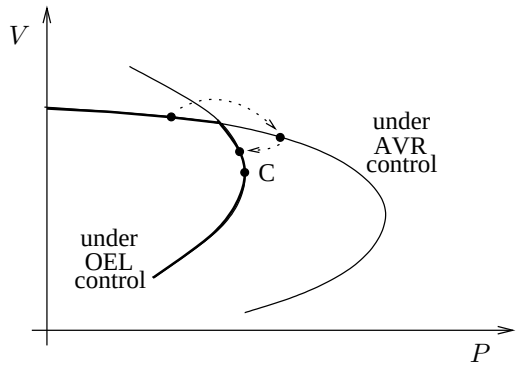

Figure 2.5: Effect on PV curves of generator limitation

2.3.2 Example of LT2 instability

Let us come back to the example of Fig. 2.4, with the PV curves reproduced in Fig. 2.6. The system is initially operating at the point A on the pre-disturbance network characteristic. As in the previous example, a disturbance causes post-disturbance characteristic

to no longer intersect the long-term load characteristic $P = P_o$, thereby leading to LT1 instability. Before the LTC starts acting the operating point jumps to B (the intersection between the dotted short-term load characteristic and the new network curve). The subsequent load restoration takes the system along the post-disturbance curve, passing successively through the points D,E,F and G. This is shown in Fig. 2.6 with a series of dotted short-term characteristics.

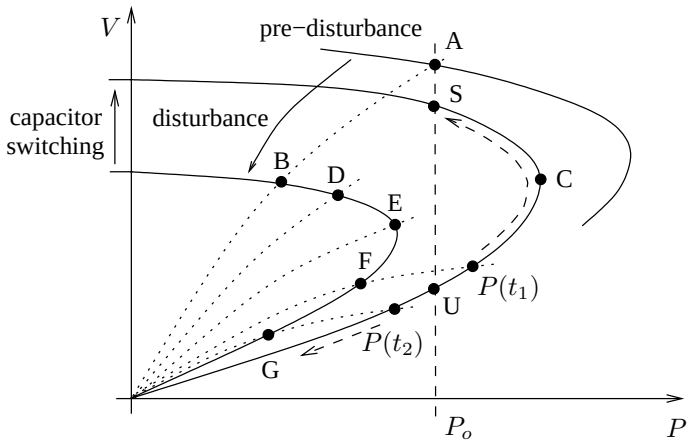

Figure 2.6: Loss of attraction towards a long-term equilibrium

Let us assume that a significant amount of shunt compensation is available at the load bus (see Fig. 2.3), and is switched in the system after some delay [BTS96]. This yields a new post-control network PV characteristic, on which there are now two long-term equilibrium points S and U. It can be easily shown [VCV98] that S (resp. U) is stable (resp. unstable) with respect to the long-term dynamic of the LTC.

Let t_1 be the time instant at which the capacitor switching takes place. The short-term equilibrium point jumps accordingly from F to the point with the consumed power $P(t_1)$ (see Fig. 2.6). Since at this point the load power exceeds that of the long-term characteristic P_o, it results from equations (2.6) that $V_2 > V_2^o$. Consequently, the LTC will increase the ratio r in order to decrease the voltage V_2 and the system will be attracted by the stable equilibrium S. Now, if the switching action is taken at the time $t_2 > t_1$, when the system operates at the point G, the power consumed just after switching is $P(t_2)$. From $P(t_2) < P_o$ it results that $V_2 < V_2^o$ and consequently the LTC will keep on decreasing the ratio r and instability will continue. In fact, the region of attraction of the stable equilibrium S is bounded by the unstable equilibrium U. This example shows that if the control is too much delayed, instability takes place by lack of attraction towards the final equilibrium (LT2 mechanism).

Chapter 3

Evaluation of voltage security margins

While the previous chapter offered a succinct introduction to voltage instability phenomenon, this one focuses on security issues. We first introduce the conceptually attractive notion of security region. We then consider two levels of security analysis: the evaluation of contingencies at a given operating point and the determination of security margins with respect to contingencies. After describing practical procedures for the computation of these margins, we address the important problem of filtering a large set of contingencies. We present numerical results of margin computations and contingency filtering obtained on two real-life systems. The chapter ends up with an approach to evaluate reactive power reserves with respect to contingencies, as a by-product of margins computation.

3.1 Security analysis

Power system security can be defined as the ability of the system to withstand any "credible" contingency. Withstanding a contingency implies two aspects. First, the system must reach a post-contingency equilibrium as well as survive the transition towards it. Second, at this point no physical constraints must be violated.

The above characterization of system security underlines two aspects of its analysis [DL74, FC78, CTF02]:

- *static security analysis* which involves steady-state analysis of the post-contingency system conditions to verify that no equipment rating and voltage constraint is violated;
- *dynamic security analysis* which involves the examination of the different categories of system instability (rotor angle, frequency and voltage) described in the previous chapter.

Security analysis consists in checking the system ability to undergo specified contingencies. When voltage instability and thermal overload are of concern, the system is said to

be *secure* if none of the specified contingencies causes an unstable voltage evolution or leads to branch currents above their physical limits. Otherwise it is *insecure*.

Credible contingencies are disturbances with a reasonable probability of occurrence. For both long-term voltage stability and thermal overload analysis, the relevant contingencies are outages of transmission or generation facilities. In this time frame the sequence of events that leads to such outages does not really matter. On the contrary, for short-term voltage stability, the system response to short-circuits must be investigated, in addition to outages. A well-known criterion is the $N-1$ security, according to which a system must be able to withstand any single transmission or generation outage without major consequences. In some cases, multiple outages having a single cause may be considered as an $N-1$ contingency. Besides, multiple ($N-k$) contingencies may also be considered, for instance the tripping of all equipments connected to a bar owing to a bus-bar fault.

System protection devices may contribute to stabilizing the system in post-contingency configuration and hence must be taken into account in contingency evaluation. We may distinguish between "normal" countermeasures, which do not affect the quality of power delivery, as opposed to "emergency" countermeasures. Compensation switching, increase in generator voltage set-points and secondary voltage control are examples of the former, while LTC blocking, LTC voltage reduction, and in the last resort, load curtailment belong to the second category. A common practice is to assess the system ability to survive credible contingencies with the sole help of normal countermeasures.

3.2 Contingency evaluation approaches

The well-known linear nature of thermal overload problems allows to devise rather simple contingency evaluation approaches. The simplest and fastest one is the DC load flow [BS70, WW96]. The latter serves only for computing MW flows on transmission elements but gives no indication on what happens to voltage magnitudes or both Mvar and MVA flows. In cases where pre- and post-contingency voltage magnitudes remain close to their nominal values the DC load flow provides sufficient accuracy with respect to MW flows. Let us recall, however, that overcurrent protections and conductor heating have to do with Ampères and not MegaWatts. Although, in practice, high currents are determined mostly by active rather than by reactive power flows, neglecting the Mvar flows represents another source of inaccuracy of this technique.

An accurate evaluation of pre- and post-contingency branch currents can be obtained using a full (or AC) load flow. Nowadays computers are fast enough to easily perform on-line thermal security analysis based on AC load flow computations. One should rely on more detailed techniques, e.g. QSS simulation (see Section 2.2) only when the post-contingency load flow may diverge due to the impossibility to take into account some discrete post-contingency controls or when voltage and thermal problems are strongly coupled.

As regards voltage security, the benchmark technique for contingency evaluation is the *multi-time scale numerical simulation* [SBD89, DS93, VCV98]. It provides the best mod-

elling accuracy, the highest interpretability of results (in terms of the sequence of events leading to voltage instability or collapse), the possibility to obtain information on remedial actions and the possibility to capture all types of voltage instability. On the other hand, it is much time consuming and therefore almost impossible to use during the short time period of on-line analysis.

Static methods are more suitable to cope with these strong time requirements. Basically, they focus on the computation of a post-contingency long-term equilibrium point. The simplest static approach is the post-contingency load flow. However, the load flow divergence may result from purely numerical problems which do not relate to a physical voltage instability. Another shortcoming of this technique is the lack of additional information (nature and location of the problem, possible remedies) in a truly unstable case. These aspects are somewhat improved when using the "non-divergent" load flow [STA71] or the VQ curve technique [CTF87]. Nevertheless, two common drawbacks of all static approaches still remain: they cannot take into account the post-contingency controls whose activation depends on the system time evolution (e.g. shunt compensation switching, OEL) and the existence of a post-contingency equilibrium does not guarantee a stable system behaviour, when instability results from a lack of attraction towards this equilibrium (see example of Section 2.3.2).

The *Quasi-Steady State (QSS) simulation* [VCJ95] is a third type of contingency evaluation technique. Its principle was presented in Section 2.2. This approach realizes a good compromise between the accuracy and diagnosis capability of dynamic methods, and the speed of computations of static methods. It is perfectly applicable within a real-time environment [CCM00, VMK03].

In this work we rely on QSS simulation to evaluate contingencies, though, as explained before, thermal security can be efficiently dealt with through the simpler AC load flow. In this context, contingencies are evaluated with QSS simulation and, if the post-contingency state is voltage stable, branch currents are checked at the final operating point. Note that an unstable voltage scenario leaves no information about branch currents.

3.3 Security regions

3.3.1 Introduction

A security analysis which relies on contingency evaluation only is however unsatisfactory in two respects. First, when available, post-contingency voltages do not provide an explicit measure of system security [1]. Second, it focuses on a particular operating point. Even when the system is voltage and thermal secure at a given operating condition, it is desirable to know how far the system can move away from its current operating point and still remain secure.

[1] post-contingency currents may, however, quantify the degree of system security with respect to thermal overload

As regards voltage stability, there are two approaches to predict the proximity (in terms of system response to increases in power transfers) to voltage instability:

- *state-based voltage stability indices* are based only on the current operating state information. For most of them no particular power transfer pattern is specified. They range from voltage drops to sensitivities, eigenvalues and singular values [TMI83, KG86, GMK92, YHC97, Bul98, VCV98, BFD98, Can02]. Although very fast, most of them have a tendency to abruptly change when generators reach their reactive limits, which generally yields a poor prediction capability;
- *direct methods* compute explicitly the maximal power transfer point [AJ89, Cut91, AC92, CTF94, IWT97, VCV98, Bul98, CMM99, Can02]. They have been often used as the benchmark for analyzing the prediction capability of the former methods.

In the thermal case, as long as voltage magnitudes remain nearly constant, sensitivities of branch currents to power injections permit a very good prediction of overload due to changes in the operating point. These sensitivities can be easily derived from the set of equations used in DC load flow, AC load flow or QSS simulation, as will be explained in the next chapter.

3.3.2 Notations

Let us consider the $2m$-dimensional space (where m is the total number of buses of the system) of the active and reactive power injections, which we will call *power injection space* for short. Such a space is defined for both *pre-* and *post-*contingency states. Each point of the pre- (resp. post-) contingency space corresponds to a particular value of *pre-* (resp. *post-*) contingency power injections.

Let us denote by P_i and Q_i the active and reactive power injections at the i-th bus ($i = 1, \ldots, m$), which we decompose into:

$$P_i = P_i^o + \Delta P_i = P_i^o + \Delta P_i^+ - \Delta P_i^- \qquad \Delta P_i^+,\ \Delta P_i^- \geq 0 \tag{3.1}$$

$$Q_i = Q_i^o + \Delta Q_i = Q_i^o + \Delta Q_i^+ - \Delta Q_i^- \qquad \Delta Q_i^+,\ \Delta Q_i^- \geq 0 \tag{3.2}$$

where P_i^o (resp. Q_i^o) is the base case value of the active (resp. reactive) power injection, ΔP_i (resp. ΔQ_i) the corresponding variation with respect to the base case, ΔP_i^+ (resp. ΔQ_i^+) the additional active (resp. reactive) power *injected into* the network, and ΔP_i^- (resp. ΔQ_i^-) the one *drawn from* the network, all relative to bus i.

3.3.3 Security regions in the pre-contingency power injection space

We first define two regions of the power injection space relative to the system in its pre-contingency state.

The set of pre-contingency points for which power system operation is feasible (i.e. a load flow solution exists for the given vector of power injections) defines the *pre-contingency feasible region* $\mathcal{F}_o$. Inside $\mathcal{F}_o$, the set of pre-contingency points for which all branch currents are under their limits defines the *pre-contingency viability region* $\mathcal{V}_o$. Note that, in this work, viability refers to thermal constraints only, albeit, it may also concern bus voltage magnitudes, generators reactive power productions, etc.

We now define two regions relative to a set of contingencies.

We define the *voltage secure region* $\mathcal{S}_V$ as the set of pre-contingency points for which the system responds in a stable way to each of the specified contingencies. Stable response of the system requires the existence of a post-contingency equilibrium and the system attraction towards the latter. This sub-space is bounded by a (nonlinear) boundary $\mathcal{B}_V$.

In practice, clearly, the determination of a security region depends to some extent on the computational tool used to evaluate the system response to the contingencies. If a load flow was used (instead of QSS time simulation as in this work), $\mathcal{S}_V$ could be defined as the set of points for which the post-contingency load flow converges after any of the specified contingencies.

We finally define the *thermal secure region* $\mathcal{S}_T$ as the set of pre-contingency points for which no branch current is above its limit after any specified contingency. This sub-space is bounded by a boundary $\mathcal{B}_T$.

For a single contingency, a graphical representation of the above concepts in a two-dimensional power injection space is given in the left part of Fig. 3.1, where A_o, B_o and C_o represent three vectors of power injections. For the sake of simplicity, we only show that part of the power injection space corresponding to positive (indifferently active or reactive power) injections P_1,P_2. Let us mention that P_1,P_2 can also stand for the ΔP_1^+, ΔP_2^+ or ΔP_1^-, ΔP_2^- power variations, which are positive by definition. For instance, these injections can represent two generator outputs, two load powers or a combination of both.

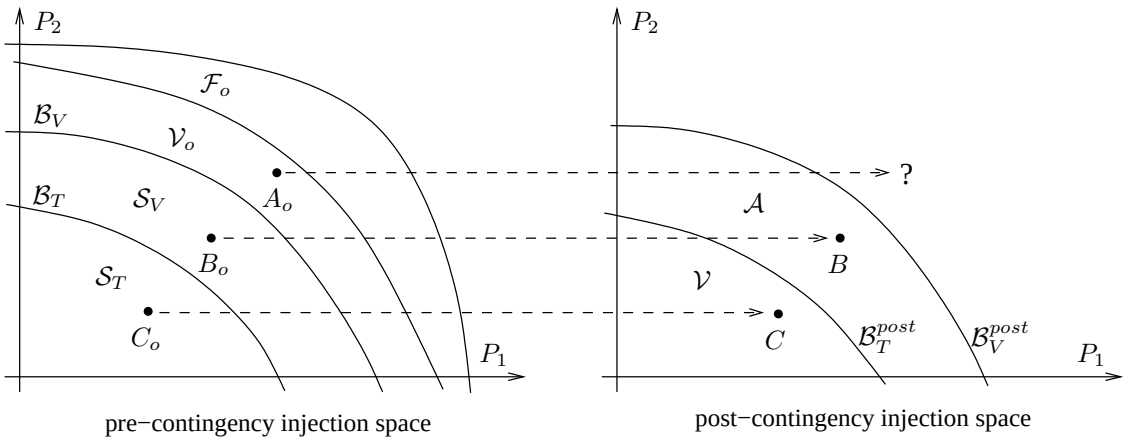

Figure 3.1: Secure regions in the power injection space

Note that the above defined regions are expected to satisfy the general relationship:

$$\mathcal{F}_o \supseteq \mathcal{V}_o \supseteq \mathcal{S}_V \supseteq \mathcal{S}_T \tag{3.3}$$

For a system operating point corresponding to an injection vector located outside $\mathcal{S}_V$, such as A_o in Fig. 3.1, there is either no post-contingency equilibrium or not enough attraction towards the existing equilibrium. Hence post-contingency thermal overloads cannot be checked, since the latter are typically checked at a long-term equilibrium of the system. It results that the thermal secure region $\mathcal{S}_T$ is included into the voltage secure region $\mathcal{S}_V$. Therefore, $\mathcal{S}_T$ can be also defined as the set of points for which no one of the specified contingencies causes voltage instability or thermal overload.

3.3.4 Security regions in the post-contingency power injection space

Before defining security regions in the post-contingency power injection space, let us recall that for a power system at a given operating point, the pre- and post-contingency power injections are generally different. Indeed, if the considered contingency is the loss of a generator, the resulting production deficit is compensated in the post-contingency situation by the other generators participating in frequency regulation. If the contingency is a line outage that does not cause network splitting, the pre- and post-contingency power generations are only slightly different since only transmission losses change and this variation is again shared by the various generators participating in frequency control. A major reason for having different power injections after a contingency is the sensitivity of loads to voltage[2]. However, if loads are controlled by LTCs, a very common situation of interest in voltage stability studies, and the system is long-term stable with no LTC limit met, the load voltages and hence the load powers are restored close to their pre-contingency values. Nevertheless, under the effect of LTC deadbands, the load voltages and powers do not exactly come back to their pre-contingency values. Incidentally, these effects are seldom taken into account in standard load flow computations, where it is common to consider constant power loads. However, even in this simplified analysis, the variation of generated powers under the effect of the contingency still remains.

We now define two regions of the power injection space relative to the system in its post-contingency state.

We define the *post-contingency attracting region* $\mathcal{A}$ as the set of post-contingency points such that the pre-contingency point belongs to $\mathcal{S}_V$. In other words, whatever the point of $\mathcal{S}_V$ there exist a point in $\mathcal{A}$ which is its long-term equilibrium and the system is attracted towards the latter. This sub-space is bounded by a (nonlinear) boundary $\mathcal{B}_V^{post}$.

For instance, in the example of Fig. 3.1, if the system operates initially at point $B_o \in \mathcal{S}_V$, there is a post-contingency equilibrium point B and the system is attracted towards it, while for $A_o \notin \mathcal{S}_V$, the system either has no post-contingency long-term equilibrium or has such an equilibrium but without sufficient attraction.

[2] and frequency if the latter changes significantly

Once again, if a load flow is used (instead of QSS simulation) to determine the system response to contingencies, only the loss of post-contingency equilibrium can be captured only, not the lack of attraction towards such an equilibrium. In this case, the region $\mathcal{A}$ is thus approximated as the set of post-contingency injection vectors such that both the pre- and post-contingency load flows converge.

Finally, we define the *post-contingency viability region* $\mathcal{V}$ as the set of post-contingency injection vectors from $\mathcal{A}$ for which no post-contingency branch current is above its limit. The boundary of this region is denoted as $\mathcal{B}_T^{post}$.

3.4 Security limits and margins

3.4.1 System stress

The security margins considered in this work rely on the definition of a *system stress*. The latter consists in changes in bus power injections which make the system weaker by increasing power transfers over relatively long distances and/or drawing on reactive power reserves.

In an open access environment any transaction can be expressed in terms of two typical stresses:

A) a power transfer from a generation to a load area, characterized by:

$$\Delta P_i^+ = \alpha_i \, S \qquad i \in G^+ \tag{3.4}$$
$$\Delta P_i^- = \beta_i \, S \qquad i \in L \tag{3.5}$$
$$\Delta Q_i^- = \beta_i \, S \, tg\varphi_i \qquad i \in L \tag{3.6}$$

B) a power transfer between two generation areas, characterized by:

$$\Delta P_i^+ = \alpha_i \, S \qquad i \in G^+ \tag{3.7}$$
$$\Delta P_i^- = \beta_i \, S \qquad i \in G^- \tag{3.8}$$

where S, referred to in the sequel as the *system stress*, is the total additional power transferred (in MW), (α_i, β_i) are positive real numbers, defining the "direction of stress", φ_i is the phase angle between voltage and current at bus i, G^+ (resp. G^-) is the set of increased (resp. decreased) generators and L the set of increased loads. G^+ (resp. G^- and L) will be called hereafter as *source* (resp. *sink*).

In this whole thesis, loads are assumed to vary under constant power factor $cos\varphi_i$ *in the pre-contingency configuration*[3]. If reactive load variations were considered independent,

[3] when lacking information about the power factor, a common practice is to use the base case one, i.e. $cos\varphi_i = cos\varphi_i^o = \frac{P_i^o}{\sqrt{(P_i^o)^2+(Q_i^o)^2}}$

the equations of type (3.6) would be adjusted and straightforwardly handled by the methods described in the sequel.

With the above notation, ΔP_i^+ corresponds to a generation increase only, while ΔP_i^- corresponds to either a load increase (as in stress A) or a generation decrease (as in stress B). ΔQ_i^- corresponds to a load increase only.

The participation factors are normalized according to:

$$\sum_{i \in L \, or \, G^-} \beta_i = 1 \qquad \sum_{i \in G^+} \alpha_i = 1 + \delta \tag{3.9}$$

where δ takes into account the losses. The latter are thus assumed to vary linearly with S, for simplicity.

Taking (3.4-3.8) into account, equations (3.1, 3.2) can be written in vector form as:

$$\mathbf{P} = \mathbf{P}^o + S\,\mathbf{d} \tag{3.10}$$

where $\mathbf{P}$ is a vector of bus injections, $\mathbf{P}^o$ its base case value, and $\mathbf{d}$ a vector defining the direction of stress.

3.4.2 Secure operation limit and margin

Procedures to compute security limits and margins involve two steps: computation of the stressed states and contingency simulation. Depending on the order in which these two steps are carried out, one may distinguish between [VCV98]:

- *a post-contingency loadability limit* for which one first simulates the contingency, then stresses the system progressively until it reaches instability, and
- *a secure operation limit* for which one stresses the system progressively until its response to the contingency becomes unstable.

Given a direction of system stress, the Secure Operation Limit (SOL) with respect to a contingency corresponds to the most stressed among the operating points, such that the system can withstand the contingency. Accordingly, the secure operation margin M relative to a contingency is the maximum value of S such that the system can withstand the contingency. Such a margin refers to pre-contingency parameters that operators can either observe (e.g. load increase) or control (e.g. generation rescheduling). Unlike a post-contingency loadability limit, an SOL refers to the present, i.e. pre-contingency, system configuration and provides a security margin that is easier to interpret in system operation [CMM99].

An SOL encompasses three types of information: direction of system stress, operator/controller actions while the system is stressed and post-contingency controls. We briefly comment hereafter on the last two aspects.

Prior to any contingency, operators or controllers react to the stress imposed to the system. Most often they role is to keep the voltage profile within limits and to maximize reactive reserves readily available to face incidents. Typical examples of such actions are: shunt capacitor/reactor switching, secondary voltage control, operator adjustment of generator voltages to keep network voltages within limits (e.g. at the high voltage of the step-up transformer), operator adjustment of ratios of transformers connecting two transmission levels, etc.

As mentioned earlier in this chapter, post-contingency controls are typically automatic and hence faster than human operators, who play a role in the pre-contingency situation only.

Note that, if one neglects both pre-contingency operator/controller actions and post-contingency, the post-contingency loadability limit and the secure operation limit should be close to each other.

3.4.3 Intuitive view of a secure operation limit

Figure 3.2 illustrates graphically the concept of SOL within the context of security regions defined in Section 3.3.3. In this figure the thermal security region $\mathcal{S}_T$ is tinted in gray and is included in the voltage security region $\mathcal{S}_V$, as explained earlier. Each point of $\mathcal{B}_V$ (resp. $\mathcal{B}_T$) can be seen as corresponding to a voltage (resp. thermal) secure operation limit, for a particular direction of stress. For instance, when considering the stress direction $\mathbf{d}_1$, the voltage (resp. thermal) security limit corresponds to point L_V (resp. L_T), the intersection between the boundary $\mathcal{B}_V$ (resp. $\mathcal{B}_T$) and the straight line corresponding to $\mathbf{d}_1$. For this stress direction the thermal overload margin is lower than the voltage stability one. In practice, one may encounter situations where voltage instability is more constraining than thermal overload, i.e. no branch is overloaded in the post-contingency state corresponding to the voltage secure operation limit. In some neighbourhood of such a limit boundaries $\mathcal{B}_V$ and $\mathcal{B}_T$ coincide. In Fig. 3.2 this situation occurs for the stress direction $\mathbf{d}_2$ with the overall limit corresponding to point L.

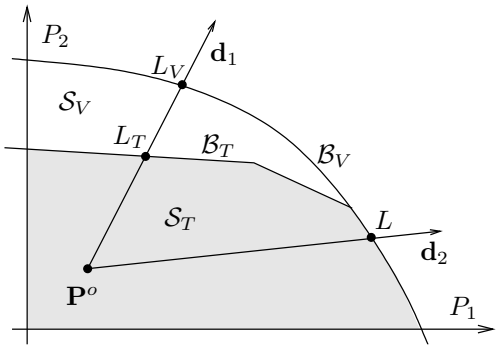

Figure 3.2: Intuitive view of an SOL by means of security regions

3.4.4 Formal description of a secure operation limit

We attempt to provide hereafter a more formal description of an SOL, although the equations shown cannot capture the full complexity of a practical SOL determination, as illustrated in Section 3.7.

Let us consider the set of long-term dynamics equations (2.2, 2.3, 2.4, 2.5) written in a compact form as:

$$\dot{\mathbf{z}} = \mathbf{h}(\mathbf{x}, \mathbf{y}, \mathbf{z}) \tag{3.11}$$
$$\mathbf{0} = \mathbf{f}(\mathbf{x}, \mathbf{y}, \mathbf{z}) \tag{3.12}$$
$$\mathbf{0} = \mathbf{g}(\mathbf{x}, \mathbf{y}, \mathbf{z}) \tag{3.13}$$

where equations (3.11) relate to both the continuous and the discrete long-term dynamics (conveniently replaced by a continuous-time approximation), and thus replace (2.3) and (2.4).

Assuming that voltage instability stems from the loss of a long-term equilibrium point (which is the main cause in practice: see example of Section 2.3.1), the determination of an SOL, for a given direction of stress $\mathbf{d}$, can be formulated as an optimization problem:

$$\max S \tag{3.14}$$
$$subject\ to: \quad \mathbf{0} = \mathbf{h}_o(\mathbf{x}, \mathbf{y}, \mathbf{z}, \mathbf{P}^o + S\,\mathbf{d}) \tag{3.15}$$
$$\mathbf{0} = \mathbf{f}_o(\mathbf{x}, \mathbf{y}, \mathbf{z}, \mathbf{P}^o + S\,\mathbf{d}) \tag{3.16}$$
$$\mathbf{0} = \mathbf{g}_o(\mathbf{x}, \mathbf{y}, \mathbf{z}, \mathbf{P}^o + S\,\mathbf{d}) \tag{3.17}$$
$$\mathbf{0} = \mathbf{h}(\mathbf{x}_{post}, \mathbf{y}_{post}, \mathbf{z}_{post}, \mathbf{P}_{post}) \tag{3.18}$$
$$\mathbf{0} = \mathbf{f}(\mathbf{x}_{post}, \mathbf{y}_{post}, \mathbf{z}_{post}, \mathbf{P}_{post}) \tag{3.19}$$
$$\mathbf{0} = \mathbf{g}(\mathbf{x}_{post}, \mathbf{y}_{post}, \mathbf{z}_{post}, \mathbf{P}_{post}) \tag{3.20}$$

where $\mathbf{P}^o$ is the vector of bus injections in the base case, $\mathbf{P}^o + S\,\mathbf{d}$ is the corresponding vector after pre-contingency stress and $\mathbf{P}_{post}$ is the vector of bus injections at the post-contingency long-term equilibrium point reached by the system. Note that $\mathbf{P}_{post}$ generally differs from $\mathbf{P}^o + S\,\mathbf{d}$, as explained in Section 3.3.4.

The pre-contingency long-term equilibrium equations (3.15-3.17) express that the limit is sought among steady-state operating points. On the other hand, equations (3.18-3.20) express that in the post-contingency configuration the system settles at a long-term equilibrium. Additionally, operating constraints may be imposed to this long-term equilibrium, but the latter have not been included for the sake of clarity.

The solution of this optimization problem is the secure operation margin M and the SOL corresponds to the injection vector $\mathbf{P}^\star = \mathbf{P}^o + M\,\mathbf{d}$.

Note that if a post-contingency loadability limit (or margin) was sought, only the post-contingency equations would be kept in the above optimization problem. Supposing that $\mathbf{P}^o_{post}$ is the post-contingency equilibrium point when the system operates in the base case

$\mathbf{P}^o$, the optimization problem would take on the form:

$$\max S \tag{3.21}$$

$$subject\ to: \quad \mathbf{0} = \mathbf{h}(\mathbf{x}_{post}, \mathbf{y}_{post}, \mathbf{z}_{post}, \mathbf{P}^o_{post} + S\,\mathbf{d}) \tag{3.22}$$

$$\mathbf{0} = \mathbf{f}(\mathbf{x}_{post}, \mathbf{y}_{post}, \mathbf{z}_{post}, \mathbf{P}^o_{post} + S\,\mathbf{d}) \tag{3.23}$$

$$\mathbf{0} = \mathbf{g}(\mathbf{x}_{post}, \mathbf{y}_{post}, \mathbf{z}_{post}, \mathbf{P}^o_{post} + S\,\mathbf{d}) \tag{3.24}$$

Note that any point of $\mathcal{B}_V^{post}$ (see Fig. 3.1) can be seen as corresponding to a post-contingency loadability limit, for a particular direction of stress. Indeed, as far as the security margin is computed with respect to voltage instability, the post-contingency long-term equilibrium that corresponds to the maximum pre-contingency stress $\mathbf{P}^\star$ is "on the verge of instability". It is thus a loadability limit of the system in its post-contingency configuration.

These considerations are illustrated graphically in Fig. 3.3 using simple PV curves and assuming that the load restores to constant power under the effect of an LTC. For a pre-contingency stress larger than M, the system has no post-contingency long-term equilibrium since the long-term load characteristic does not intersect the post-contingency network characteristic (see Section 2.3.1). For a pre-contingency stress equal to M, the system settles down at the "ultimate" long-term equilibrium point C. As shown by the figure, C is a loadability limit, since any further increase in load would make the equilibrium disappear.

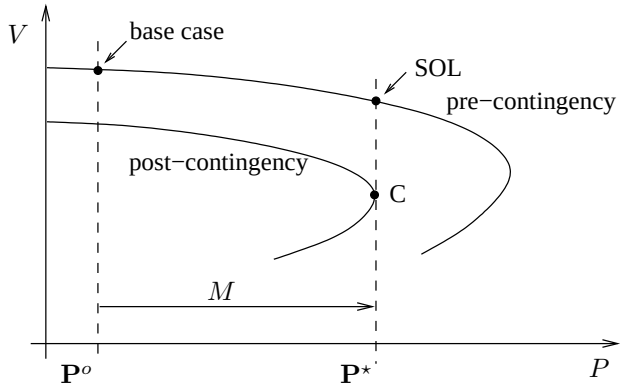

Figure 3.3: Saddle-node bifurcation

In the terminology of System Theory, C is a *Saddle-Node Bifurcation* point (SNB) of the long-term dynamics [Dob92, VCV98].

The necessary condition for an equilibrium of the general model (3.11-3.13) to be an SNB, is the singularity of the Jacobian $\mathbf{J}$ of the corresponding equations, i.e. $\det \mathbf{J} = 0$, which is equivalent to say that $\mathbf{J}$ has a zero eigenvalue. In order to identify a zero eigenvalue of $\mathbf{J}$ a small-disturbance analysis is needed. The system (3.11-3.13) is thus linearized into:

$$\begin{bmatrix} \Delta\dot{\mathbf{z}} \\ \mathbf{0} \\ \mathbf{0} \end{bmatrix} = \underbrace{\begin{bmatrix} \mathbf{h_z} & \mathbf{h_y} & \mathbf{h_x} \\ \mathbf{g_z} & \mathbf{g_y} & \mathbf{g_x} \\ \mathbf{f_z} & \mathbf{f_y} & \mathbf{f_x} \end{bmatrix}}_{\mathbf{J}} \begin{bmatrix} \Delta\mathbf{z} \\ \Delta\mathbf{y} \\ \Delta\mathbf{x} \end{bmatrix} \tag{3.25}$$

Eliminating $\Delta\mathbf{y}$ and $\Delta\mathbf{x}$ yields:

$$\Delta\dot{\mathbf{z}} = \mathbf{A}\Delta\mathbf{z} \tag{3.26}$$

with

$$\mathbf{A} = \mathbf{h_z} - \begin{bmatrix} \mathbf{h_y} & \mathbf{h_x} \end{bmatrix} \underbrace{\begin{bmatrix} \mathbf{g_y} & \mathbf{g_x} \\ \mathbf{f_y} & \mathbf{f_x} \end{bmatrix}^{-1}}_{\mathbf{J}_s} \begin{bmatrix} \mathbf{g_z} \\ \mathbf{f_z} \end{bmatrix} \tag{3.27}$$

where $\mathbf{J}_s$ is assumed to be nonsingular.

Using the determinant Schur's formula:

$$\det \mathbf{J} = \det \mathbf{J}_s \cdot \det \mathbf{A} \tag{3.28}$$

implies that, when $\mathbf{J}_s$ in nonsingular, $\mathbf{A}$ and $\mathbf{J}$ become singular together.

An SNB point thus satisfies the set of equations:

$$\mathbf{0} = \mathbf{h}(\mathbf{x}, \mathbf{y}, \mathbf{z}) \tag{3.29}$$
$$\mathbf{0} = \mathbf{f}(\mathbf{x}, \mathbf{y}, \mathbf{z}) \tag{3.30}$$
$$\mathbf{0} = \mathbf{g}(\mathbf{x}, \mathbf{y}, \mathbf{z}) \tag{3.31}$$
$$\det \mathbf{J} = \det \mathbf{A} = 0 \tag{3.32}$$

Note that the reactive power limits of generators may yield another type of loadability limits, namely the *Breaking-Points* (BP) [DL92b, VCV98], also called *limit-induced bifurcations* by some authors [Can02]. The case where the ultimate post-contingency long term equilibrium is a BP is shown graphically in Fig. 3.4.

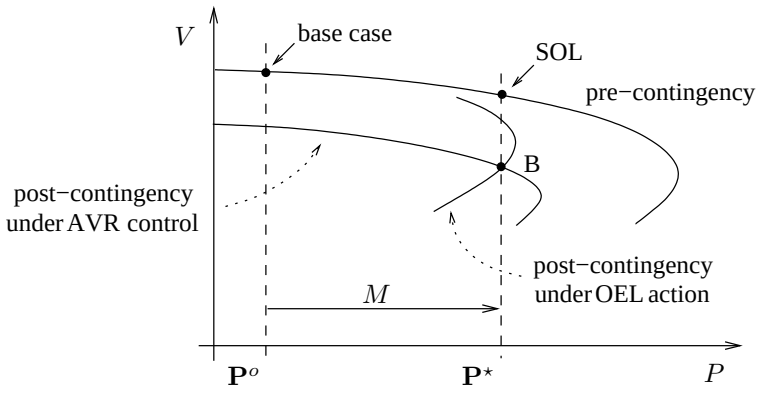

Figure 3.4: Breaking point

A BP also corresponds to a maximum stress in the post-contingency configuration but does not obey equation (3.32), i.e. $\mathbf{J}$ is nonsingular at a BP.

Let us finally mention that in an SOL computation, the post-contingency long-term equilibrium may be requested not only to exist but also to satisfy operating constraints, for instance to have all voltages above some minimal value. Clearly, it will not be an SNB or a BP, if this constraint is met before the equilibrium is lost in the post-contingency configuration.

3.5 Practical determination of secure operation limits

3.5.1 Binary search: handling of a single contingency

The margin relative to a contingency can be determined by *Binary Search* (BS) (also referred to as *bisection method* or *dichotomic search*) which is a simple and robust method. This consists in building a smaller and smaller interval $[S_\ell\ S_u]$, where S_ℓ corresponds to an acceptable post-contingency evolution and S_u to an unacceptable one, until $S_u - S_\ell$ becomes lower than a tolerance Δ. The search starts with $S_\ell = 0$, the base case and $S_u = S_{max}$, a maximum stress of interest. At each step, the interval is divided in two equal parts; if the midpoint is found acceptable (resp. unacceptable) it is taken as the new lower (resp. upper) bound. The final value of S_ℓ is the sought margin M.

This procedure is illustrated in Fig. 3.5 by means of PV curves. The pre-contingency (resp. post-contingency) curve is sketched with dashed (resp. solid) line. Let us assume once more that the load restores to constant power under the effect of an LTC. In this illustrative example we consider as acceptable a post-contingency system evolution for which there is a stable long-term equilibrium point. Stress levels S_{max}, S_1, S_2, S_3 and S_4 are tested successively. For the stress levels S_1, S_2, and S_4 the post-contingency system evolution is acceptable while for S_{max} and S_3 it is unacceptable. The SOL correspond to the marginally acceptable case.

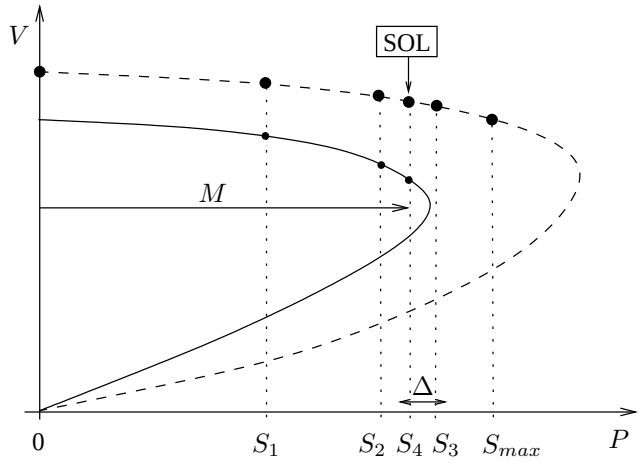

Figure 3.5: Binary search

Note that, for the sake of simplicity, we have drawn a single PV curve for all pre-contingency situations as well as a single curve for all post-contingency ones. In reality, there is a family of such curves determined by both pre-contingency and post-contingency control actions.

Whether the system response to a contingency is acceptable must be defined with respect to appropriate criteria. At least, voltage stability is required, but in addition to being stable, the system might be requested to meet some post-contingency viability constraints,

i.e. post-contingency voltage magnitudes and branch currents to be within limits:

$$V_i^{min} \leq V_i \leq V_i^{max} \quad i = 1, \ldots, m \tag{3.33}$$

$$I_j \leq I_j^{max} \quad j = 1, \ldots, b \tag{3.34}$$

In these equations, V_i is the post-contingency voltage at the i-th bus, V_i^{min} (resp. V_i^{max}) is the minimal (resp. maximal) allowed value of this voltage, I_j is the post-contingency current in the j-th branch (b is the number of branches) and I_j^{max} is the maximum allowed current in the j-th branch. In this situation one can compute at the same time an overall security margin with respect to voltage instability, voltage quality and thermal overload.

There are basically two computational tasks involved in a binary search, namely the pre-contingency stress and the contingency evaluation. The system operating states corresponding to various stress levels S can be computed with a standard load flow (or possibly an optimal power flow) in which the operator/controller reaction to the system stress is taken into account, as already discussed. We use the QSS simulation in order to evaluate the impact of a contingency at a given stress level.

3.5.2 Binary search: handling of several contingencies

When the objective is to determine the SOL with respect to the severest contingency of a given set, it would be a waste of time to compute the individual limit of each contingency and finally keep the smallest value as the global limit. It is more efficient to perform a *Simultaneous Binary Search* (SBS) [CMM99]. In this procedure, at a given step of the binary search, the various contingencies stemming from the previous step are simulated. If at least one of them is unacceptable, the acceptable ones are discarded since their limits are higher than the current stress level; the search proceeds with the unacceptable ones only. By so doing, the procedure provides for each contingency an interval containing its SOL. The more dangerous the contingency, the smaller the width of this interval. In particular, for the severest contingency the width of this interval is slightly less than the requested accuracy Δ.

The procedure is illustrated in Fig. 3.6 for a simple case of three contingencies. C1, C2 and C3 are the post-contingency PV curves relative to these contingencies, while the pre-contingency curve is depicted with dashed line. At maximum stress, the third contingency is found acceptable and is thus already discarded. The same happens at the stress S_1 for the second contingency. The severest contingency is the first one, and its SOL is thus the overall SOL.

3.5.3 Linear methods for thermal limits

When security margins are sought with respect to thermal overloads only, the binary search method becomes too complex. Indeed, this problem being often linear, simpler approaches can be thought of, as explained hereafter.

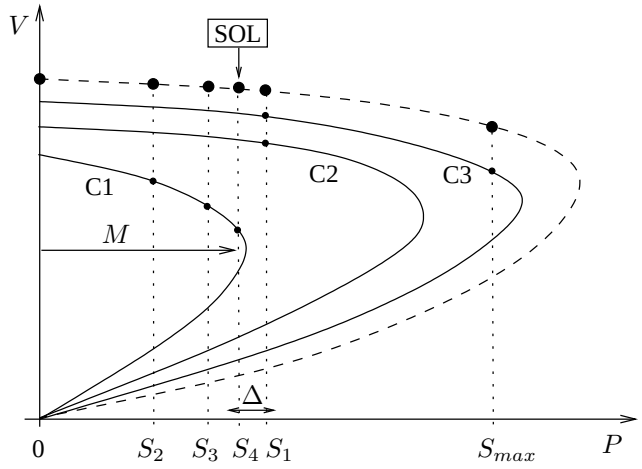

Figure 3.6: Simultaneous binary search

In order to compute a thermal security margin one has to determine which post-contingency branch current will first reach its maximum allowed value following a system stress in the specified direction. To this purpose one can rely on sensitivities of branch currents with respect to system stress. An analytical derivation of these sensitivities will be presented in Section 4.2.

It is well known that (pre- or post-contingency) branch currents vary almost linearly with bus power injections and, thereby, with the stress S which is nothing but a linear combination of power injections. The post-contingency thermal viability constraints (3.34) can thus be linearized into:

$$I_j = I_j^o + \frac{\partial I_j^o}{\partial S}\Delta S \leq I_j^{max} \quad j = 1, \ldots, b \tag{3.35}$$

where I_j^o is the post-contingency current in the j-th branch when the system operates at base case and $\dfrac{\partial I_j^o}{\partial S}$ is the sensitivity of the same current to system stress.

Figure 3.7 presents a simple example of linear approximation of a thermal security margin for a simple case with two branches. Let us denote by I_1 (resp. I_2) the current in the first (resp. second) branch. If only the first (resp. second) branch constraint is taken into account, the thermal margin is M_1 (resp. M_2) and corresponds to the projection onto the stress axis of point A (resp. B). It is easily seen that the first branch is the most constraining for the stress under concern because its current reaches the maximal value while the second branch current is still under its limit. Obviously the overall margin is the smallest among the two margins, i.e. M_1. Note that the difference between the maximal and base case currents as well as their sensitivity to the stress matter for establishing the margin. In this example, despite the fact that the second branch is closer to its maximum current ($I_2^{max} - I_2^o < I_1^{max} - I_1^o$) the first branch first reaches its maximum current due to its greater current sensitivity to stress ($\partial I_1^o/\partial S > \partial I_2^o/\partial S$ and $\dfrac{I_1^{max} - I_1^o}{\dfrac{\partial I_1^o}{\partial S}} < \dfrac{I_2^{max} - I_2^o}{\dfrac{\partial I_2^o}{\partial S}}$).

This figure suggests a first way to compute a thermal security margin which consists of

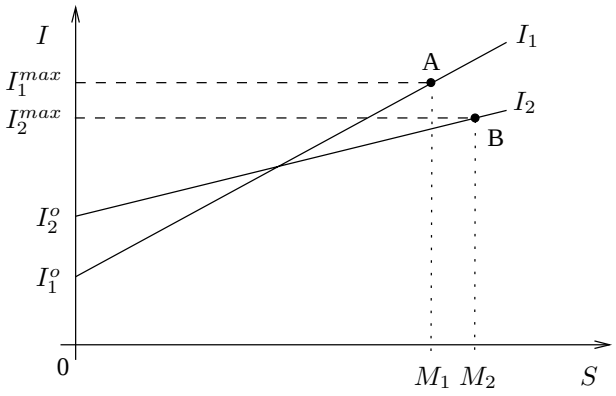

Figure 3.7: Linear approximation of a thermal security margin

estimating the margin for each branch separately, and finally keeping the smallest among these values. This can be expressed in mathematical terms as:

$$M = \min_{j=1,\dots,b} \frac{I_j^{max} - I_j^o}{\frac{\partial I_j^o}{\partial S}} \tag{3.36}$$

This approach involves the simulation of the contingency in the base case as well as the computation of the $\partial \mathbf{I}/\partial S$ sensitivities at the post-contingency equilibrium point of the system. The computation of these sensitivities requires the solution of a single linear system, as we will show in Section 4.2.

To account for nonlinearities, one can check all branch currents at the estimated value of margin M. If they are too far from their predicted values, especially for the most constraining branch, one can improve each $\partial I_j^o/\partial S$ sensitivity by using instead the ratio $(I_j^M - I_j^o)/M$, where I_j^M represents the post contingency current in the j-th branch for the system operating at the stress level M. The margin may then be computed by interpolation or extrapolation.

A second technique to compute a thermal security margin consists in computing branch currents for two different stress levels [4] and directly determining the margin by interpolation or extrapolation. Thus, this approach uses a finite-difference approximation of $\partial \mathbf{I}/\partial S$ sensitivities. Since nonlinearities are better taken into account, this technique is appropriate for cases where voltages and currents are strongly coupled. On the other hand, it is a bit more time consuming because it requires to solve a second load flow instead of a single linear system as in the first approach.

Let us finally mention that it is also possible to compute a thermal security margin by solving the simple linear optimization problem:

$$\max S \tag{3.37}$$

$$subject\ to: \quad I_j^o + \frac{\partial I_j^o}{\partial S} S \leq I_j^{max} \quad j = 1, \dots, b \tag{3.38}$$

[4] one of them may be the base case

3.5.4 Increasing an interface flow as system stress

In some systems (mainly in North America) security limits are expressed on *interface flows*, i.e. on the total power flowing through a set of branches linking two adjacent systems. To obtain such a limit, sources can be placed on one side of the interface and sinks on the other side.

Obviously if there is no parallel flow spanning third systems, the stress defined previously in this chapter will coincide with the interface flow (if one ignores variations of losses)[5] [SKL00, GLB01].

On the other hand, if there is a parallel path between the two adjacent systems, some power will flow through this path when increasing the stress [6]. In this case, one can only say that there is a one-to-one correspondence between the overall system stress and the interface flow. The limit value of the latter can be taken as the power flowing in the interface when the system stress is at its limit M. Alternatively, it is possible to directly use the interface flow as the varied pre-contingency parameter, while constraining sources and sinks to follow this increase. To this purpose, one can re-use a technique first proposed in [Bri69], as follows:

- in the pre-contingency load flow, add a new equation corresponding to the interface flow:

$$\sum_{j \in \mathcal{I}} F_j - F_{des} = 0 \tag{3.39}$$

  where $\mathcal{I}$ is the set of branches crossing the interface, F_j the power flowing in the j-th branch and F_{des} the desired interface flow;

- in the combined equations (3.1, 3.4 and 3.5):

$$P_i = P_i^o + \alpha_i S - \beta_i S$$

  S becomes an unknown, balancing the additional equation (3.39). The participation factors α_i and β_i are chosen as previously explained in this chapter;

- perform the binary search on the value of F_{des}.

The remaining of this work relies on the formulation presented in the previous sections of this chapter and does not consider the interface flow formulation.

[5] in the case of the UCTE system, for instance, this would apply to the interface between Portugal and Spain, or Spain and France.

[6] this is typically the case of the French-Belgian interface: when a transfer takes place from France to Belgium, most of the power enters Belgium across its South border, but the remaining flows through Germany and the Netherlands before entering Belgium from the North

3.6 Contingency filtering

3.6.1 Introduction

When a large set of contingencies has to be processed, contingency filtering (or selection) becomes essential. This holds true for operational planning studies but even more for real-time applications.

Contingency selection has been first investigated within the context of static security analysis [ILS79, EW79, ZWP80]. The goal is to quickly identify those contingencies which can lead to the violation of operating constraints, e.g. branch currents or bus voltage magnitudes outside limits. Two-three decades ago, post-contingency thermal overloads were identified by using very fast techniques such as the DC load flow [BS70] or the fast decoupled load flow [SA74, ABH82]. The AC load flow provided better accuracy for the filtering of contingencies likely to cause thermal overloads, but was found too slow. In the meantime, computers have achieved very high computation speeds such that, nowadays, evaluating contingencies with a standard load flow is not a real problem anymore.

Recently, emphasis has been put on contingency filtering within the context of security margin computations [RAU93, Ove94, EIM96, CWF97, SMC98, VFX99, GDA99, CMM99, BZM00, Cap00, FGD02]. Here, the objective of contingency selection is to quickly identify those contingencies whose security margin is lower than some threshold.

Contingency selection techniques generally have two steps. The contingencies under concern are first ranked according to a Severity Index (SI). Then, contingencies with an SI smaller than a threshold are discarded while the others are kept for a more detailed analysis.

Ideally, the lower the security margin, the greater the index. Setting up an SI that varies monotonically with the voltage security margin is not an easy task [Cap00]. Indeed, such an SI must take into account not only the disturbance but also the direction of system stress, since the respective severities of contingencies usually change with the assumed stress. Also, what matters is how the SI decreases when the stress increases rather than the SI value at a given stress level. Finally, as discussed in the sequel, it may be impractical to compare contingencies with different impacts on the system.

However, as long as the objective is to filter out harmless contingencies, by discarding those with an SI smaller than a threshold value, the SI does not need to be sophisticated. “In the large” it should be larger for contingencies with low margins, but some “irregularities” can be tolerated. Clearly, the rejection threshold should be chosen prudently: low enough to avoid missing harmful contingencies and high enough to avoid too many false alarms.

Methods to rank contingencies must find the best compromise between accuracy and speed. From this perspective two types of methods may be distinguished.

The first type of method simulates the contingency explicitely and exploits post-contingency system information [RAU93, Ove94, EIM96, CWF97, VFX99, CMM99, Cap00]. Some

of these methods yield fairly accurate SIs with acceptable time requirements. For instance, we proposed in [Cap00] to rank contingencies according to the sum of the squared mismatches provided by a "non divergent" post-contingency load flow computation .

The second type of method relies on first or second order sensitivity information [GDA99, BZM00, FGD02]. These techniques are appealing because they attempt to provide additionally estimates of security margins. They are faster than the former because no explicit contingency simulation is required. For instance, Refs. [GDA99, FGD02] propose to first compute the pre-contingency loadability limit of the system for the assumed stress direction. If this limit corresponds to a saddle-node bifurcation, the security margin of a line outage is then approximated by the sensitivity of the pre-contingency system loadability limit with respect to either the branch admitance, as in [GDA99], or the power flow in the lost branch, as in [FGD02]. Note, however, that the accuracy of these methods is questionable when the instability mode of the pre-contingency loadability limit differs significantly from the post-contingency instability mode [SMC98]. This partly explains the errors obtained with these techniques [GDA99]. A slightly improved ranking is obtained by using the second term of the Taylor series expansion [GDA99].

On the other hand, Ref [BZM00] aims at ranking line outages according to the line loadability margin (the system stress being the increase of a line power flow at a time). It uses the sensitivity of the maximal singular value of the inverse load flow Jacobian to the power flow of the contingent branch. Obviously, the higher the power flowing on the contingent branch, the less accurate the linear estimate of the margin. In this case using the second order sensitivity information yields a considerably improved ranking.

If an accurate ranking of the contingencies is sought, one should take into account that it makes no physical sense to compare contingencies which relate to (very) different voltage instability modes. Ref. [SMC98] points out three types of voltage instability modes, namely: wide, middle and narrow. They are related to the two major causes of voltage instability: (i) the exhaustion of reactive reserves leading to the loss of voltage control at some buses (wide mode) and (ii) the increase of electrical distance between loads and generators (middle and narrow modes) [Sch98].

Let us finally mention that in large power systems several weak areas prone to voltage instability may exist. Obviously, security analysis and hence contingency selection should be performed for each of them separately. Moreover, in a weak area (or a whole system) exhibiting multiple instability modes, for some SIs it may be required to split the initial contingency set in clusters of comparable contingencies. These clusters, however, should be updated when operating conditions (mainly topology) change. Such treatments may lack the computational efficiency and the reliability required by automatic real-time applications.

3.6.2 The proposed approach

We describe hereafter a practical contingency filtering procedure which has been found to provide very satisfactory results on several tested systems. This procedure is aimed at being applied before the SBS described in Section 3.5.1.

A form of filtering takes place at the first step of the SBS, i.e. at maximum stress S_{max}, when discarding contingencies which yield an acceptable system response. Thus harmless contingencies may be discarded at the (low) cost of a single QSS simulation per contingency. However, in spite of the QSS simulation speed, it may take too long to simulate the system response to each contingency of a long list.

Hence, the idea of performing a pre-filtering test in order to identify those contingencies likely to yield an unacceptable system evolution at maximum stress. Note that this does not require to define an SI, but just to label each contingency as potentially harmful or potentially harmless. From there on, only potentially harmful contingencies are going to be processed by SBS. In a majority of systems, the post-contingency load flow can be advantageously used to this purpose.

Load flow equations with constant power loads and enforcement of generator reactive limits correspond to the long-term equilibrium that prevails after load voltage restoration by LTCs and machine excitation limitation by OELs. Insofar as voltage instability results from the loss of such an equilibrium, the corresponding load flow equations no longer have a solution and the Newton-Raphson algorithm diverges. However, using the divergence as an instability criterion meets the following difficulties:

1. divergence may result from purely numerical problems (this is particularly true when controls have to be adjusted and/or many generators switch under limit)
2. some dynamic controls that help stability cannot be taken into account in the static load flow calculation
3. conversely, some system dynamics may be responsible for an instability not detected by the load flow.

Within the context of filtering, errors 1 and 2 will induce false alarms and hence some more computational effort for the binary search. Error 3, on the other hand, will mask some potentially dangerous contingencies. To reduce this second risk, a contingency is declared potentially harmful not only if the load flow diverges but also if some voltages drop by more than some amount [7].

To reduce the above errors, it is essential that the load flow data match closely the model used in QSS simulation. More particularly:

- generator reactive power limits must be updated with the active power output and terminal voltage;
- any active power imbalance (caused by a generator tripping or a loss of connexity) must not be left to the slack-bus but distributed over the generators according to frequency control.

To speed up the post-contingency load flows we use the following short-cuts:

[7] it is more reliable to check voltage drops than post-contingency voltages themselves since in some cases low voltages may exist even in pre-contingency situation, which will lead to many false alarms.

- divergence is early detected by monitoring the square root of the sum of squared mismatches $\varphi(\mathbf{y}) = \sqrt{\sum_i g_i^2(\mathbf{y})}$, where $g_i(\mathbf{y}) = 0$ denotes the i-th load flow equation and $\mathbf{y}$ is the vector of bus voltage magnitudes and phase angles. If $\varphi(\mathbf{y})$ increases from an iteration to the next, divergence is declared and the computation stops. If the load flow equations have no solution, the Newton-Raphson algorithm diverges, which is quickly observed through an increase of φ. On the other hand, if an increase of φ is only due to a temporary convergence difficulty, the contingency is misclassified as potentially harmful. However, this situation is rarely observed in practice; most of the time, the value of this function decreases from one iteration to the next. This rule is illustrated in Fig. 3.8 where the computation is stopped at points C and D, and divergence is declared. This test is skipped at the iteration which follows the enforcement of generator reactive limits, since $\varphi(\mathbf{y})$ increases owing to the added generator reactive power equations, not necessarily because of divergence. The latter situation corresponds to point B in the same figure;

- tolerances on mismatches are somewhat relaxed and the maximum number of iterations somewhat decreased. Additionally, as soon as $\varphi(\mathbf{y})$ falls below a threshold φ_{min}, a situation which corresponds to point E in Fig. 3.8, the computation is stopped;

- controls which moderately improve voltage stability margins may be ignored. A typical example is secondary voltage control [8] [PLT87, VPL96]. Thus the supplementary iterations for adjusting generator terminal voltages are skipped. Moreover, being a conservative choice, it goes hand in hand with security.

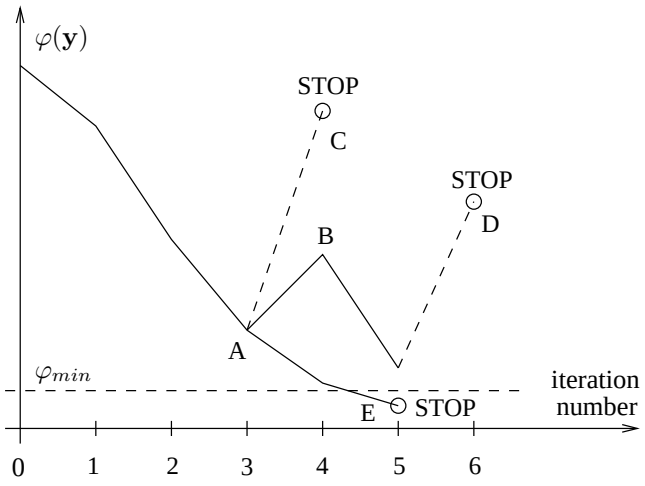

Figure 3.8: Iterations stop

Note finally that this approach is also suitable for filtering contingencies which do not cause thermal overload at S_{max}.

[8] this approximation is used in the filtering load flow, not in the subsequent QSS simulations

3.7 Practical examples

3.7.1 Examples from the RTE system

By way of illustration, we first give an example of SOL computation on the RTE system. A description of this system is provided in Appendix A.2.

The stress considered is a national load increase ($S_{max} = 7000$ MW), compensated by French generators.

We consider a set of 105 contingencies involving mainly two regions (West and South-East) where voltage stability is known to be a concern, and including: single and double line outages, single and double generator outages, busbar faults with two to four lines lost.

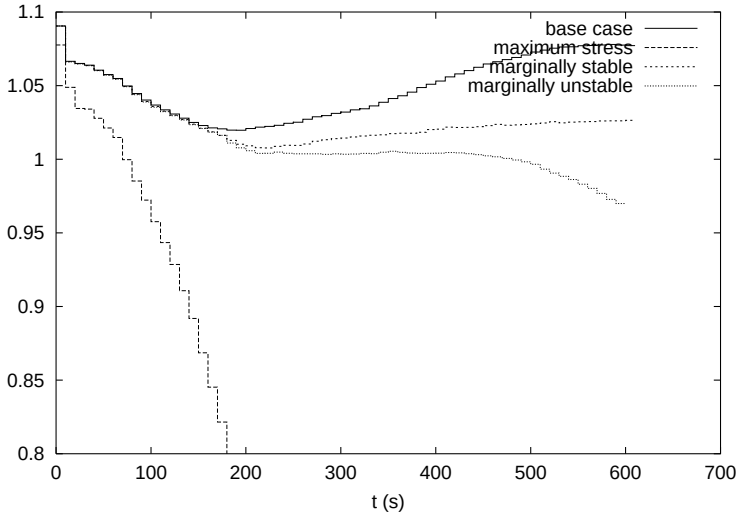

Figure 3.9: QSS evolutions of a pilot bus voltage (in pu)

Figure 3.9 shows the QSS time evolution of the voltage at a pilot bus of the Western region after a severe busbar fault, at four levels of pre-contingency stress S: 0, 0.08 S_{max}, 0.10 S_{max} and S_{max}. The time step of QSS simulation is 10 s. The contingency is applied at t=10 s. The pre-contingency voltage is the same in the first three cases due to secondary voltage control, while at maximum stress the reactive reserves were already exhausted in the pre-contingency situation making it impossible to maintain the pilot bus voltage. In the base case, the voltage recovers to almost its pre-disturbance value. This holds true in the marginally stable case as well but for a longer time simulation (about 900 s). The "mild" evolution of voltages in this system is due to the rather smooth nature of post-contingency controls.

Table 3.1 describes the various steps of the SBS applied to the 19 contingencies found unstable by the QSS simulation at maximum stress. The overall SOL is the limit of contingency Nb. 16, and is in the interval [0.1250 ; 0.1406] S_{max} = [875 ; 984] MW.

The computing time on a 500-MHz 128-Mb Pentium III PC (running Windows NT 4.0) is

Table 3.1: RTE system: successive steps of the SBS

successive stress levels	unstable contingencies	stable contingencies
1.000	92,94,58,45,39,44,54,103,105,21, 100,35,89,60,102,56,99,24,16	86 others
0.5000	56,99,24,16	39,92,94,58,45,44,54,21, 103,105,100,35,89,60,102
0.2500	56,99,24,16	
0.1250		56,99,24,16
0.1875	56,99,16	24
0.1562	16	56,99
0.1406	16	

of 2 min 30 s for the SBS [9]. In order to refine the SOLs of the remaining 18 harmful contingencies, one can process them through individual BS. The corresponding computing time is around 2 minutes. The method is thus fully compatible with real-time requirements.

In this system, contingencies can be pre-filtered very efficiently by a post-contingency load flow, as confirmed by the following results.

A post-contingency load flow is run for each contingency, at maximum stress, and only those contingencies declared potentially harmful will be processed in the BS. The shortcuts listed at the end of Section 3.6.2 have been used as well. Secondary voltage control is taken into account when computing the pre-contingency operating points and obviously in the QSS simulations, but not in the filtering post-contingency load flows.

Table 3.2 lists both the false alarms and the masked contingencies obtained with four filtering criteria, namely:

A : load flow divergence

B : load flow divergence or some voltage drops $\Delta V \geq 0.20$ pu

C : load flow divergence or some voltage drops $\Delta V \geq 0.15$ pu

D : load flow divergence or some voltage drops $\Delta V \geq 0.10$ pu

When criterion A is used, 4 contingencies (out of the 19 harmful ones) are not detected. Note that the SOL of the severest among them is rather high (about 5633 MW). Let us also underline that in all cases the early stop technique of Fig. 3.8 has correctly anticipated the divergence of the full load flow. By adding a voltage drop criterion, as with criterion B, one more harmful contingency is identified. Decreasing the threshold ΔV (C and D criteria) makes false alarms appear but expectedly more harmful contingencies are identified as well.

[9] on recent computers equipped with 2.5-GHz processors, this computing time can be merely divided by 5.

Criterion C leads to a good compromise between the two types of errors; the single masked contingency is the same as with criteria B and A. Let us repeat that all false alarms introduced by the load flow filtering technique are discarded by the first QSS simulation at maximum stress. It is thus more convenient to accept some more false alarms in order to detect almost all harmful contingencies. Note also that the filtering procedure correctly points out the most critical contingencies.

Table 3.2: Classification errors with post-contingency load flows performed at 7000 MW of stress

criterion	potentially harmful contingencies	undetected harmful contingencies	false alarms
A	15	4	0
B	16	3	0
C	21	1	3
D	32	0	13

By choosing the maximum stress a bit larger, for instance $S_{max} = 7500$ MW, while still seeking to identify contingencies with margins below 7000 MW, the filtering is improved, as shown by the results of Table 3.3.

Table 3.3: Classification errors with post-contingency load flows performed at 7500 MW of stress

criterion	potentially harmful contingencies	undetected harmful contingencies	false alarms
A	19	1	1
B	20	0	1
C	24	0	5
D	36	0	17

The computing time for the pre-filtering load flow on a 500-MHz PC is of 19 s.

Extensive tests of this contingency filtering approach on the RTE system, for a different operating point than that used in the above examples, have been also reported in [EDF00]. In this study a set of 1555 contingencies belonging to 8 areas has been considered. Instead of considering a national stress, as in the above examples, each area has been stressed separately.

Table 3.4 synthesizes the filtering results for each area and different values of the threshold ΔV. These results clearly illustrate the compromise between false alarms and undetected harmful contingencies. In this case, a threshold $\Delta V = 0.07$ pu proves to be a very good choice.

The following are some guidelines for the choice of ΔV. In principle, ΔV should be adapted to S_{max} and the contingencies. As regards the dependence on S_{max}, generally the higher the maximum stress, the larger the voltage drops between pre- and post-contingency system states. As regards the contingencies, ΔV should be adjusted when the basic set of contingencies change significantly, e.g. when adding some $N-2$ contingencies. On the other hand, the choice of ΔV is generally quite robust with respect to variations of the operating point. An off-line simulation of contingencies at maximum stress usually suffices to obtain a good threshold ΔV.

Table 3.4: Contingency filtering: overall results for different ΔV values

Area No	total number of contingencies	$\Delta V(\%)$	undetected harmful contingencies	false alarms	filtered contingencies
1	290	5	0	56	234
		7	0	36	254
		10	1	16	274
		20	2	8	282
2	239	5	1	20	219
		7	1	15	224
		10	1	9	230
		20	1	5	233
3	225	5	0	25	199
		7	0	19	206
		10	0	10	215
		20	0	7	218
4	167	5	0	15	152
		7	1	10	157
		10	2	7	160
		20	6	3	164
5	284	5	0	37	247
		7	3	21	263
		10	5	13	271
		20	11	10	274
7	148	5	0	11	137
		7	0	10	138
		10	0	9	139
		20	0	6	142
8	123	5	0	23	100
		7	1	18	105
		10	3	2	121
		20	3	0	123

The computing time on a 500-MHz PC is around 2 hours and 10 minutes for the exhaustive computation by BS of the security limits of all 1555 contingencies. When using the pre-filtering load flow the same operations are performed in 40 minutes which highlights the importance of the filtering.

The above results confirm that, in systems with rather smooth post-contingency controls, contingencies can be very efficiently and reliably filtered using a post-contingency load flow. Incidentally, very good results were also obtained on the Nordic 32 test system [Cap00].

3.7.2 Example from the Hydro-Québec system

We proceed with an example of SOL computation on the Hydro-Québec (HQ) system whose description is provided in Appendix A.3. As indicated in this appendix, the system is equipped with automatic shunt reactor tripping devices, named MAIS [10] which significantly contribute to stabilizing the post-contingency evolution of transmission system voltages.

The stress considered corresponds to a load increase in the Montréal area ($S_{max} = 3000$ MW above the base case, the system load being around 33000 MW) with 55 $\%$ (resp. 45 $\%$) of the power provided by the James Bay (resp. Churchill Falls and Manic-Outardes) generators.

For test purposes, a set of 90 various contingencies has been considered, including: 31 single line outages at the 735-kV level, the same with 330-Mvar shunt reactor tripping, 8 line outages each with the loss of an SVC, the same with 330-Mvar shunt reactor tripping, 6 double line outages, the same with 330-Mvar shunt reactor tripping.

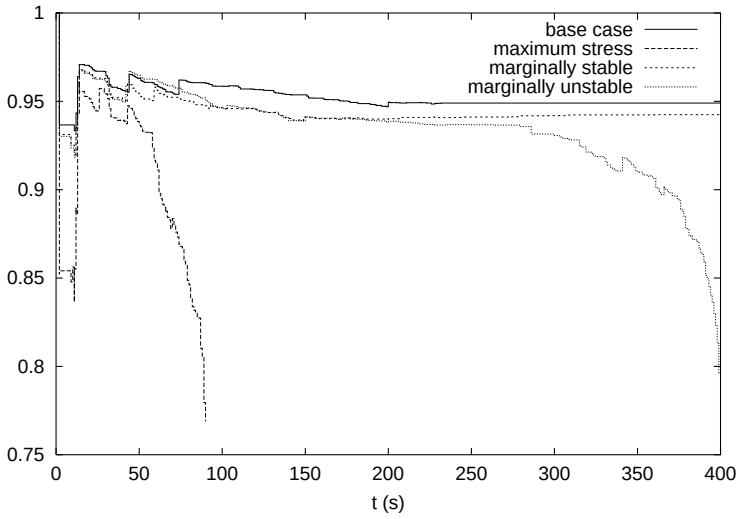

Figure 3.10: QSS evolution of a 735-kV bus voltage (in pu)

Figure 3.10 shows the QSS time evolution of the voltage near Québec City after the most severe contingency (applied at t=1s), at four levels of pre-contingency stress S: 0, 0.17 S_{max}, 0.19 S_{max} and S_{max}. The time step of the QSS simulation is 1 s. This figure confirms that voltage dynamics are strongly influenced by the MAIS (responsible for the many jumps). The number and the timing of reactor trippings strongly influences voltage stability.

Table 3.5 describes the various steps of the SBS. The overall SOL is the limit of contingency Nb. 6, and is in the interval [0.1719 ; 0.1875] S_{max} = [516 ; 563] MW.

Note that on the Hydro-Québec system it was found impossible to filter contingencies

[10] french acronym for "Manoeuvre Automatique d'Inductances Shunt"

Table 3.5: Hydro-Québec system: successive steps of the SBS

successive stress levels	unstable contingencies	stable contingencies
1.000	6,9,16,19,38,39,40,51,67,83,85	79 others
0.500	6,51	9,16,19,38,39,40,67,83,85
0.2500	6	51
0.1250		6
0.1875	6	
0.1562		6
0.1719		6

with a post contingency load flow. Such a static tool does not allow to guess how many and when reactor switchings take place. In this system, one has to rely on QSS simulation to filter out contingencies at the maximum stress.

In order to assess the efficiency of QSS simulation, the above set of 90 contingencies has been analyzed in 10 system configurations differing by the lines out of service and/or the number of MAIS devices in operation. The average computing time on a 500-MHz PC ranges between 1 min 20 s and 4 minutes.

Note that the QSS computational efficiency can be considerably improved, without affecting quality, by adding a self-stopping criterion within the QSS simulation [CCM00, Cap00]. The aim of the self-stopping strategy is to anticipate as soon as possible whether a post-contingency scenario is stable or not. Further details can be found in [CCM00, Cap00].

On the average, with respect to the computation of all individual SOLs, SBS allows to save 50 % of the computing time while SBS together with the self-stopping criterion allows to a 75 % saving.

Let us finally mention that, in very large systems, it may be advantageous to distribute contingencies on several computers in order to improve the filtering speed, at low software development costs.

3.8 On the evaluation of reactive power reserves

3.8.1 Motivation

Following a disturbance, most generators, synchronous condensers and static var compensators of a power system react to maintain their voltages at (almost) constant values, by producing more reactive power. This is possible as long as no physical limit prevents this additional reactive power from being produced. When such limits are encountered, transmission voltages fall down more or less progressively, until instability occurs either in the form of a loss of synchronism (insufficient voltage support to transfer active power

over long distances) or a voltage instability at the load ends (inability of the transmission and generation system to meet the load demand).

Reactive reserves are thus necessary for both angle and voltage stability. Although we focus on the second aspect, let us mention that the proposed method can be used in a more general context.

It is rather easy to compute or measure the individual reactive reserve available on the above components. However, it is well-known that reactive power cannot be transmitted over long distances. For instance, remote generators cannot provide a significant voltage support. Even if a generator has a large reserve with respect to its physical limit, its effective ability to help remote incidents may be limited. In other words, in large systems, reactive reserves cannot be obtained by merely summing up individual reserves.

Although the above facts are well known, there is no clear method to evaluate reactive power reserves with respect to a contingency.

Reference [AF92] proposed to monitor reactive margins on voltage zones in order to assess the voltage profile quality. A voltage zone is defined as a group of "tightly coupled" generator buses, together with the union of the sets of load buses that they mutually support. The voltage zone margin is the difference between: (i) the zone reserve, obtained by adding the individual reserves of generators within the zone, and (ii) the additional reactive generation needed to maintain acceptable voltage levels after any given contingency. The partition of the system into zones relies on load flow sensitivity information.

References [Sch98, SHC91] rely on the notion of voltage control area, defined as the set of load and generator buses whose voltages respond "coherently" to outside changes in reactive load and generation. The "reactive reserve basin" of the area is then defined as the sum of the reactive reserves exhausted at the minimum of the VQ curve [Tay94, VCV98] relative to any bus of the area. The percentage of basin reactive reserve remaining after a disturbance is used as a measure of proximity to voltage instability.

As long as the above voltage (control) areas are identified from sensitivity analysis of a pre-contingency configuration, their validity may be questioned when seeking reserves with respect to instability (not just voltage profile quality) and severe contingencies.

Two methods for determining the "effective" reactive reserve of a specific voltage area are outlined in [TR98]. The first method relies on VQ curves determined at one bus or for one area. The reserve is taken as the sum of individual reserves of the generators under limit at the minimum of the curve. It is thus an image, on the generation side, of a particular load power margin. The second method computes an effective power reserve as the weighted sum of individual reserves; the weights are based on sensitivities of generator reactive outputs to reactive loads.

The evaluation of reactive power reserves has gained attention within the context of unbundling of generation and transmission. Provision of reactive power reserve is an ancillary service that has to be valuated and paid accordingly. The value of this service must be assessed with respect to the capability of helping the system to face incidents.

To valuate individual reactive reserves, reference [XZdS00] proposes an "equivalent reactive compensation" method. The latter consists of adding fictitious synchronous condensers at all or selected load buses, and switching all reactive sources under constant power. The synchronous condenser outputs are monitored while the production of each source is varied from base case to maximum capability. This provides a basis for comparing the relative efficiencies of the various sources. Note, however, that transferring voltage control from the generation to the load side results in a fundamental change of system behaviour: problems of load flow divergence, overvoltage and unusual sensitivities can be experienced. The proper location of the synchronous condensers is a key step in this method, to avoid abnormal operating conditions and obtain meaningful results.

In this work we propose to evaluate reactive reserves as a by-product of the secure operation margin computation.

3.8.2 Towards a definition of reactive reserves

3.8.3 Effective capability of generators

Consider the simple 3-bus system of Fig. 3.11. In this system, the load at bus L is fed by generator 1, electrically close to bus L, and generator 2, located farther away (the lines in Fig. 3.11 represent both step-up transformers and transmission lines).

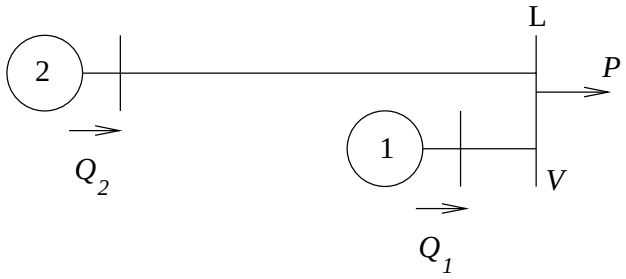

Figure 3.11: Simple 3-bus system

We denote the generator reactive power capabilities by Q_1^{lim} and Q_2^{lim}, respectively. As is well-known, these limits are mainly dictated by the thermal overload capability of the field or armature winding, as depicted by the machine capability curves [Tay94, Kun94, VCV98].

Figure 3.12.a shows the PV curve relating the load voltage V to the load active power P. The load is assumed to increase under constant power factor and the two generators respond to the active demand increase according to some participation factors. The breakpoint B corresponds to the loss of voltage control by generator 1, under the action of an overexcitation (or, possibly, a stator current) limiter. P^{max} is the maximum power that can be delivered to the load by the combined generation/transmission system.

The reactive power response of each generator is considered in Fig. 3.12.b. Under the effect of reactive power losses, both productions increase more than linearly. As long

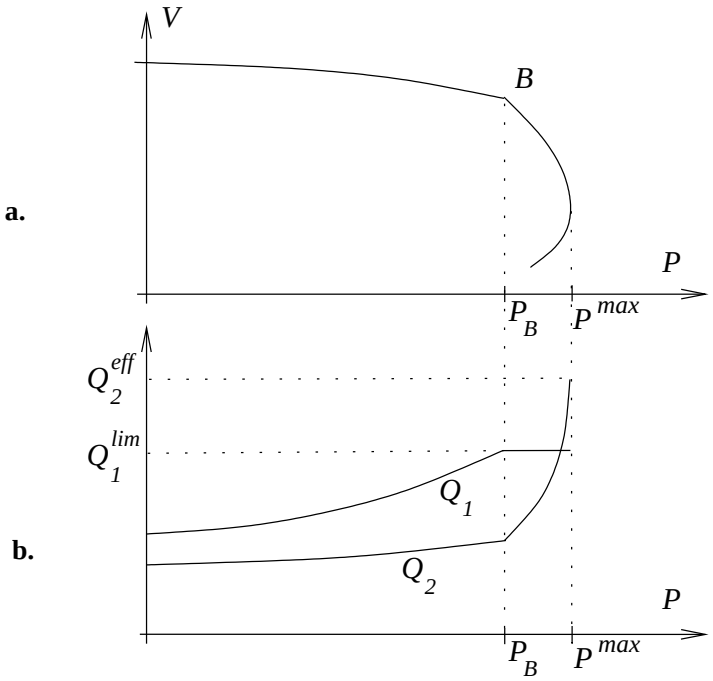

Figure 3.12: PV and PQ curves of the 3-bus system

as it controls its voltage, generator 1, located closer to the load, is more responsive, as indicated by the higher slope of the Q_1 vs. P curve. For simplicity, we assume that, once under limit, generator 1 has a constant reactive power output Q_1^{lim} [11]. When the system operates above $P = P_B$, the whole reactive power has to come from the farther generator 2. Hence, the slope of the Q_2 vs. P curve increases suddenly when passing through point B. At the loadability limit $P = P^{max}$, this curve has an infinite slope, a well-known characteristic of saddle-node bifurcations [VCV98].

Let Q_2^{eff} be the reactive production of generator 2 at the loadability limit. We call this value the *effective reactive limit* of generator 2, as opposed to the *physical limit* Q_2^{lim}. For generator 1, which produces Q_1^{lim} at the bifurcation point, both limits coincide. For generator 2, on the other hand, transmission system constraints prevent from taking advantage of $Q_2^{lim} - Q_2^{eff}$ Mvars, at least when load is increased at bus L.

The total reactive reserve with respect to the effective capabilities is given by:

$$R = (Q_1^{eff} - Q_1) + (Q_2^{eff} - Q_2)$$

Clearly, this reserve decreases as the load increases and vanishes at the loadability limit point, i.e.

$$R \to 0 \quad \text{when} \quad P \to P^{max} \tag{3.40}$$

What has been said applies to all reactive power sources. We will continue speaking of generators but the proposed definition and method apply to synchronous condensers and static var compensators as well.

[11] this simplifying assumption is not needed if the QSS simulation is used

3.8.4 Reactive reserve with respect to a contingency

Consider a power system with g generators in service. We denote by Q_i^o the reactive production of the i-th generator $(i = 1, \ldots, g)$ at the current operating point and by Q_i^{lim} its reactive capability (or physical limit).

Following a contingency, most controlled reactive power sources react by increasing their production in order to keep their controlled voltages (almost) constant. In other words, the contingency will "consume" some of the reactive power reserve available on generators. We know that the farther the generator, the lower its support. Hence, the question: *out of the total reserve* $\sum_i Q_i^{lim} - Q_i^o$*, how much is needed and on which generators, in order the system to respond to the contingency in an acceptable way ?*

Whether the system response to a contingency is acceptable must be defined with respect to appropriate criteria. At least, voltage stability is required, but in addition to being stable, the system might be requested to meet some operating constraints.

The approach followed here consists in stressing the system in its pre-contingency configuration, until reaching an unacceptable post-contingency response. A simple analysis of the last acceptable situation, or *marginally stable* case, will provide us with the sought information, as explained hereafter.

Let M be the security margin with respect to the contingency. We denote by:
• $Q^M_{pre,\,i}$ the reactive power production of the i-th generator in the pre-contingency configuration, after the system has been stressed at the critical level M
• $Q^M_{post,\,i}$ the reactive power production of the same generator in the post-contingency situation, for the same level of stress.

Since M is such that the system response is marginally acceptable after the contingency has occurred, we consider $Q^M_{post,\,i}$ as the effective capability of the i-th generator. Similarly to what was said in section 3.8.3 for a load increase :
• any additional Mvar available on this machine cannot be used to face the contingency in an acceptable way;
• in this particular post-contingency state, some generators may be at their limits while others may still have some reserve. For the latter the effective capability is smaller than the physical one, while for the former both limits coincide.

The system response to the contingency in the marginally stable case is given by:

$$R_M = \sum_{i=1}^{g} Q^M_{post,\,i} - Q^M_{pre,\,i} \tag{3.41}$$

Now, those generators not involved in (e.g. located far away from) the contingency are characterized by:

$$Q^M_{post,\,i} \simeq Q^M_{pre,\,i} \tag{3.42}$$

and hence, will not significantly contribute to the above sum. In practice, we identify the set of generators involved in the contingency as:

$$\mathcal{E} = \{i : Q^M_{post,\,i} - Q^M_{pre,\,i} > \epsilon\} \tag{3.43}$$

where ϵ is a tolerance. Thus, for a small enough ϵ, we have:

$$R_M \simeq \sum_{i \in \mathcal{E}} Q^M_{post,\,i} - Q^M_{pre,\,i} \tag{3.44}$$

This formulation conveys a bit more information in the sense that it focuses on generators playing a significant role.

The corresponding reserve at an operating point characterized by productions Q^o_i is given by:

$$R = \sum_{i \in \mathcal{E}} Q^M_{post,\,i} - Q^o_i \tag{3.45}$$

Note that generators not involved in the contingency may respond to the stress and hence be characterized by:

$$Q^M_{pre,\,i} > Q^o_i$$

or, taking (3.42) into account:

$$Q^M_{post,\,i} > Q^o_i$$

Hence, extending the sum in (3.45) over all generators would include in reserve R a significant contribution from generators that do not respond to the contingency. Therefore, it is essential to restrict the summation in (3.45) to the set $\mathcal{E}$ only. Unless otherwise specified, we will use the corresponding formula (3.44) for the system response to contingency in the marginally stable case, for the sake of symmetry.

Finally, note that there is a risk of not including a significant generator in the $\mathcal{E}$ set, if: (i) it approaches its (physical) limit by less than ϵ in the stressed pre-contingency situation, and (ii) hits its limit after the contingency. In this case, one could re-simulate the contingency, at the stress level M, with the limit removed. If the "freed" generator responds by more than ϵ to the contingency, it is included in $\mathcal{E}$.

3.8.5 A security index

It follows from the above derivation that:

$$R \to R_M \quad \text{when} \quad S \to M \tag{3.46}$$

which is an extension of (3.40) considering the contingency effect. In fact, (3.40) can be seen as a particular case of (3.46) for an infinitely mild disturbance that can be faced without consuming any reactive reserve, i.e. $R_M = 0$.

Clearly, the system is secure with respect to the contingency as long as:

$$R > R_M$$

or in dimensionless form:

$$I = \frac{R - R_M}{R_M} > 0 \tag{3.47}$$

The larger the index I, the higher the system robustness with respect to the contingency of concern.

The above indices depend to some extent on the stress chosen to push the system towards its limits. This aspect is further discussed in Section 3.8.7.

3.8.6 Computational procedure

The determination of R_M and R relies on $Q^M_{pre,\,i}$ and $Q^M_{post,\,i}$ which in turn require to determine the security margin M. This can be done using the binary search algorithms of Section 3.5.1. In this context, the reactive reserves are obtained at no cost as a by-product of the limit search. In some sense, the index I is an alternative way of presenting results, looking from the generator side. In addition, it brings complementary information on the generators responsible for unacceptable voltage profiles.

3.8.7 Numerical results from the RTE system

We present results relative to two $N-2$ contingencies, namely the tripping, in the Western part of the system, of two double-circuit 400-kV lines, referred to as A and B, respectively.

We first take as system stress a national load increase covered by French generators. Table 3.6 gives the corresponding values of margin M, number of generators in $\mathcal{E}$, response to the contingency (3.41) at the security limit, reserve (3.45), and security index (3.47). A threshold $\epsilon = 20$ Mvar has been chosen to identify the set $\mathcal{E}$. The loss of line A is a contingency with local effects, the system becoming voltage unstable in its very Western extremity. The margin is small and so is the index I. The loss of line B has a wider impact but the load must be increased by a much larger amount before this contingency becomes harmful. Expectedly, this system has only a small subset of generators involved in each contingency. The more local the contingency, the smaller this subset.

Table 3.6: RTE system : margins and reserve

contingency: loss of	M (MW)	nb of gen. in $\mathcal{E}$	R_M (Mvar)	R (Mvar)	$\frac{R - R_M}{R_M}$
line A	490	13	1350	1461	0.08
line B	4142	30	2897	5165	0.78

Figure 3.13 relates to generators in $\mathcal{E}$ only. It confirms that the loss of line A has a more local impact. For both contingencies, generators A1 and A2 are the closest to the tripped lines and are field current limited in the marginally accepted post-contingency situation. Generator B1 (resp. B2) has a large reactive capability but the effective reserve is only one half (resp. one third) of it.

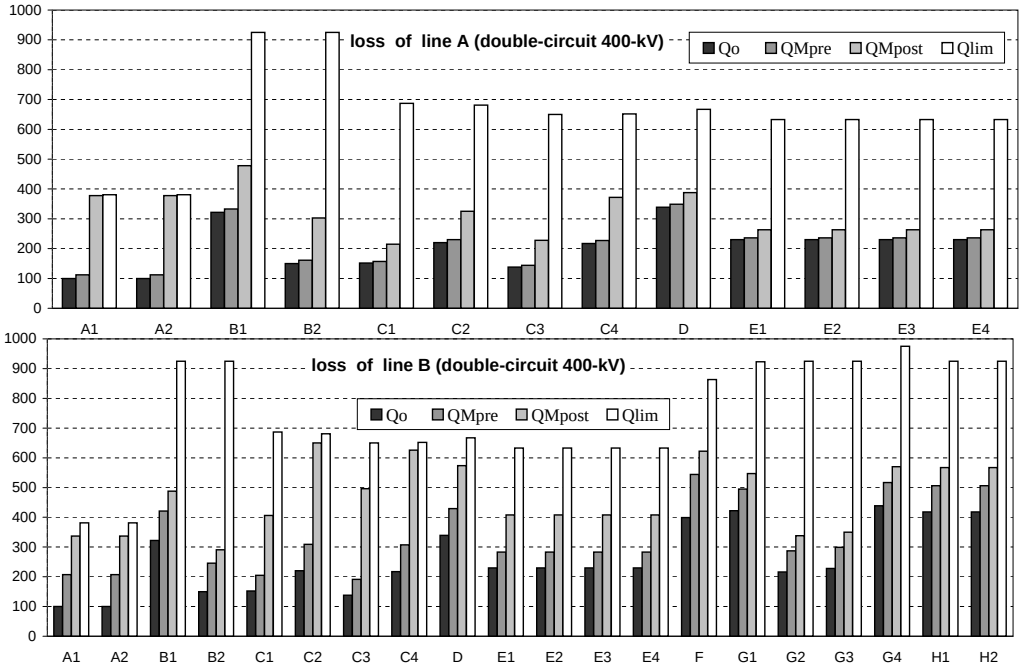

Figure 3.13: RTE system : values of Q_i^o, $Q_{pre,\,i}^M$, $Q_{post,\,i}^M$ and Q_i^{lim} of generators in $\mathcal{E}$

Figures 3.14 and 3.15 show how the value of R and R_M relative to a given (base case) operating point changes with the direction of stress used to compute them. To this purpose, loads have been increased homothetically in 12 "concentric" areas, all including the area most affected by the contingency. The abscissa in Figs. 3.14 and 3.15 is the base case load power consumed in the stressed area. Each figure shows M, R_M and R, respectively. The left (resp. right) plot of each of these figures corresponds to the loss of line A (resp. line B).

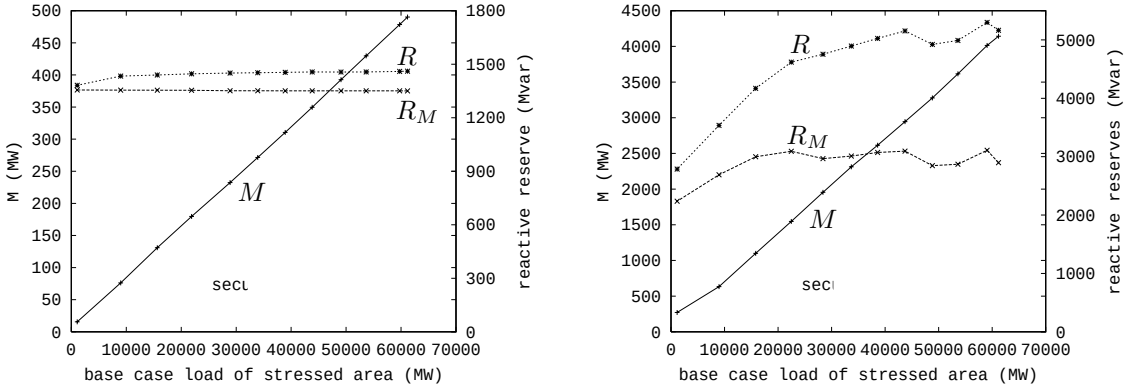

Figure 3.14: Influence of stressed area (left plot: loss of line A, right plot: loss of line B)

The plots of Fig. 3.14 have been obtained in the absence of secondary voltage control. When the latter is in operation, the curves of Fig. 3.14 become those of Fig. 3.15. This figure shows the expected improvement in the margin M relative to each contingency.

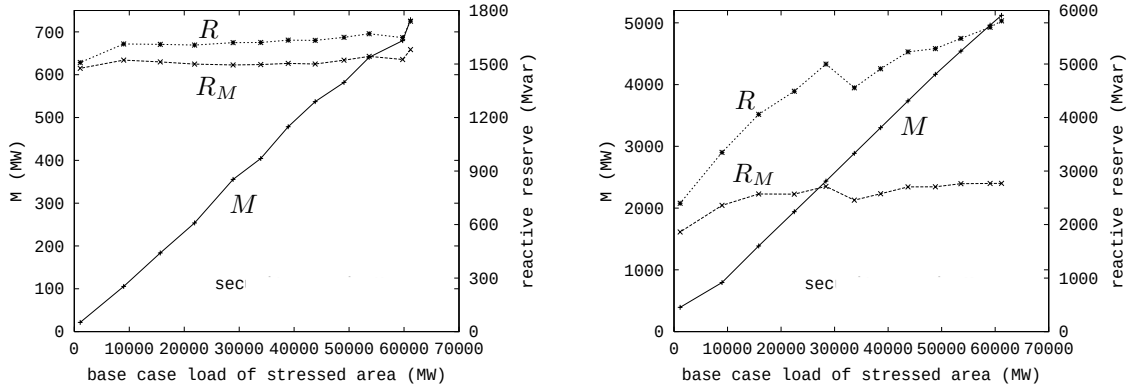

Figure 3.15: Same as Fig. 3.14 with secondary voltage control

The corresponding security index I is also larger.

As can be seen, the security margin M decreases (almost) linearly with the size of the stressed area. The response R_M, on the other hand, remains rather constant, provided that the stressed area does not approach too much the "heart of instability". The invariance of R_M for the most dangerous contingency (loss of line A) is noteworthy. The reserves R undergo more important changes, which seem to follow those of R_M.

Figures 3.16 and 3.17 show how the reserve evolves with the system stress. Let us emphasize that in these figures, a national load increase is assumed to compute R and R_M (this corresponds to the rightmost point in each plot of Fig. 3.14).

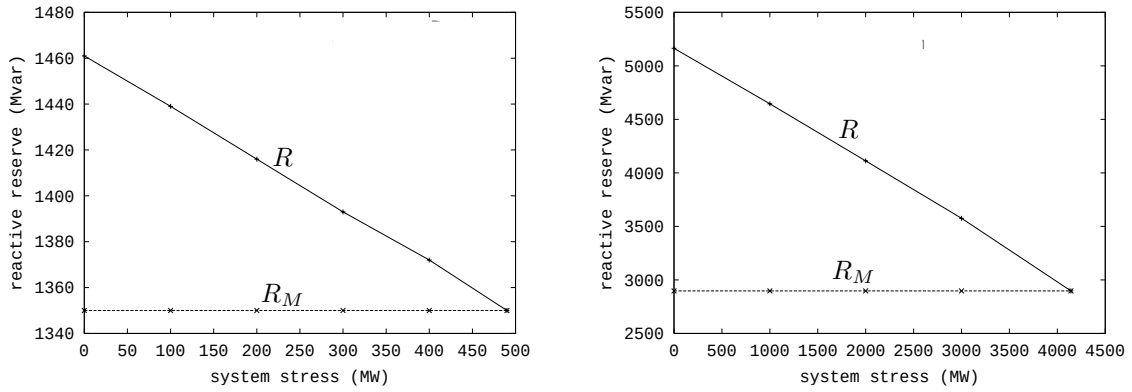

Figure 3.16: Evolution of reserve with stress (left plot: loss of line A, right plot: loss of line B), same stress used to compute reserve

In the plots of Fig. 3.16 the system is stressed along the direction assumed when computing the reserves. As the stress increases, the available reserve R decreases. Due to the way it is computed, the system response in the marginally stable case R_M remains unchanged. The R and R_M curves necessarily intersect at a stress level equal to the margin M given

in Table 3.6. The linear variations of R (and hence of I) are noteworthy.

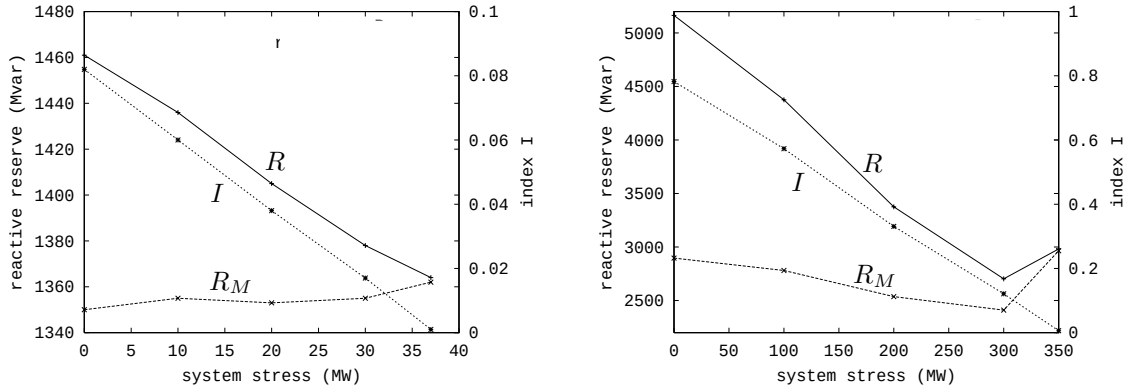

Figure 3.17: Evolution of reserves with stress when the system is locally stressed (left plot: loss of line A, right plot: loss of line B)

In the plots of Fig. 3.17, on the other hand, the system is stressed more locally, which yields much smaller margins (37 and 355 MW, respectively). Despite the fact that, at each operating point, R and R_M were computed assuming a national load increase, the R and R_M curves still intersect at a stress level equal to the margin M. The final increase observed in the right plot of Fig. 3.17 is due to some generators lately entering the set $\mathcal{E}$ as well as a slightly larger response $Q^M_{post,\,i} - Q^M_{pre,\,i}$ to the contingency. The method could still be improved to avoid such variations. Note, however, that the security index I decreases linearly towards zero as the stress approaches the margin M.

3.8.8 Summary and final remarks

The ideas developed in this section can be summarized as follows:

1. the reactive power produced by a generator at the post-contingency operating point corresponding to its security limit is taken as the effective capability of this generator, for the contingency of concern. For most generators of a (large enough) system, the effective capability is smaller than the physical one, due to the impossibility of transmitting reactive power over long distances;

2. at a given pre-disturbance operating point, the reactive reserve R available to face the contingency is a sum of differences between the effective capability and the current production. This sum extends over the set $\mathcal{E}$ of generators responding significantly to the contingency;

3. the response R_M needed to face a contingency is the total reactive power produced in response to the contingency, when the system has been previously stressed at its security limit;

4. the ratio $(R - R_M)/R_M$ is a convenient, dimensionless security index.

Although the proposed method can be used in any context where it makes sense to compute reactive power reserves, we focused here on voltage instability.

Further encouraging results obtained on the Nordic 32 as well as the RTE systems can be found in [CVC01].

There is some dependency of the so obtained reactive reserves on the direction of stress used to compute them. However, the results presented here tend to show that, up to some point, the R_M is rather insensitive to the above choice. Also, even if the system is being stressed along another direction than the one assumed to compute the reserves, the difference $R - R_M$ between the current reserve and the system response to the contingency at the security limit - and hence the I index - decreases towards zero as the system approaches an operating point where the contingency becomes harmful. A linear decrease has been observed in many cases.

Whereas the key role of reactive reserves is to support the voltage profile in response to contingencies and stress, and thereby contribute to system security, the concepts summarized under items 1 to 3 above constitute a basis for the valuation of reactive reserves. With respect to a single contingency, it sounds reasonable to reward a generator up to the amount corresponding to its effective capability (see item 1). To take the whole set of credible contingencies into account, one could either consider the maximum effective capability over all scenarios or a weighted sum cumulating the effects of the various contingencies.

A possible drawback of our approach concerns the criterion used to incorporate a generator into the set $\mathcal{E}$. The criterion used here appears somewhat rigid especially when a generator responds to a contingency a bit less than the threshold ϵ, and, consequently is not included in $\mathcal{E}$. It may be advantageous to use weights in the formula of R and R_M, for instance:

$$R_M = \sum_{i=1}^{g} w_i \, (Q^M_{post,\,i} - Q^M_{pre,\,i})$$

However a satisfactory definition of weights w_i remains to be found.

Chapter 4

Ranking of preventive controls for security enhancement

This chapter is devoted to the ranking of candidate control actions according to their efficiency in enhancing security. We first recall a useful general sensitivity formula. We then consider the (simpler) case of thermal security. We proceed with the case of voltage security where two appealing approaches are presented. We finally derive general security constraints with respect to thermal overload and voltage instability.

4.1 The two levels of security analysis

Before presenting the methods for ranking the controls, we briefly introduce the two security levels which will be considered throughout this thesis:

- *security restoration* requires that no one of the specified contingencies causes voltage instability or thermal overloads. This is basically a "point-wise" analysis performed on the system current operating conditions. The analysis consists in checking whether the present injection vector belongs to $\mathcal{S}_T$, or $\mathcal{S}_V$, or none of these two regions [1];

- *security margin restoration* additionally requires the system to have sufficient voltage and thermal security margins with respect to the postulated contingencies. The computation of voltage (resp. thermal) security margin requires to find the intersection point between the straight line that characterizes the assumed stress direction and the boundary $\mathcal{B}_V$ (resp. $\mathcal{B}_T$), as shown in Fig. 3.2. Thus, the present injection vector must not only belong to the security region of concern but the distance (measured in MW/Mvar) between this point and the security region boundary should be larger than some threshold.

[1] for instance, at point C_o of Fig. 3.1, the system is secure from the voltage stability and thermal overload viewpoints; at point B_o the system is voltage but not thermally secure

When, following a security analysis, the system is deemed as insecure one has to answer to the twofold question: *where* and of *how much* to act in order to restore security (margin) ?

In this chapter we focus on the first part of the question, while the second one will be treated in the next chapter. In this respect, we concentrate here on the ranking of candidate control actions (mainly changes in power injections) according to their efficiency.

4.2 Sensitivity of dependent variables with respect to power injections

In this section we recall the derivation of a general sensitivity formula [DT68, FOC90, WW96, VCV98] which will be used at several places in this work.

Let us consider a power system in steady state described by a set of algebraic equations, which we write in compact form as:

$$\boldsymbol{\varphi}(\mathbf{u}, \mathbf{P}) = \mathbf{0} \tag{4.1}$$

where $\boldsymbol{\varphi}$ is a vector of smooth functions, $\mathbf{u}$ is the vector of algebraic variables and $\mathbf{P}$ is the $2m$-dimensional vector of power injections. In the context of QSS simulation, these equations are the long-term equilibrium equations (3.11, 3.12, 3.13) and $\mathbf{u} = (\mathbf{x}, \mathbf{y}, \mathbf{z})$. In the reminder of this thesis we denote by $nbeq$ the total number of long-term equilibrium equations. If a simple load flow model is used, there are only $2m$ network equations and $\mathbf{u} = \mathbf{y}$, the vector of bus voltage magnitudes and phase angles.

Let η be a scalar quantity of interest which we consider, for simplicity, to depend only on $\mathbf{u}$ and not on $\mathbf{P}$ [2]. η can be for instance the reactive power output of a generator, a bus voltage magnitude, a branch current, etc.

If some changes in power injections $\mathbf{P}$ take place, the system will generally operate at another value of $\mathbf{u}$ still satisfying (4.1). As a result, η will also change. For small changes in $\mathbf{P}$ we are interested in determining the sensitivity of η to each P_i:

$$\frac{\partial \eta}{\partial P_i} = \lim_{\Delta P_i \to 0} \frac{\Delta \eta}{\Delta P_i} \tag{4.2}$$

Differentiating $\eta(\mathbf{u})$ according to the chain rule yields:

$$d\eta = \mathbf{du}^T \frac{\partial \eta}{\partial \mathbf{u}} \tag{4.3}$$

On the other hand, differentiating (4.1) gives:

$$\boldsymbol{\varphi}_\mathbf{u}\, \mathbf{du} + \boldsymbol{\varphi}_\mathbf{P}\, \mathbf{dP} = \mathbf{0} \tag{4.4}$$

[2] the case where η depends explicitly on $\mathbf{P}$ can be straightforwardly taken into account

where $\boldsymbol{\varphi}_{\mathbf{u}}$ is the Jacobian of the long-term equilibrium equations (4.1). It is a $nbeq \times nbeq$ matrix containing the partial derivatives of each long-term equilibrium equation with respect to each component of $\mathbf{u}$. Assuming that $\boldsymbol{\varphi}_{\mathbf{u}}$ is nonsingular one obtains:

$$\mathbf{du} = -\boldsymbol{\varphi}_{\mathbf{u}}^{-1}\, \boldsymbol{\varphi}_{\mathbf{P}}\, \mathbf{dP} \tag{4.5}$$

Introducing (4.5) into (4.3) yields:

$$d\eta = -\mathbf{dP}^T \boldsymbol{\varphi}_{\mathbf{P}}^T ({\boldsymbol{\varphi}_{\mathbf{u}}}^T)^{-1} \frac{\partial \eta}{\partial \mathbf{u}} \tag{4.6}$$

and hence the sought sensitivity vector is given by:

$$\frac{\partial \eta}{\partial \mathbf{P}} = -\boldsymbol{\varphi}_{\mathbf{P}}^T ({\boldsymbol{\varphi}_{\mathbf{u}}}^T)^{-1} \frac{\partial \eta}{\partial \mathbf{u}} \tag{4.7}$$

In the above formula:

- $\boldsymbol{\varphi}_{\mathbf{P}}$ is a very sparse $nbeq \times 2m$ matrix. The only $2m$ nonzero elements correspond to the derivative of the i-th (active and reactive) power mismatch equation with respect to the i-th power injection[3];
- $\dfrac{\partial \eta}{\partial \mathbf{u}}$ is a $2m$-dimensional vector. It is also sparse in as much as the η function involves few $\mathbf{u}$ variables.

Note that, following the same reasoning, one can derive the sensitivity of a vector of quantities $\boldsymbol{\rho}$ with respect to a given power injection P. The formula is:

$$\frac{\partial \boldsymbol{\rho}}{\partial P} = -\boldsymbol{\rho}_{\mathbf{u}} {\boldsymbol{\varphi}_{\mathbf{u}}}^{-1} \frac{\partial \boldsymbol{\varphi}}{\partial P} \tag{4.8}$$

where:

- $\dfrac{\partial \boldsymbol{\varphi}}{\partial P}$ is a $nbeq$-dimensional vector of zeros except for the component which corresponds to the sole mismatch equation involving P;
- $\boldsymbol{\rho}_{\mathbf{u}}$ is an $a \times nbeq$ matrix, where a is the dimension of the vector $\boldsymbol{\rho}$. This matrix is also very sparse in as much as $\boldsymbol{\rho}$ involves few $\mathbf{u}$ variables.

The implementation of the above sensitivity formulas is rather straightforward. Indeed, the Jacobian matrix $\boldsymbol{\varphi}_{\mathbf{u}}$ needs to be computed and factorized only once. Then, each vector of sensitivities is obtained by solving a linear system having the appropriate sparse vector as independent term. Note also that the sensitivities need to be computed only for a restricted number of injections P_i.

[3] in QSS simulation there is one active and one reactive power mismatch equation at each bus of the system.

4.3 Thermal security restoration

When dealing with a thermal overload one has to identify the best controls to decrease the magnitude of some branch currents. To this purpose it is appropriate to rely on sensitivities of currents to injection.

In principle we need to compute the sensitivities of post-contingency currents with respect to *pre*-contingency power injections. To solve this problem exactly, two analytical solutions have been proposed, based on the Inverse Matrix Modification Lemma [SAM87] or the compensation method [AST83], respectively. In this work, we approximate the derivatives of post-contingency currents to *pre*-contingency injections by the derivatives of post-contingency currents to *post*-contingency injections. The latter can be obtained as a direct application of the sensitivity formulae (4.7) or (4.8).

4.3.1 Derivation of branch current sensitivities with respect to power injections

Let us assume that the j-th branch (which can be a line or a transformer) links buses i and k. A general equivalent scheme of a branch is given in Fig. 4.1, where the shunt elements have been neglected for simplicity. This scheme contains the branch resistance R_j and reactance X_j and an ideal transformer of ratio r. When it is used to represent a transformer, r is the transformer ratio and the primary and secondary currents are given by:

$$I_2 = rI_1 = rY_j\sqrt{V_i^2 + (rV_k)^2 - 2rV_iV_k\cos(\theta_i - \theta_k)} \tag{4.9}$$

where $Y_j = 1/\sqrt{R_j^2 + X_j^2}$ and V_i (resp. θ_i) is the magnitude (resp. the phase angle) of the voltage at bus i, and similarly for bus k. When this scheme is used to represent a line, $r = 1$ and $I_1 = I_2 = I_j$. For a transformer we monitor only the side which is more loaded i.e. $I_j = \max(I_1/I_1^{max}, I_2/I_2^{max})$ where I_1^{max} (resp. I_2^{max}) is the maximal allowed current on the primary (resp. secondary) transformer side.

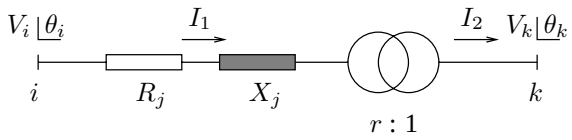

Figure 4.1: A simplified scheme of a line or transformer

The sensitivity of the current in the j-th branch to a change ΔP_i in the i-th power injection is given by:

$$\frac{\partial I_j}{\partial P_i} = \lim_{\Delta P_i \to 0} \frac{\Delta I_j}{\Delta P_i} \qquad j = 1, \ldots, b \qquad i = 1, \ldots, 2m \tag{4.10}$$

and indicates how much the current in the j-th branch varies when either:

- 1 pu of active power is injected at the i-th bus, this excess power being compensated by the generators. In QSS simulation, we mainly focus on primary frequency control and hence generators participate according to their speed droops (provided they are not limited). In a classical load flow calculation, this excess active power is absorbed by the slack-bus only;

- 1 pu of reactive power is injected at the i-th bus, this additional power being compensated by the generators controlling their terminal voltages. In practice, only generators close to the i-th bus will react.

The first approach to come to mind for computing the above sensitivities is that of *finite differences*. In this "brute-force" approach, ΔP_i MW (or Mvar) are successively injected at each bus of the system and the corresponding variation ΔI_j ($j = 1, \ldots, b$) of each branch current is computed. This requires to compute the new branch currents $2m$ times and the procedure must be repeated for each post-contingency configuration. Although very simple, this technique remains too computationally demanding, especially for on-line applications.

For this reason it is more efficient to rely on the sensitivity formulae detailed in Section 4.2.

In equation (4.7), $\dfrac{\partial \eta}{\partial \mathbf{u}}$ contains only four nonzero elements, namely the partial derivatives of I_j with respect to V_i, V_k, θ_i and θ_k. These derivatives are easily obtained from (4.9).

In equation (4.8), the j-th line of the $\boldsymbol{\rho}_{\mathbf{u}}$ matrix contains only four nonzero elements, namely the partial derivatives of I_j with respect to V_i, V_k, θ_i and θ_k.

Let us finally mention that in order to further increase efficiency we use formula (4.7) when the number of controls is greater than the number of branches overloaded or likely to be overloaded, and formula (4.8) otherwise.

4.4 Thermal security margin restoration

We now seek to rank controls aimed at increasing an insufficient thermal security margin. To this purpose we rely on the sensitivities of this margin to power injections, i.e. $\dfrac{\partial M^T}{\partial P_i}$. The latter can also be computed analytically.

We have explained in Section 3.5.3 that, for a given stress direction, a single branch generally determines the value of the thermal margin. Let us denote by k this branch. For small enough injection variations the same branch will remain the most constraining for the new thermal margin. Considering that the margin M^T is a function of the current I_k, which in turn is a function of the injections $\mathbf{P}$ one can write:

$$\frac{\partial M^T}{\partial P_i} = \frac{\partial M^T}{\partial I_k}\frac{\partial I_k}{\partial P_i} \tag{4.11}$$

The sensitivities of branch current to power injections can be determined using formula (4.7), as explained in the previous section. The sensitivity of the thermal margin to the k-th branch current results from (3.36) as:

$$\frac{\partial M^T}{\partial I_k} = \frac{\partial M^T}{\partial I_k^o} = -\frac{1}{\dfrac{\partial I_k}{\partial S}} \tag{4.12}$$

Alternatively the above sensitivity may be computed from the optimization problem (3.37) in Section 3.5.3. Indeed, at the optimum solution of this problem, the Lagrange multiplier associated to each branch current constraint is nothing but the sensitivity of the thermal margin with respect to the branch current, i.e.

$$\mu_j = \frac{\partial M^T}{\partial I_j} \quad j = 1, \ldots, b \tag{4.13}$$

Whereas only the k-th branch current is active at the optimum $\mu_k \neq 0$ while for the other branches $\mu_j = 0, \ \ \forall j \neq k$.

Now, depending on the magnitude of the variation ΔP_i it may happen that the most constraining branch changes. In this case, we have to identify the new constraining branch by computing the new operating point and use the latter in (3.36). Formula (4.11) still applies to the new constraining branch.

4.5 Controls ranking for voltage security restoration: first approach

In this section we answer the question: if a contingency triggers voltage instability, *where* should one act, before the contingency occurrence, in order the system to have a post-contingency stable response ? Compared to thermal overload, this problem is more complex in the sense that in a voltage unstable scenario the system has no post-contingency equilibrium. Nevertheless, we can extract information from the unstable post-contingency evolution and use it for ranking controls in the pre-contingency state.

The material of this section is largely borrowed from [VCJ95, VCV98, MVC99].

4.5.1 Information provided by the normal vector

Let us consider that, before the contingency, the system operates at the point $\mathbf{P}^o = \mathbf{P}(0^-)$ inside the pre-contingency feasible region $\mathcal{F}_o$ but outside the voltage security region $\mathcal{S}_V$ (see the left plot of Fig. 4.2). Under the effect of the contingency the operating point $\mathbf{P}(0^-)$ jumps to $\mathbf{P}(0^+)$ (see the right plot of Fig. 4.2) mainly due to the load sensitivity to voltage. Then, for reasons explained in Section 3.3 (mainly load restoration and frequency control) the system will evolve along the trajectory $\mathbf{P}(t)$ *tending* to attain a point $\mathbf{P}^d$

located outside region $\mathcal{A}$, as sketched in the right plot of Fig. 4.2. During this evolution the system trajectory "touches" the boundary $\mathcal{B}_V^{post}$ at the so-called *critical point* $\mathbf{P}^c$. At this point one real eigenvalue of the matrix $\mathbf{A}$, given by (3.27), goes from negative to positive. The same holds for the unreduced Jacobian $\mathbf{J}$, given by (3.25). The left eigenvector associated to the zero eigenvalue of $\mathbf{A}$ is closely related to the normal vector $\mathbf{n}$ to the boundary $\mathcal{B}_V^{post}$. From both $\mathbf{P}^c$ and $\mathbf{n}$, a linear approximation of the boundary surface $\mathcal{B}_V^{post}$ can be built, in the form of the tangent hyperplane $\mathcal{H}$ (see Fig. 4.2) whose equation is:

$$\mathbf{n}^T(\mathbf{P} - \mathbf{P}^c) = 0 \tag{4.14}$$

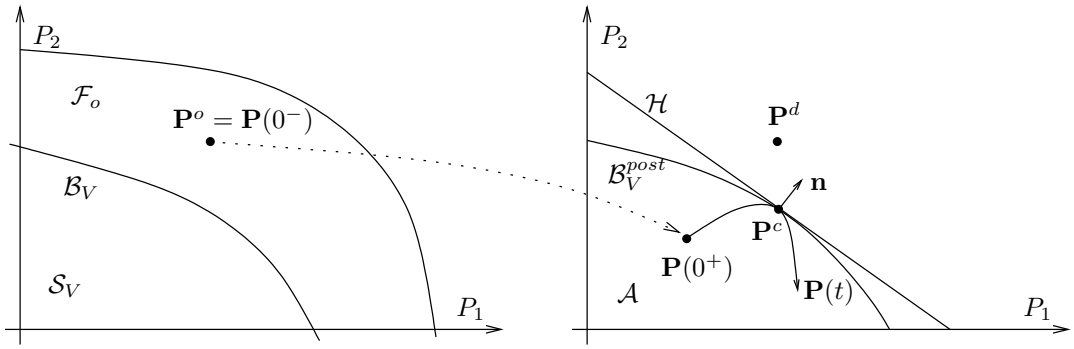

Figure 4.2: Portrait of a voltage unstable post-contingency scenario

Let $\Delta\mathbf{P}$ be a vector of injection variations. In order $\mathbf{P}^d + \Delta\mathbf{P}$ to be brought back on the stable side of $\mathcal{H}$, $\Delta\mathbf{P}$ must satisfy:

$$\begin{aligned} & \mathbf{n}^T(\mathbf{P}^d + \Delta\mathbf{P} - \mathbf{P}^c) \leq 0 \\ \Leftrightarrow \quad & -\mathbf{n}^T\Delta\mathbf{P} \geq \mathbf{n}^T(\mathbf{P}^d - \mathbf{P}^c) \end{aligned} \tag{4.15}$$

Assuming that only the i-th injection is changed, the amount required to come back on the stable side of $\mathcal{H}$ is given by:

$$\Delta P_i \geq -\frac{\mathbf{n}^T(\mathbf{P}^d - \mathbf{P}^c)}{n_i} \qquad i = 1, \ldots, 2m \tag{4.16}$$

Since the numerator in the right-hand side is the same for all buses, we conclude that the higher the normal vector component corresponding to an injection, the smaller the amount of the action needed and thereby the more efficient this control.

4.5.2 Identification of the critical point

The critical point of the system corresponds to a smooth passage through zero of one eigenvalue of the unreduced Jacobian $\mathbf{J}$. It is not a long-term equilibrium ($\mathbf{h}(\mathbf{x}, \mathbf{y}, \mathbf{z}) \neq \mathbf{0}$) but only a point of the system trajectory which satisfies:

$$\mathbf{0} = \mathbf{f}(\mathbf{x}, \mathbf{y}, \mathbf{z}) \tag{4.17}$$

$$\mathbf{0} = \mathbf{g}(\mathbf{x}, \mathbf{y}, \mathbf{z}) \tag{4.18}$$

$$\det \mathbf{A} = \det \mathbf{J} = 0 \tag{4.19}$$

A critical point can be identified using the sensitivities of the *total* reactive generation Q_g to the various reactive loads [CGS84, BP92, VCJ95, VCV98]. These sensitivities can be obtained from the general formula (4.7):

$$\frac{\partial Q_g}{\partial \mathbf{Q_l}} = -\boldsymbol{\varphi}_{\mathbf{Q_l}}^T ({\boldsymbol{\varphi}_{\mathbf{u}}}^T)^{-1} \frac{\partial Q_g}{\partial \mathbf{u}} \tag{4.20}$$

where for the QSS simulation $\boldsymbol{\varphi}_{\mathbf{u}}$ is the $\mathbf{J}$ matrix defined by (3.25), $\dfrac{\partial Q_g}{\partial \mathbf{u}}$ is an $nbeq$-dimensional vector and $\boldsymbol{\varphi}_{\mathbf{Q_l}}$ is an $nbeq \times m$ very sparse matrix.

Let us decompose the Jacobian matrix $\boldsymbol{\varphi}_{\mathbf{u}}$ into:

$$\boldsymbol{\varphi}_{\mathbf{u}} = \mathbf{V}\, \Lambda\, \mathbf{W} \tag{4.21}$$

where:

- Λ is a diagonal matrix containing the eigenvalues $\lambda_1, \ldots, \lambda_{nbeq}$ of $\boldsymbol{\varphi}_{\mathbf{u}}$, which we assume all distinct for simplicity
- $\mathbf{V}$ is a matrix whose i-th column is the right eigenvector $\mathbf{v}_i$ of $\boldsymbol{\varphi}_{\mathbf{u}}$ relative to λ_i
- $\mathbf{W}$ is a matrix whose i-th row is the left eigenvector $\mathbf{w}_i$ relative to λ_i.

Under the above assumption of distinct eigenvalues, the left and right eigenvectors relative to two different eigenvalues are orthogonal to each other. We assume moreover that all eigenvectors have been normalized, so that:

$$v_i^T w_j = \begin{cases} 0 & \text{if } i \neq j \\ 1 & \text{if } i = j \end{cases} \tag{4.22}$$

which shows that $\mathbf{W} = \mathbf{V}^{-1}$.

Inverting and transposing (4.21) we get:

$$({\boldsymbol{\varphi}_{\mathbf{u}}}^T)^{-1} = \mathbf{W}^T \Lambda^{-1} \mathbf{V}^T = \sum_{i=1}^{nbeq} \frac{\mathbf{w}_i \mathbf{v}_i^T}{\lambda_i} \tag{4.23}$$

Taking (4.23) into account the sensitivity formula (4.20) becomes:

$$\frac{\partial Q_g}{\partial \mathbf{Q_l}} = -\boldsymbol{\varphi}_{\mathbf{Q_l}}^T \left[\sum_{i=1}^{nbeq} \frac{\mathbf{w}_i \mathbf{v}_i^T}{\lambda_i} \right] \frac{\partial Q_g}{\partial \mathbf{u}} \tag{4.24}$$

This formula clearly shows that when the Jacobian $\boldsymbol{\varphi}_{\mathbf{u}}$ is singular, or equivalently has a zero eigenvalue, the above sensitivities tend to infinity.

By way of illustration, the time evolution of one such sensitivity is shown in the right plot of Fig. 4.3, relative to the unstable voltage evolution shown in the left plot. The critical point is crossed at $t = 370$ s, where sensitivities change sign "going through infinity".

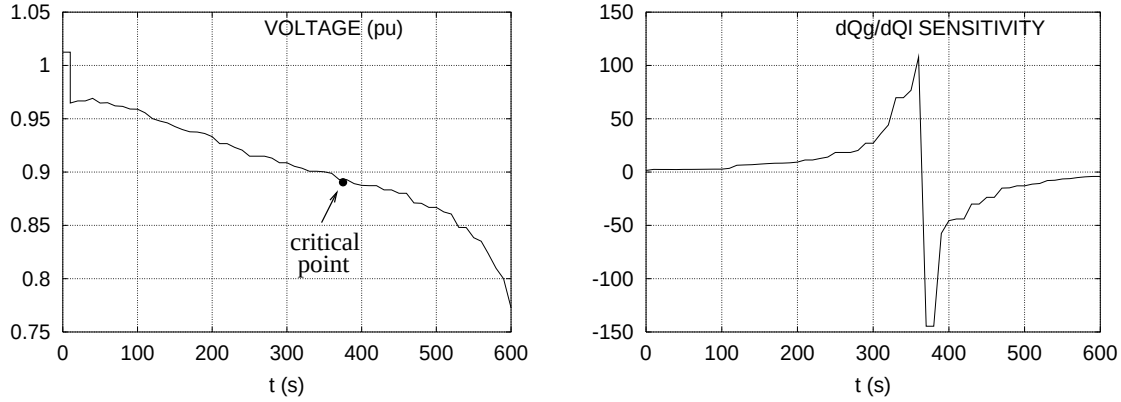

Figure 4.3: Time evolution of a bus voltage and a $\partial Q_g/\partial Q_l$ sensitivity in an unstable scenario

4.5.3 Determination of the normal vector

Let $\mathbf{w}$ be the left eigenvector corresponding to the zero eigenvalue of the unreduced Jacobian $\mathbf{J}$ at the critical point. Therefore, $\mathbf{w}^T\mathbf{J} = \mathbf{0}$. It can be shown [Dob92] that the normal vector $\mathbf{n}$ is given by:

$$\mathbf{n} = \begin{bmatrix} \mathbf{0} & \mathbf{0} & \mathbf{g}_\mathbf{P}^T \end{bmatrix} \mathbf{w} \tag{4.25}$$

where $\mathbf{g_P}$ is the Jacobian of $\mathbf{g}$ (see Eq. 3.13) with respect to the power injections vector $\mathbf{P}$.

In practice the dominant real eigenvalue and the corresponding left eigenvector $\mathbf{w}$ can be obtained by applying the Simultaneous Iteration method to the matrix $\mathbf{A}$ [RVC96]. An unreduced Jacobian formulation allows to use the sparse $\mathbf{J}$ matrix in all the involved linear systems.

Under the effect of field current limiters, it may happen that the dominant real eigenvalue "jumps" from a negative to a positive value (e.g. [VCV98], pp. 255-260), instead of smoothly passing through zero. This situation corresponds to the system going through a breaking point (see Fig. 3.4). The above sensitivities correspondingly switch from positive to negative without assuming very large values. As reported in [MVC99], in all practical cases, we found it satisfactory to compute $\mathbf{w}$ at the first point where negative sensitivities are observed.

4.6 Controls ranking for voltage security restoration: second approach

In the previous section we have presented a control ranking technique based on the normal vector $\mathbf{n}$. In this section, we propose an alternative ranking criterion which offers some advantages over the $\mathbf{n}$-based criterion, for equally good ranking capabilities.

4.6.1 Principle

It is well known that long-term voltage instability develops as a progressive fall of voltages. If successive "snapshots" are taken along an unstable system evolution and if the bus voltage magnitudes are sorted out, a rather constant pattern is observed, pointing out the most affected area of the transmission system. Depending upon the instability mode, this area may be more or less extended.

Within the context of preventive actions, it thus makes sense to take actions that will prevent the lowest transmission voltage to fall. Hence the idea of:

- identifying the transmission bus which undergoes the largest voltage decay. We will assume that this occurs at the ℓ-th bus [4] and will refer to the latter as the weakest bus;
- identifying those control actions able to increase the voltage V_ℓ of the weakest bus. To this purpose, we propose to evaluate the sensitivities of this voltage to the (active and reactive) power injections, i.e. $\dfrac{\partial V_\ell}{\partial \mathbf{P}}$.

This raises the question of choosing the operating point at which the above sensitivities are computed. Our simulations have shown that the choice of this linearization point, although easy, is crucial for the success of the method, as is the choice of the weakest bus. Before addressing this question, we briefly explain how these sensitivities are computed.

4.6.2 Analytical derivation of the sensitivities

The sensitivities

$$\frac{\partial V_\ell}{\partial \mathbf{P}} = \left[\frac{\partial V_\ell}{\partial P_1}, ..., \frac{\partial V_\ell}{\partial P_i}, ..., \frac{\partial V_\ell}{\partial P_{2m}}\right]^T \tag{4.26}$$

can be easily obtained from the general sensitivity formula presented in Section 4.2, which yields:

$$\frac{\partial V_\ell}{\partial \mathbf{P}} = -\boldsymbol{\varphi}_{\mathbf{P}}^T \left(\boldsymbol{\varphi}_{\mathbf{u}}^T\right)^{-1} \frac{\partial V_\ell}{\partial \mathbf{u}} = -\boldsymbol{\varphi}_{\mathbf{P}}^T \left(\boldsymbol{\varphi}_{\mathbf{u}}^T\right)^{-1} \mathbf{e}_\ell \tag{4.27}$$

where $\mathbf{e}_\ell$ is a unit vector with $e_i = 0, \ \forall i \neq \ell$ and $e_\ell = 1$.

Note the strong similarity with the $\dfrac{\partial Q_g}{\partial \mathbf{Q}_l}$ sensitivities presented in Section 4.5.2, given by (4.24) and used to identify the critical point along a voltage unstable trajectory. Both sensitivities involve the inverse of the $\boldsymbol{\varphi}_{\mathbf{u}}$ Jacobian and hence change sign passing through infinity when crossing the critical point. For this reason, one could think of using the sensitivities $\dfrac{\partial V_\ell}{\partial \mathbf{P}}$ instead of $\dfrac{\partial Q_g}{\partial \mathbf{Q}_l}$ to identify critical points. However, this would raise

[4] ℓ for "lowest"

the question of choosing the weakest bus, which is not known beforehand. On the contrary, because they involve the reactive power generation of the whole system, the $\frac{\partial Q_g}{\partial \mathbf{Q}_l}$ sensitivities allow a global monitoring of the system.

4.6.3 Linearization point

Following a similar reasoning as for the $\frac{\partial Q_g}{\partial \mathbf{Q}_l}$ sensitivities and normal vector $\mathbf{n}$, we propose to compute the $\frac{\partial V_\ell}{\partial \mathbf{P}}$ sensitivities along the unstable post-contingency trajectory of the system [5].

Clearly, the absolute and relative values of these sensitivities change with the point of the post-contingency evolution at which the system equations are linearized. This change results from generators reaching their reactive limits and from the load restoration process. This raises the question of chosing the point at which it is appropriate to evaluate $\wp_{\mathbf{u}}$ and therefrom (4.27), in order the sensitivities to accurately indicate which controls can increase the minimal voltage V_ℓ.

We propose to carry out this computation near the critical point. This choice is motivated by the fact that at the critical point the unrestored load is at (or close to) its minimum (see example of Section 2.3.1). More importantly, at the critical point, we know which generators are responsible for the limitation of the power deliverable to loads. Just after the contingency, many generators may still be under voltage control, because load restoration has not taken place yet, or their OELs have not acted yet or their field currents are still low because many generators share the effort. On the other hand, long after the critical point has been crossed, many generators may switch under limit due to the system degradation. It is therefore not suitable to compute the sensitivities either too early before or too late after the crossing of the critical point. At this point, the sensitivities will have "the mark" of load restoration and generator reactive power limitation.

This choice is further justified by the analytical considerations of the next section.

For already mentioned reasons, near the critical point, the sensitivities will assume very large values. The absolute values have no real interpretation and we will thus consider normalized sensitivities, obtained by dividing the vector $\frac{\partial V_\ell}{\partial \mathbf{P}}$ by its component with the largest magnitude. In other words, the most effective injection to act on will be ranked with a 1. The lower the magnitude of a sensitivity, the less effective the corresponding injection. Note that sensitivities with respect to active power injections may be negative, as will be illustrated in Section 4.8.4.

[5] an extension to stable but low-voltage scenarios will be discussed in Section 4.6.5

4.6.4 Relationship between $\mathbf{n}$ and $\dfrac{\partial V_\ell}{\partial \mathbf{P}}$

Substituting (4.23) for $(\boldsymbol{\varphi}_\mathbf{u}{}^T)^{-1}$ into the sensitivity formula (4.27) we obtain:

$$\frac{\partial V_\ell}{\partial \mathbf{P}} = -\sum_{i=1}^{nbeq} \frac{\boldsymbol{\varphi}_\mathbf{P}^T \mathbf{w}_i \mathbf{v}_i^T \mathbf{e}_\ell}{\lambda_i} \tag{4.28}$$

As already mentioned, the Jacobian $\boldsymbol{\varphi}_\mathbf{u}$ is singular at the critical point or, equivalently, it has a zero eigenvalue. In the neighbourhood of this point, it has an almost zero eigenvalue, which we denote by λ_c. Putting in evidence the term relative to λ_c in (4.28) yields:

$$\frac{\partial V_\ell}{\partial \mathbf{P}} = -\sum_{i\neq c} \frac{\boldsymbol{\varphi}_\mathbf{P}^T \mathbf{w}_i \mathbf{v}_i^T \mathbf{e}_j}{\lambda_i} - \frac{\boldsymbol{\varphi}_\mathbf{P}^T \mathbf{w}_c \mathbf{v}_c^T \mathbf{e}_\ell}{\lambda_c} = -\sum_{i\neq c} \frac{\boldsymbol{\varphi}_\mathbf{P}^T \mathbf{w}_i \mathbf{v}_i^T \mathbf{e}_\ell}{\lambda_i} - \frac{k}{\lambda_c}\mathbf{n} \tag{4.29}$$

where $\mathbf{n} = \boldsymbol{\varphi}_\mathbf{P}^T \mathbf{w}_c$ is the normal vector and

$$k = \mathbf{v}_c^T \mathbf{e}_\ell \tag{4.30}$$

Hence, as we approach the critical point, the magnitude of the last term in (4.29) becomes larger and larger ($||\mathbf{n}k/\lambda_c|| \to \infty$) and, the other eigenvalues being nonzero, the last term dominates the other ones, so that the sensitivities can be approximated by this term only:

$$\frac{\partial V_\ell}{\partial \mathbf{P}} \cong -\frac{k}{\lambda_c}\mathbf{n} \tag{4.31}$$

It results that the vector of $\dfrac{\partial V_\ell}{\partial \mathbf{P}}$ sensitivities is collinear with the normal vector $\mathbf{n}$. In other words, after a proper normalization, both vectors will coincide. Hence, under the above assumptions, the normal vector and these sensitivities computed at the critical point provide essentially the same information about the ranking of controls. In theory, this result holds true whatever the bus ℓ.

In practice, however, the eigenvalue λ_c is close to but not equal to zero and hence, the contribution of the other terms in (4.29) may not be negligible. This is even more true in large systems having a large number of eigenvalues (and hence a large number of terms). In order the last term to be dominant, the value of k should be as large as possible. From (4.30), it is easily seen that bus ℓ should correspond to the largest entry of the right eigenvector $\mathbf{v}_c$.

Now, it has been shown in Ref. [Dob92] that the right eigenvector $\mathbf{v}_c$ indicates how the various system states u_i are affected by the voltage collapse. More precisely, the higher the voltage drop at a bus, the larger the corresponding component of the right eigenvector $\mathbf{v}_c$. In particular, the largest component of the right eigenvector is expected to point out the voltage which drops the most.

To summarize, the choice of bus ℓ as the one experiencing the largest voltage drop does not only make sense from a physical viewpoint but allows the sensitivities $\dfrac{\partial V_\ell}{\partial \mathbf{P}}$ to bring the same information as the normal vector $\mathbf{n}$.

4.6.5 Advantages of the $\frac{\partial V_\ell}{\partial \mathbf{P}}$-based ranking

The $\frac{\partial V_\ell}{\partial \mathbf{P}}$-based ranking offers advantages over the $\mathbf{n}$-based one in several respects:

1. *efficiency*: both approaches require a single computation and factorization of the Jacobian $\mathbf{J}$ [6]. However, while the sensitivities require to solve a single linear system, the simultaneous iteration method used to compute $\mathbf{w}_c$ (and therefrom $\mathbf{n}$) requires to solve a sequence of such systems [RVC96];

2. *reliability*: although the simultaneous iteration method works well in most cases, it may experience convergence problems when the initial estimate of the dominant eigenvalue is not accurate enough. We have experienced this problem around breaking points, where the (real) dominant eigenvalue does not go smoothly through zero but rather "jumps" from a negative to a (non negligible) positive value. In such a case, it may be required to execute the simultaneous iteration algorithm several times with progressively larger initial estimates. On the other hand, the sensitivities can always be computed as long as the system has a post-contingency short-term equilibrium. They thus appear more reliable for an industrial application.

3. *extension to low but stable voltage problems*. As mentioned in Section 3.5.1, in practice, lower bounds may be imposed on the post-contingency voltages (see equation 3.33). It is thus possible that the system settles at unacceptably low but still stable voltages, in which case no critical point is crossed and the derivation of Section 4.5 does not apply. The sensitivities, on the other hand, can be computed at that final operating point. They will carry information about how to restore viability rather than stability. From this viewpoint they appear to be a more general approach to tackle voltage problems.

As already mentioned, only the relative values of the sensitivities are meaningful when the computation is carried out near a critical point, for stability restoration. On the contrary, when the problem is to increase a low final voltage (see item 3 above), absolute values can be interpreted.

4.6.6 Summary : practical procedure

The procedure for ranking the control actions for voltage security restoration can be summarized as follows:
1. Simulate the post-contingency evolution of the system until the specified time horizon is reached, or unacceptable low voltages are met, or short-term equilibrium is lost;
2. at the various points of the simulated system evolution, check for $\partial Q_g/\partial \mathbf{Q}_l$ sensitivities changing sign through infinity;
3. if this takes place, compute the $\partial V_\ell/\partial \mathbf{P}$ sensitivities at the short-term equilibrium point

[6] $\mathbf{J} - \hat{\lambda}\mathbf{I}$ in the eigenvalue computation, where $\hat{\lambda}$ is an estimate of the sought dominant eigenvalue

where the sign change takes place. Normalize them by dividing by the sensitivity with the largest magnitude;
4. if no sign change has been detected, compute the sensitivities at the final operating point and use the absolute values, provided that $\partial Q_g/\partial \mathbf{Q}_l$ is smaller than a threshold.

Obviously, the sensitivities $\partial V_\ell/\partial \mathbf{P}$ cannot be checked if the system loses its short-term equilibrium right after the contingency is applied, which is the case of short-term voltage instability.

4.7 Numerical results

We exemplify hereafter some of the ideas exposed in this section on one test and two real systems. We focus on comparing the controls ranking given by the $\partial V_\ell/\partial \mathbf{P}$ sensitivities and the normal vector, respectively.

4.7.1 Example from Nordic 32 system

We first consider the Nordic 32 system (see Appendix A.1).

A comparison of controls ranking for an unstable scenario resulting from the loss of the line linking buses 4011 and 4021 is given in Table 4.1. At the critical point, the smallest voltage is observed at bus 4022 and is about 0.92 pu. From this table one can easily remark that the sensitivities of this voltage with respect to active generator injections practically coincide with the corresponding components of the normal vector. As already explained, this result is attributable to the relatively small number of eigenvalues of this system.

Table 4.1: Nordic 32 system: comparison of controls ranking

gen	n	dV_ℓ/dP	gen	n	dV_ℓ/dP	gen	n	dV_ℓ/dP
g7	1.000	1.000	g18	0.914	0.912	g21	-0.075	-0.075
g6	0.955	0.954	g19	0.903	0.900	g22	-0.075	-0.074
g17b	0.954	0.953	g11	0.788	0.785	g10	-0.075	-0.074
g17	0.954	0.953	g12	0.542	0.537	g1	-0.076	-0.075
g16	0.941	0.939	g8	0.429	0.425	g2	-0.083	-0.083
g15	0.941	0.939	g5	0.023	0.023	g3	-0.084	-0.084
g14	0.924	0.922	g9	-0.073	-0.073	g4	-0.105	-0.104

4.7.2 Example from the RTE system

In this example we consider a contingency whose security margin is about 4800 MW. During the marginally unstable scenario (4900 MW of stress) the system passes through the critical point at t=130s. We have chosen to display the results relative to 19 significant generators among a total of 176.

Figure 4.4 shows the ranking of these generators according to both criteria. As expected, both rankings are in a very good agreement. Nevertheless, small discrepancies can be observed for generators 2 to 6. They are slightly greater than those observed for the Nordic 32 system, likely because of the higher value of the first term in equation (4.29).

Figure 4.5 presents the ranking obtained according to $\partial V_\ell / \partial \mathbf{P}$ sensitivities computed at four different snapshots: just after the contingency (t=20s), at the critical point (t=130s), at t=290s and at t=300s just before the short-term equilibrium is lost. One can conclude that the sensitivity ranking is more and more distorted with respect to that of the normal vector when moving away from the critical point. This applies to the values of the sensitivities as well as to the order in which generators are ranked. That is attributable to the fact that, after the critical point, more and more generators attain their reactive limits. This causes the relative values of some generators to become more important. Comparatively, the ranking obtained just after the contingency is less distorted.

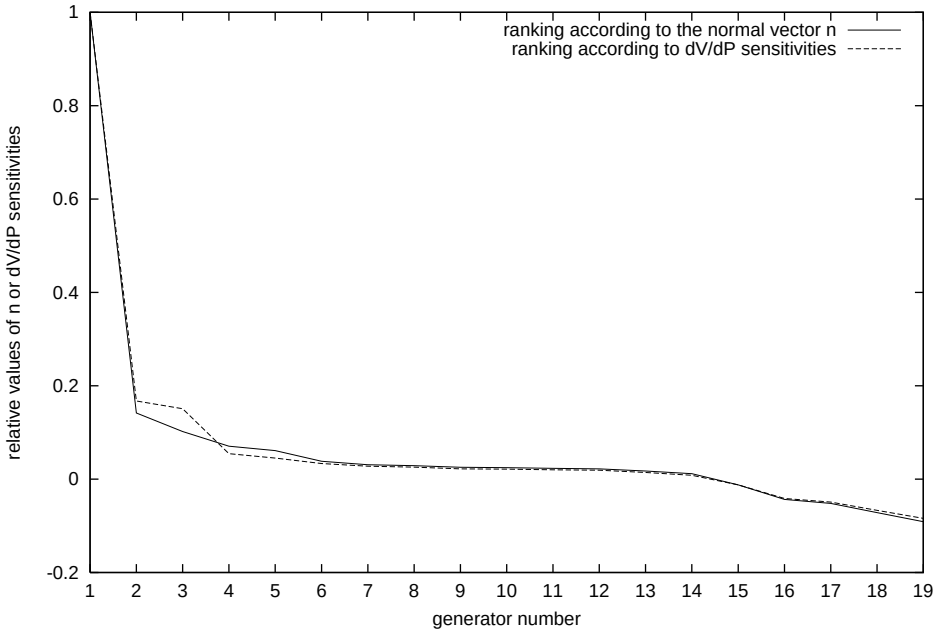

Figure 4.4: RTE system: generators ranking according to normal vector and $\partial V_\ell / \partial \mathbf{P}$ sensitivities

Figure 4.6 compares the generators ranking provided by sensitivities relative to four different "weak" buses. Bus 0 undergoes the highest voltage drop between its pre-contingency and critical point values and is thus considered as the best choice. The other three buses are located at some distance, in different directions, from bus 0. For buses 2 and 3 the ranking is very different, while for bus 1 located near bus 0, the ranking is only slightly different. This result underlines the importance of deriving the sensitivities at a location where the voltage drop is large enough but at the same time it shows that the choice between various buses of the same weak area is not critical.

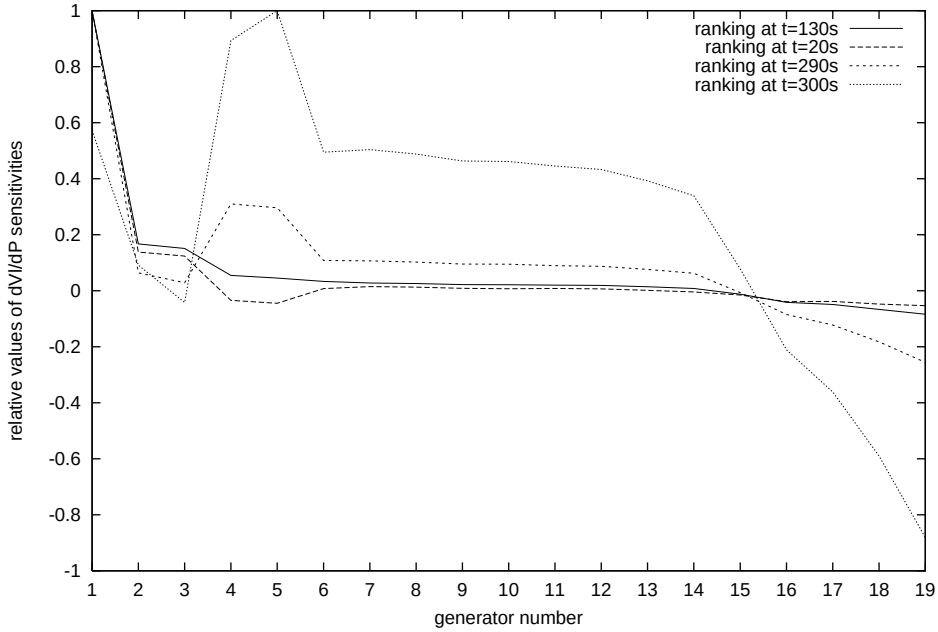

Figure 4.5: RTE system: generators ranking according to $\partial V_\ell / \partial \mathbf{P}$ sensitivities computed at different time instants

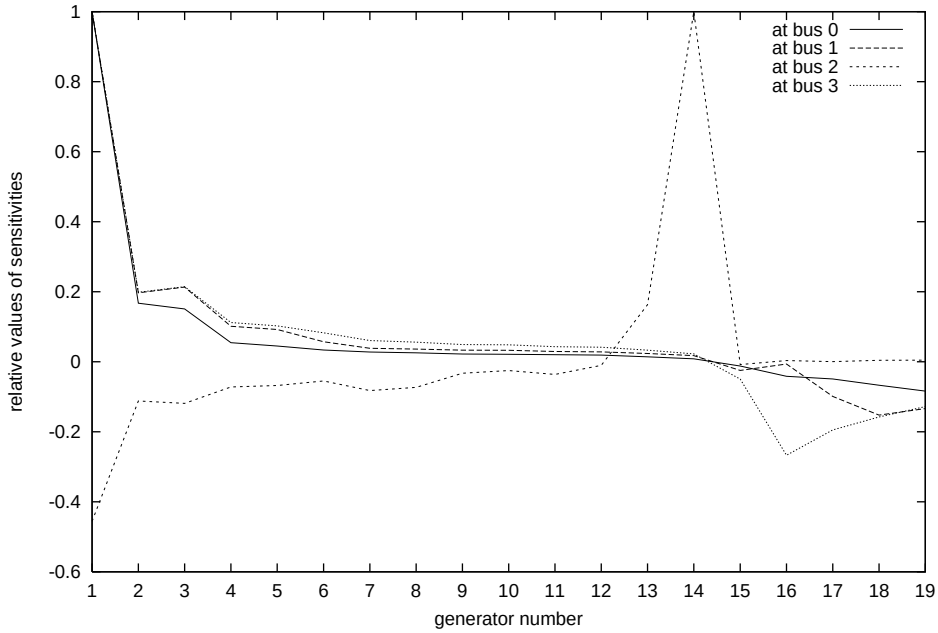

Figure 4.6: RTE system: generators ranking according to $\partial V_\ell / \partial \mathbf{P}$ sensitivities computed at different buses

4.7.3 Example from the Hydro-Québec system

A comparison of generators ranking according to normal vector and $\dfrac{\partial V_\ell}{\partial \mathbf{P}}$ sensitivities for this system is given by Fig. 4.7. We consider the marginally unstable scenario of a binary search relative to the loss of a line between MO and MQ areas. Note that,

during the post-contingency evolution the system switches back and forth three times between sensitivities of opposite sign (at t=2 s, 14 s and 30 s respectively), as shown in the left plot of Fig. 4.8. The last two switches are due to MAIS devices that trip shunt inductances at successive time instants to counteract the system degradation owing to LTCs, and maintain for some time the system around its critical point. The critical point is crossed for the first time at t=2 s, i.e. just after the contingency, when the dominant eigenvalue of the system λ_c jumps from -0.057 to 0.551 (see the right plot of Fig. 4.8). At that point we rank the 84 generators of the system according to both criteria. Bus 705 whose voltage is the lowest at the critical point (about 0.92 pu) is taken as the weak bus. One can remark that, in spite of the large value of λ_c, the sensitivity-based ranking, drawn with dotted line, is quite close to that of the normal vector, drawn with solid line.

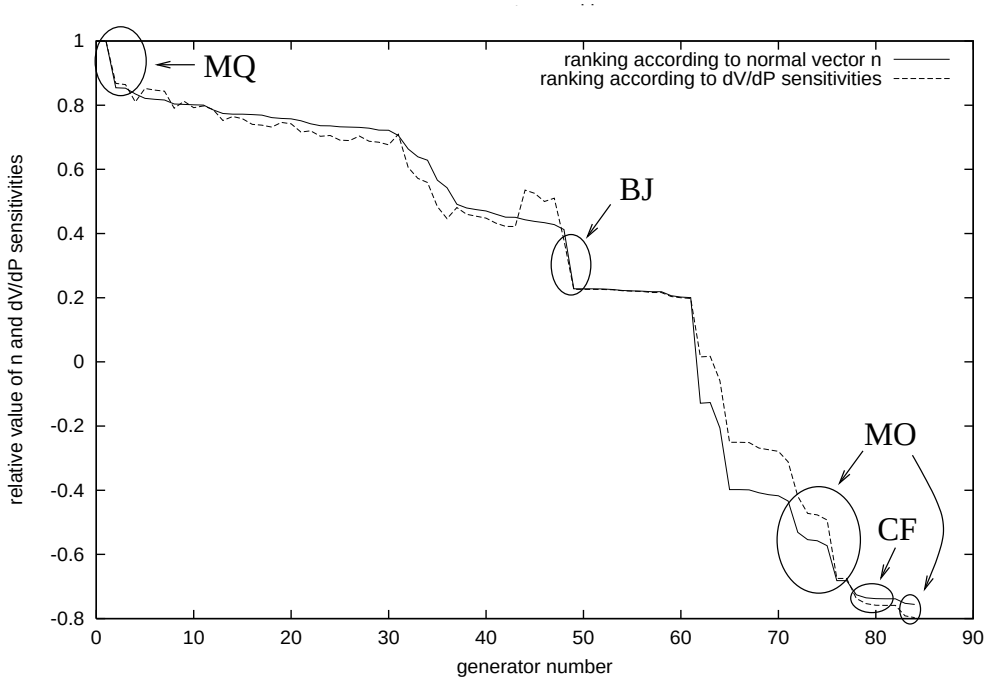

Figure 4.7: Hydro-Québec system: generator ranking according to normal vector and $\partial V_\ell / \partial \mathbf{P}$ sensitivities

Figure 4.7 also shows that increasing active power injections in the BJ area, located one thousand kilometers from the weak bus 705, has a significant effect (about a quarter of the largest sensitivity, relative to the MQ area). Expectedly, injecting reactive power at the same place does not influence the weak bus voltage at all.

Moreover, the MO and CF areas exhibit negative sensitivities, which indicate that active power generation should be decreased in these areas. Indeed, they are located in the corridor where the contingency takes place.

4.8 Voltage security margin restoration

In the previous sections, we have considered the problem of ranking control actions with respect to their efficiency in restoring voltage stability. In this section, we consider the

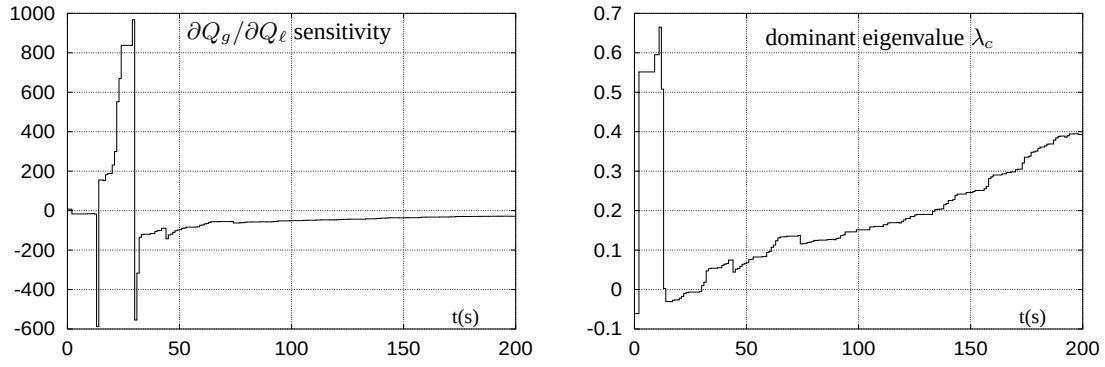

Figure 4.8: Left plot: time evolution of $\partial Q_g/\partial Q_l$ sensitivity at a load bus. Right plot: time evolution of the dominant eigenvalue λ_c

problem of additionally restoring a security margin, and we correspondingly derive the sensitivities of margins to power injections.

4.8.1 Voltage security margin sensitivity with respect to power injections

For a given contingency, the sensitivity of the pre-contingency margin M^V to a small change ΔP_i of the i-th power injection is given by:

$$\frac{\partial M^V}{\partial P_i} = \lim_{\Delta P_i \to 0} \frac{\Delta M^V}{\Delta P_i} \qquad i = 1, \ldots, 2m \tag{4.32}$$

which should be interpreted as indicated in Section 4.3.1.

Let us assume that before the contingency, the system operates at point $\mathbf{P}^o$ inside the voltage secure region $\mathcal{S}_V$, as shown in the left plot of Fig. 4.9. For a given direction of stress $\mathbf{d}$, the security limit corresponds to point $\mathbf{P}^\star$. Let us denote by M^V the corresponding security margin. We aim at determining the sensitivity of the margin M^V to the base case power injections $\mathbf{P}^o$. To this purpose we assume a small variation $d\mathbf{P}^o$ of power injections around the initial point $\mathbf{P}^o$. The new security limit, for the same stress direction, is now the point $\mathbf{P}^\star + d\mathbf{P}^\star$ and the new security margin changes accordingly into $M^V + dM^V$.

4.8.2 Approach by finite differences

A simple, brute force approach consists in approximating the sensitivities by a ratio of finite differences, assuming a small variation ΔP_i and evaluating the resulting margin variation ΔM^V. To guarantee accuracy, the magnitude of ΔP_i must be properly chosen and the margins must be computed with a tolerance Δ smaller than what is usually needed for practical security monitoring. This requires to perform more steps in the binary search. On the other hand, each binary search can start from a narrower interval $[S_\ell \; S_u]$.

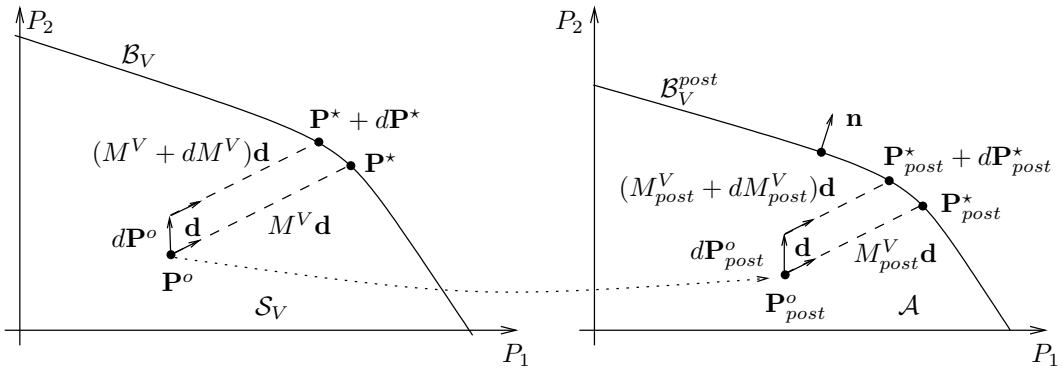

Figure 4.9: Effect of small power injection changes on a voltage security margin

4.8.3 Analytical approach

Deriving an accurate analytical expression of the sensitivities is a challenging – if at all solvable – problem. Indeed, we seek to determine how far changes in the *pre*-contingency operating point influence the maximum stress that can be imposed to the system, such that its response to a contingency is stable.

Given the difficulty of this problem, we approximate the sensitivity of *pre*-contingency margin to *pre*-contingency injections with the sensitivity of *post*-contingency margin to *post*-contingency injections. A contribution of this thesis is to show that the latter sensitivities provide reasonably accurate information for the pre-contingency control.

The derivation in the post-contingency configuration is as follows [DL92a, Gre98, VCV98].

Let $\mathbf{P}^o_{post}$ be the post-contingency equilibrium point of the system operating initially at $\mathbf{P}^o$ (see the right plot in Fig. 4.9). Let also $\mathbf{P}^\star_{post}$ be the post-contingency security limit of the system in the direction $\mathbf{d}$ and M^V_{post} its corresponding margin. Let $\mathbf{P}^\star_{post} + d\mathbf{P}^\star_{post}$ (resp. $M^V_{post} + dM^V_{post}$) be the new security limit (resp. margin) after a small injection variation $d\mathbf{P}^o_{post}$ around $\mathbf{P}^o_{post}$.

As mentioned above, we make the approximation:

$$\frac{dM^V}{d\mathbf{P}^o} \cong \frac{dM^V_{post}}{d\mathbf{P}^o_{post}}$$

and for the sake of clarity, we drop the lowerscript "post" in the following derivation.

We have shown in Section 3.4.4 that any point of surface $\mathcal{B}_V^{post}$ is a loadability limit for a particular direction of stress. Let us now assume that these points are of the SNB type, i.e. the Jacobian $\mathbf{J}$ is singular at each of these points.

At the post-contingency security limits $\mathbf{P}^\star$ and $\mathbf{P}^\star + d\mathbf{P}^\star$ we have respectively:

$$\boldsymbol{\varphi}(\mathbf{u}^\star, \mathbf{P}^\star) = \boldsymbol{\varphi}(\mathbf{u}^\star, \mathbf{P}^o + M^V\mathbf{d}) = \mathbf{0} \tag{4.33}$$

$$\boldsymbol{\varphi}(\mathbf{u}^\star + \mathbf{du}^\star, \mathbf{P}^\star + d\mathbf{P}^\star) = \boldsymbol{\varphi}(\mathbf{u}^\star + \mathbf{du}^\star, \mathbf{P}^\star + d\mathbf{P}^o + dM^V\mathbf{d}) = \mathbf{0} \tag{4.34}$$

together with the singularity conditions:

$$\det \boldsymbol{\varphi}_{\mathbf{u}}|_{\mathbf{u}=\mathbf{u}^\star} = 0 \tag{4.35}$$

$$\det \boldsymbol{\varphi}_{\mathbf{u}}|_{\mathbf{u}=\mathbf{u}^\star+\mathbf{du}^\star} = 0 \tag{4.36}$$

A Taylor series expansion yields:

$$\boldsymbol{\varphi}(\mathbf{u}^\star + \mathbf{du}^\star, \mathbf{P}^\star + d\mathbf{P}^\star) = \boldsymbol{\varphi}(\mathbf{u}^\star, \mathbf{P}^\star) + \boldsymbol{\varphi}_{\mathbf{u}}\mathbf{du}^\star + \boldsymbol{\varphi}_{\mathbf{P}}[d\mathbf{P}^o + dM^V\mathbf{d}] \tag{4.37}$$

Premultiplying with $\mathbf{w}^T$ and taking (4.33, 4.34) into account, we get:

$$\mathbf{w}^T\boldsymbol{\varphi}_{\mathbf{u}}\mathbf{du}^\star + \mathbf{w}^T\boldsymbol{\varphi}_{\mathbf{P}}d\mathbf{P}^o + \mathbf{w}^T\boldsymbol{\varphi}_{\mathbf{P}}dM^V\mathbf{d} = \mathbf{0} \tag{4.38}$$

Now, since $\mathbf{w}^T\boldsymbol{\varphi}_{\mathbf{u}} = 0$ and $\mathbf{n} = \mathbf{w}^T\boldsymbol{\varphi}_{\mathbf{P}}$, and assuming that $\mathbf{w}^T\boldsymbol{\varphi}_{\mathbf{P}}\mathbf{d} \neq 0$, we obtain the sought sensitivity as:

$$\frac{dM^V}{d\mathbf{P}^o} = -\frac{\mathbf{w}^T\boldsymbol{\varphi}_{\mathbf{P}}}{\mathbf{w}^T\boldsymbol{\varphi}_{\mathbf{P}}\mathbf{d}} = -\frac{\mathbf{n}^T}{\mathbf{n}^T\mathbf{d}} \tag{4.39}$$

In practice, for each contingency of interest, these sensitivities are computed in the *marginally unstable* case of the binary search used to determine the margin.

4.8.4 Numerical example

We consider the Nordic 32 test system. The stress of concern is a load increase in the South area ($S_{max} = 600$ MW/180 Mvar) covered by a slightly greater generation increase in the North area (due to system losses), each according to participation factors.

Let us recall that there is no slack-bus in the QSS model; instead, generators respond to a disturbance according to governor effects [VCV98]. Moreover, it is assumed that only the generators of the North area participate to frequency control (i.e. the others have infinite speed droops).

Table 4.2 shows the sensitivities of margins to controls given by (4.39), for the five severest contingencies and for different controls. The sensitivity to an active generation is the margin increase for a small increase on this generation, balanced by a decrease of Northern generations, as dictated by frequency control. Such values are presented in the first four rows of Table 4.2. The last two rows, on the other hand, correspond to a shift of power from one generator to another. The values have been obtained by subtracting the corresponding sensitivities.

For comparison purposes, Table 4.3 shows the same sensitivities obtained by finite differences. For each generator of concern, a 50 MW production increase has been considered, properly compensated by the other generators. All margins have been computed with a Δ tolerance of 2 MW for the sake of accuracy.

Numerical discrepancies are to be expected considering that a finite difference is used, tap changers deadband make the QSS simulation somewhat insensitive, etc. Nevertheless,

Table 4.2: Nordic 32 system : sensitivities given by (4.39)

control :		contingency : loss of				
gener.	balanced by	g14	g17	line A	g15	g8
g17b	North	0.84	0.91	0.93	0.84	0.91
g18	North	0.80	0.84	0.92	0.80	0.88
g4	North	-0.09	-0.07	-0.12	-0.09	-0.09
g1	North	-0.02	0.00	-0.09	-0.02	-0.02
g17b	g4	0.93	0.98	1.05	0.93	1.00
g18	g1	0.82	0.84	1.01	0.82	0.90

Table 4.3: Same system: sensitivities obtained by finite differences

control :		contingency : loss of				
gener.	balanced by	g14	g17	line A	g15	g8
g17b	North	0.86	1.04	0.98	0.96	0.92
g18	North	0.80	0.92	0.94	0.90	0.88
g4	North	-0.08	-0.16	-0.14	-0.10	-0.18
g1	North	0.00	-0.02	-0.22	-0.02	0.00
g17b	g4	0.94	1.10	1.08	1.02	1.02
g18	g1	0.82	0.92	1.00	0.90	0.88

there is a good general agreement between both approaches. In particular, the ranking of control actions is the same by both approaches.

Let us finally comment on the fact that analytical sensitivities are computed in the post-contingency state and used in the pre-contingency analysis. Their derivation assumes that the system is characterized by the same set of equations in the pre-contingency base case and at the critical point of the post-contingency unstable scenario. However, very often, at the critical point some generators are under field current limit [7] while they controlled their voltages in the base case. Therefore, the system equations in the base case and at the critical point may be somewhat different, which causes some inaccuracy on the sensitivities. Neglecting the higher-order terms of the Taylor in series expansion (4.37) is another source of error [Gre98]. Nevertheless, we have observed that the so obtained sensitivities are accurate enough for control ranking.

4.9 Derivation of security constraints with respect to voltage instability and thermal overload

When, following a security analysis, the system has been found voltage and/or thermal insecure, and candidate controls have been ranked as proposed in this chapter, the next problem is to determine *how much the controls should be changed to remove the insecurity, while taking care that these actions do not create other security violations*.

[7] hence, the voltage setpoints of such generators cannot be taken as control variables, since they do no longer appear in the final set of equations

We believe that the easiest way to tackle this problem is through security constraints, which take on the form of linear inequality constraints and are derived as explained hereafter.

4.9.1 Constraints for thermal security restoration

Thermal security constraints express that no branch current is above its limit after any specified contingency:

$$I_{rj} \leq I_j^{max} \qquad r = 1, \ldots, c \qquad j = 1, \ldots, b \tag{4.40}$$

where b is the number of branches, I_{rj} is the post-contingency current in the j-th branch after the r-th contingency, c is the number of contingencies and I_j^{max} is the maximum current allowed in the j-th branch. The above inequality can be linearized into:

$$I_{rj}^o + \sum_{i=1}^{2m} \frac{\partial I_{rj}}{\partial P_i} \Delta P_i \leq I_j^{max} \qquad r = 1, \ldots, c \qquad j = 1, \ldots, b \tag{4.41}$$

where I_{rj}^o is the current in the j-th branch after the r-th contingency, when the system operates with the base case injections $\mathbf{P}^o$. Note that inequalities (4.41) can be written for pre-contingency currents as well, but post-contingency currents are generally more constraining.

The above constraints approximate the boundary $\mathcal{B}_T^{post}$ (resp. $\mathcal{B}_T$) of the post-contingency viability region $\mathcal{V}$ (resp. thermal security region $\mathcal{S}_T$) by a piece-wise linear surface, each linear part corresponding to one of the constraints (4.41) being active ($\leq$ replaced by $=$). This is illustrated in Fig. 4.10, which focuses on thermal aspects only.

It is very convenient in practice to consider the post-contingency viability region as bounded by linear constraints, because simpler linear analysis can be used. This approximation is accurate in truly thermal limited systems, where voltages remain close to their nominal values. The approximation is more questionable in the region of the injection space where the thermal security boundary approaches the voltage security boundary. A case of special interest is when an action aimed at enhancing voltage security, causes thermal overloads to become severer than voltage instability.

4.9.2 Constraints for voltage security restoration

Similarly, for any contingency causing voltage instability, a linear security constraint can be straightforwardly derived from the considerations of Section 4.5, where we have shown how the boundary $\mathcal{B}_V^{post}$ can be approximated by its tangent hyperplane $\mathcal{H}$ at the critical point $\mathbf{P}^c$, as illustrated in Fig. 4.2. The equation of $\mathcal{H}$ being given by (4.17), the secure region is thus characterized by:

$$\mathbf{n}^T(\mathbf{P} - \mathbf{P}^c) \leq 0$$

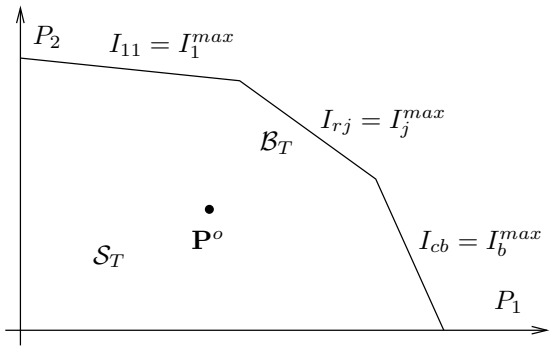

Figure 4.10: Thermal secure region in the power injection space

Assuming as before that this post-contingency information can be used for pre-contingency control, and decomposing $\mathbf{P}$ into $\mathbf{P} = \mathbf{P}^o + \Delta\mathbf{P}$, the above inequality becomes:

$$\mathbf{n}^T \Delta\mathbf{P} \leq \mathbf{n}^T(\mathbf{P}^c - \mathbf{P}^o) \leq 0$$

Adding a subscript r to refer to the r-th contingency ($r = 1, \ldots, c$) this constraint can be rewritten as:

$$\mathbf{n}_r^T \Delta\mathbf{P} \leq \mathbf{n}_r^T(\mathbf{P}_r^c - \mathbf{P}^o) \leq 0$$

or equivalently as:

$$\sum_{i=1}^{2m} n_{ri} \Delta P_i \leq C_r \tag{4.42}$$

where $C_r = \mathbf{n}_r^T(\mathbf{P}_r^c - \mathbf{P}^o)$ is a constant for the r-th contingency.

It is noteworthy that, in order to build the inequalities (4.42), all what matters is to identify a critical point of the system, and compute the corresponding normal vector $\mathbf{n}$. Therefore, such a security constraint can be also built for a contingency which does not cause voltage instability, by merely bringing the system at an (insecure, stressed) operating point $\mathbf{P}^d$ where it responds in an unstable way to the contingency. Incidentally, note that $\mathbf{P}^d$ does not appear in the linear approximation (4.15); it is merely used to bring the system to instability and therefrom obtain a linear approximation of the security boundary. On the other hand, the choice of $\mathbf{P}^d$ may influence the "quality" of the linear approximation, through $\mathbf{P}^c$ and, consequently, $\mathbf{n}$ [8].

Finally, let us emphasize that in the voltage security constraint (4.42), the normal vector may be replaced by the $\partial V_\ell / \partial \mathbf{P}$ sensitivities which have been shown to provide essentially the same ranking.

[8] moreover, for (very) mild contingencies it may be impossible to derive a voltage security constraint because the voltage secure region $\mathcal{S}_V$ almost entirely overlaps the feasible region $\mathcal{F}_o$ and, hence, the load flow could diverge at $\mathbf{P}^d$

4.9.3 Constraints for voltage and thermal security margin restoration

Let us denote by M either the voltage M^V or the thermal security margin M^T.

Security constraints relative to margins express that the system should to have a sufficient margin M_d with respect to any of the specified contingencies. These constraints take on the form:

$$M_r(\mathbf{P}^o) \geq M_d \quad r = 1, \ldots, c \tag{4.43}$$

For a small variation $\Delta\mathbf{P}$ of the power injections around the initial operating point $\mathbf{P}^o$, the inequalities (4.43) can be linearized into:

$$M_r(\mathbf{P}^o) + \sum_{i=1}^{2m} S_{ri}\Delta P_i \geq M_d \quad r = 1, \ldots, c \tag{4.44}$$

where $S_{ri} = \dfrac{\partial M_r}{\partial P_i}$ is the sensitivity of the r-th margin to the i-th power injection. These sensitivities can be computed as indicated earlier in this chapter.

4.9.4 Summary

Inequalities (4.41, 4.42 and 4.44) are at the heart of the derivations made in the later chapters of this thesis.

From a practical viewpoint, we will consider that the *relative values* of the sensitivities $\dfrac{\partial I_{rj}}{\partial P_i}$, n_{ri} and S_{ri} are accurate. However, to account for errors introduced by the linearization or by the way the constraints are derived, we will use compensation techniques, as presented in the next chapter.

4.9.5 Extension to transactions

In deregulated systems under the bilateral contract model, it is of interest to quantify security with respect to transactions. To this purpose, voltage and thermal security constraints should be derived considering transactions as control variables. A simple, linear change of variables can be used, as detailed hereafter.

A transaction is a bilateral exchange of power between a selling and a buying entity. In the sequel, the selling (resp. buying) entity is called *source* (resp. *sink*) and may comprise several generators (resp. loads). The k-th transaction ($k = 1, \ldots, t$) is defined by its volume T_k, which is the active power received by the sink, as well as by the bus participations in the source and the sink. The latter are defined by the two m-dimensional vectors:

$$\boldsymbol{\alpha}_k = [\alpha_{k1} \ldots \alpha_{ki} \ldots \alpha_{km}]^T \quad \boldsymbol{\beta}_k = [\beta_{k1} \ldots \beta_{ki} \ldots \beta_{km}]^T$$

where α_{ki} (resp. β_{ki}) is the participation factor of the generator (resp. load) at bus i in the k-th transaction. Obviously, $\alpha_{ki} = 0$ (resp. $\beta_{ki} = 0$) in the absence of a participating generator (resp. load) at bus i, and $\alpha_{ki} > 0$ (resp. $\beta_{ki} > 0$) otherwise. Furthermore, the participation factors are chosen such that:

$$\sum_{i=1}^{m} \alpha_{ki} = 1 + \delta_k \qquad \sum_{i=1}^{m} \beta_{ki} = 1$$

where δ_k accounts for the transmission losses associated with the k-th transaction.

Thus, for the k-th transaction, the active power P_{ki}^{+} ($i = 1, \ldots, m$) *injected into* and the active power P_{ki}^{-} *drawn from* the i-th bus relate to the above variables through:

$$P_{ki}^{+} = \alpha_{ki} T_k \qquad P_{ki}^{-} = \beta_{ki} T_k \qquad P_{ki}^{+},\ P_{ki}^{-} \geq 0$$

and the volume of the k-th transaction is given by:

$$T_k = \sum_{i=1}^{m} P_{ki}^{-} = \frac{\sum_{i=1}^{m} P_{ki}^{+}}{1 + \delta_k} \tag{4.45}$$

Denoting by Δ the variations from base case values, we have:

$$\Delta P_{ki}^{+} = \alpha_{ki} \Delta T_k \qquad \Delta P_{ki}^{-} = \beta_{ki} \Delta T_k$$

and the net power variation at bus i is, for all transactions:

$$\Delta P_i = \Delta P_i^{+} - \Delta P_i^{-} = \sum_{k=1}^{t} \Delta P_{ki}^{+} - \Delta P_{ki}^{-} = \sum_{k=1}^{t} \left(\alpha_{ki} - \beta_{ki}\right) \Delta T_k \tag{4.46}$$

This equation defines a mapping between the power injection and the transaction spaces.

Since a transaction is nothing but a linear combination of power injections, security constraints can be derived with respect to transactions as a particular case of those derived with respect to power injections.

The thermal security constraints (4.41) become:

$$I_{rj}^{o} + \sum_{k=1}^{t} \frac{\partial I_{rj}}{\partial T_k} \Delta T_k \leq I_j^{max} \qquad j = 1, \ldots, b \qquad r = 1, \ldots, c \tag{4.47}$$

where the partial derivative is given by:

$$\frac{\partial I_{rj}}{\partial T_k} = \sum_{i=1}^{2m} \frac{\partial I_{rj}}{\partial P_i} (\alpha_{ki} - \beta_{ki}) \tag{4.48}$$

As regards the voltage security constraints, the first term of (4.42) becomes:

$$\sum_{i=1}^{2m} n_{ri} \Delta P_i = \sum_{i=1}^{2m} n_{ri} \sum_{k=1}^{t} \left(\alpha_{ki} - \beta_{ki}\right) \Delta T_k = \sum_{k=1}^{t} \sum_{i=1}^{2m} n_{ri} \left(\alpha_{ki} - \beta_{ki}\right) \Delta T_k \tag{4.49}$$

Introducing the new coefficients:

$$\tilde{n}_{rk} = \sum_{i=1}^{2m} n_{ri}(\alpha_{ki} - \beta_{ki})$$

the constraints (4.42) can be rewritten as:

$$\sum_{k=1}^{t} \tilde{n}_{rk} \Delta T_k \leq C_r \tag{4.50}$$

Similarly, the security constraints (4.44) become:

$$M_r(\mathbf{P}^o) + \sum_{k=1}^{t} \frac{\partial M_r}{\partial T_k} \Delta T_k \geq M_d \qquad r = 1, \ldots, c \tag{4.51}$$

where the partial derivative is given by:

$$\frac{\partial M_r}{\partial T_k} = \sum_{i=1}^{2m} \frac{\partial M_r}{\partial P_i}(\alpha_{ki} - \beta_{ki}) \qquad r = 1, \ldots, c \tag{4.52}$$

Chapter 5

Management of voltage and thermal congestions

The methods presented in this chapter aim at determining, in some optimal manner, the preventive actions needed to remove voltage or thermal congestions. Congestions refer to situations where the system is either voltage or thermal insecure with respect to the previously defined security levels. Two approaches are proposed: the first one considers power injections as control variables while the second one relies on power transactions. Numerical examples of both approaches are given for a test as well as for a real-life system.

5.1 Introduction and previous works

In a deregulated environment a system is said to be "congested" when some predefined security constraints (thermal, voltage stability, angle stability, etc.) are violated in the current or in a foreseen operating state. Security constraints refer to both "N" and "N-1" configurations. Congestion management consists in controlling the system such that all security constraints are satisfied. The task of relieving or removing a congestion falls on the Transmission System Operator (TSO).

Congestion management can be carried out *preventively*, i.e. before the occurrence of any contingency, or *correctively*, i.e. after a disturbance has led to security constraints violation. Preventive congestion management is performed prior to real-time operation (e.g. after the day-ahead market is cleared) or on-line to remove an existing (or a trend towards) congestion. Preventive congestion management alone cannot guarantee that no congestion will occur because, on the one hand, there is always a mismatch between the forecasted and the real power flows and, on the other hand, unexpected disturbances may occur. Therefore, corrective congestion management appears as a required complement to preventive congestion management [CWW00].

Most authors deal with these two types of congestion management separately. However,

excessive preventive control leads to higher operating costs and, hence, to higher electricity prices for customers. On the other hand, relying too much on corrective measures increases considerably the risk of blackouts. A trade-off between preventive and corrective congestion management through the minimization of costs of combined preventive and corrective actions is proposed in [SAK98, CMP01]. However, these approaches strongly rely on the knowledge of the probability of contingency occurrence and the computation of the minimum load curtailment needed to restore feasibility after a contingency.

While a thermal overload generally leaves some time to take a remedial action, it is widely agreed that a developing voltage instability cannot be counteracted by human operators. Hence, corrective control against voltage instability must be implemented trough automatic, fast enough devices [Moo02]. The latter may increase generator (or compensator) voltages, switch shunt compensation and, in the last resort, shed load. Such a system protection scheme appears as the natural complement of preventive congestion management, allowing smaller – and hence less expensive or less market intrusive – control actions to be taken to preserve security. Note that, whereas our approach relies on QSS time simulation, existing automatic corrective control means can be taken into account (as already illustrated in Section 3.7). This chapter is devoted to preventive congestion management methods. Nevertheless, the proposed approaches apply as well to correct both mild voltage instabilities and thermal overloads.

Power systems were confronted to congestions well before deregulation has prevailed [1]. In the vertically integrated environment, congestion management most often consists in modifying the economic dispatch at the least cost until no security constraint is violated. As regards corrective control, depending on the gravity of the congestion, the objective may range from minimum action cost to minimum control deviation (with respect to pre-contingency values). Minimal load shedding to restore voltage security is an example of the second objective.

The management of *thermal overload congestions* has been widely analyzed [GI98, SHP98, WV99, WS00, CWW00, Ham00b]. It is most often based on the DC load flow model. Although valid in many practical cases, the latter approximation may be less satisfactory when voltage and thermal aspects are strongly coupled.

The management of *voltage instability congestions* has been comparatively less investigated so far [KVE00, BMZ00, Vou01, CVC02a]. Most of these publications aim at keeping security margins with respect to plausible contingencies above some threshold. Multiple contingencies are treated through heuristics [KVE00] or through constrained optimization [BMZ00, CVC02a].

So far the two types of congestions have been considered separately because voltage stability analysis requires more accurate tools than a mere DC load flow. This work proposes an integrated handling of both problems.

The methods to tackle congestions can be divided into two main categories [ESO99, CWW00]: *economical* (e.g. market splitting, auctioning) and *technical* (e.g. generation redispatch, transaction curtailment). The former methods can be used only in a preventive

[1] and many power systems are still vertically integrated

context, e.g. in the day-ahead market, while the latter are suited to both day-ahead and real-time applications. The methods considered in this work fall in the second category.

As regards the available means to remove a congestion, actions on voltages – through transformer ratios, generator voltages and reactive power injections – are limited either by the range of variation allowed for these variables or by their impact on the pre-contingency system configuration. For instance, in order to increase a security margin, it is unlikely that significant amounts of shunt compensation can be switched in the pre-contingency configuration, owing to the risk of overvoltages. The same holds true for generator terminal voltages. On the other hand, active power generation rescheduling and load curtailment can have a significant impact on both voltage stability and thermal overloads. However, these actions have a cost and hence must be taken in a transparent and optimal manner. In the sequel we will mainly concentrate on congestions that cannot be removed by "cost-free" means such as capacitors, transformer taps, FACTS devices, etc. although most of proposed algorithms could be extended to such control means.

We will consider another distinction related to control means to manage congestions. A first approach, referred to as *Injection Control* and denoted IC, relies on power injections, i.e. generator productions and load consumptions. A second approach, referred to as *Transaction Control* and denoted TC, relies on power transactions as defined in Section 4.9.5.

The IC approach can be implemented in any deregulated model. It consists in modifying the market-based generation scheme at the least cost, according to the generator bids [SHP98, Dav98, CWW00, WS00, KVE00, BMZ00, LRG02, CVC02a]. In order to ensure higher competition this method can be easily extended to also take into account load curtailment [BMZ00, Vou01, TB02, CVC02a].

As an alternative, the TC approach is applied in deregulated systems operated under the bilateral contract model. It consists in curtailing non-firm transactions in some optimal manner in order to relieve congestions [TLR97, GI98, CGM98, WV99, Ham00b, BGC00].

A Transmission Loading Relief (TLR) protocol is used by the North American Electric Reliability Council (NERC) in order to remove congestions [TLR97]. The main shortcoming of the TLR formula is its inability to take into account the benefit of counter flows, thereby implying bigger than necessary transactions curtailment [RA98, BGC00]. Improvements of the NERC protocol are suggested in [RA98, GS00, BGC00]. Reference [RA98] proposes a bid-based system, where each trader submits incremental/decremental price bids for both the supply and demand of the trader's transaction. This information would be used to determine centrally the optimal redispatch of transactions. Reference [BGC00] suggests to use multilateral trades, that is each trader is allowed to submit a balanced schedule with multiple generation and delivery points, rather than bilateral ones. An improved TLR formula which leads to curtail more on those trades with a larger influence on the congested line is additionally proposed. Finally, Ref. [GS00] suggests to compute the ATCs on an hour-ahead basis, instead of classical off-line computation which yields less accurate values.

Reference [GI98] proposes to curtail transactions according to the least distance, in the L_2-norm sense, between the operating point obtained if all desired transactions were accepted and the secure region. This approach completely disregards prices of transactions. On the contrary, Ref. [Dav98] suggests a weighted L_2-norm in which the weight associated to each transaction represents its price.

An iterative method to assess the feasibility of simultaneous transactions ahead of their scheduling time is presented in [Ham00b]. At each step of the procedure, transactions are ranked by decreasing order of their available transmission margin (ATM), which is defined as the difference between the ATC of the transaction path and the size of transaction. While the ATM of the first ranked transaction is positive, it is entirely accommodated and the ATCs of other transactions are updated. Although transparent, this procedure can be deemed unfair especially when accepted and rejected transactions have almost the same impact on security.

In Europe, within UCTE [2], the cross-border transmission capacity will be most likely allocated by a Coordinated Auctioning (CA) mechanism [ESO01, ACT02, PCH02]. Thus, TSOs organize simultaneous ("coordinated") auctions for each pair of adjacent countries. Market participants make bids which consist of a desired amount of power and a maximal price they are willing to pay for obtaining that power. As long as no congestion occurs all transactions are accepted at their desired level. Otherwise the (thermal) congestion is removed by minimizing the sum over all requested transactions of their bid price times their deviation from the requested quantity. Note that the CA is designed to manage congestions at international level, while leaving each country responsible of its internal congestions.

As regards the security requirements, most authors adopt the viewpoint of *security restoration* especially for thermal congestions, i.e. all branch currents must not exceed their upper limit in the base case as well as after any specified contingency. Comparatively less publications focus on *security margin restoration*, especially for voltage instability congestions, which requires in addition the system to have adequate security margins with respect to all postulated contingencies.

The various formulations dealing with security margin restoration aim at either maximizing a load power margin [DL92a, Can98, RCQ99, WL00] or minimizing an objective function with voltage security constraints [WET98, RCQ99, VFX99, FAM00, WPH01, Mil03]. The approach used in this work belongs to the second category.

There are basically two techniques to compute the controls aimed at increasing a security margin:

- perform a single optimization providing both the improved margin and the corresponding controls. Control and dependent variables are handled together. This optimization is performed with at least a set of equality constraints describing system operation at the limit point [DL92a, Can98, WL00]. Inequality constraints can be added on the limit point [WL00] or on both the limit and the base case oper-

[2] Union for the Co-ordination of Transmission of Electricity

ating points [RCQ99, VFX99, Mil03], which requires to incorporate the equality constraints relative to base case system operation;

- import into an optimization of the base case system operation constraints stemming from a separate margin computation and analysis [WET98, FAM00, WPH01, CVC02a].

Although it requires to iterate between margin calculation and control adjustments, the second technique is more "open": for instance, margins can be determined through more accurate, dynamic simulations, while the first technique relies on algebraic (typically load flow) equations treated as equality constraints. The second technique has been followed in this work.

All publications so far concentrate on a single configuration of the system and, where a contingency is mentioned, the control actions are taken in the post-contingency configuration. Our concern is to control the system in the pre-contingency configuration such that security margins are maintained with respect to several (dangerous or potentially dangerous) contingencies simultaneously. Again, the second technique seems more appropriate, in as much as the multiple contingencies can be handled separately (and possibly in parallel), thereby breaking down the problem into more tractable ones.

5.2 Injection control approach

Let us first recall that in any deregulated environment a *Balancing Market* (BM) operates to provide the TSO with means for compensating generation-load imbalances and managing congestions. Typically, the BM opens after the day-ahead market is cleared and operates as an auction market. Generators submit incremental (resp. decremental) bids indicating the minimal (resp. maximal) price at which they are willing to increase (resp. decrease) their outputs. Loads can also participate in the BM by bidding a minimal compensation price beyond which they agree to be curtailed.

5.2.1 Security restoration

In this section we require to operate the system so that none of the specified contingencies causes voltage instability or thermal overload. Thus, operating outside the overall security region (see Fig. 3.1), i.e. $\mathbf{P^o} \notin \mathcal{S}_T$, represents a system congestion which must be removed by bringing $\mathbf{P^o}$ back inside $\mathcal{S}_T$. In real-time, this requires to determine from the balancing market which among the cheapest (resp. most expensive) generations should be increased (resp. decreased) taking into account their efficiency in solving the congestion. In mathematical terms the objective is:

$$\min_{\Delta P_i^+, \Delta P_i^-} \sum_{i=1}^{m} (c_i^+ \Delta P_i^+ - c_i^- \Delta P_i^-) \tag{5.1}$$

where, for a generator which can be rescheduled, c_i^+ (resp. c_i^-) is the incremental (resp. decremental) bidding price, while for a load which can be curtailed, $\Delta P_i^+ = 0$ and c_i^- is the curtailment price.

In a pool market generators make incremental (resp. decremental) offers greater (resp. lower) than the system marginal price for each period of time, i.e. $c_i^+ > MP$ and $c_i^- < MP$ [CW98a, CW98b].

Note that this general congestion approach also applies to any of the unconstrained dispatch schemes established the day ahead. In this case $c_i^+ = MP$ and c_i^- represents the price bid by the i-th generators in the day-ahead market.

The TSO thus pays the generators which increase their output and receives payment from the generators which decrease their output. The incremented generators thus make more profit [3]. For instance, in a pool model, they are paid at a price $c_i^+ > MP$ for the additional power delivered ΔP_i^+. Similarly, the decremented generators save money because they refund the TSO an amount of energy at a lower price than the one paid to them by the TSO in the market settlement (pool model) or the one received from the customers (bilateral contract model). For instance, in a pool model, the decremented generators save the difference between the unconstrained marginal price of the system and its decremental bid times the amount of power decreased, i.e. $(MP - c_i^-)\Delta P_i^-$. The cost of congestion is further allocated to the market actors as an uplift cost [SHP98, Dav98, KVE00, CWW00].

Let $\Delta c_i^+ = c_i^+ - MP > 0$ and $\Delta c_i^- = MP - c_i^- > 0$ be the increment in price with respect to the initial one received by generators for their output variation. By substituting c_i^+, c_i^- from the above formulae and considering that $\sum_{i=1}^{m}(\Delta P_i^+ - \Delta P_i^-) = 0$, the objective (5.1) becomes:

$$\min_{\Delta P_i^+, \Delta P_i^-} \sum_{i=1}^{m}(\Delta c_i^+ \Delta P_i^+ + \Delta c_i^- \Delta P_i^-) \tag{5.2}$$

5.2.2 Minimal control change: a simplified formulation

An interesting particular case of the objective (5.2) is obtained when $\Delta c_i^+ = \Delta c_i^- = 1$. This disregards economics and aims at determining the minimal generation rescheduling and/or load curtailment needed to remove the congestion. This objective is attractive not only as a particular case of (5.2) but also by itself because it yields the least deviation from the unconstrained market solution and, hence, it hinders as little as possible the desired power transactions. In the sequel we will focus on this objective. Let us mention, however, that all the techniques to be discussed apply equally well to the more general objectives (5.1 and 5.2).

Incidentally this objective is appropriate to be used for the corrective control of an emergency situation. In such a case there may not be enough time to take the cheapest counter-

[3] we assume that generators make "reasonable" bids

measures, but only to minimize the amount of load shed in order to save the system from collapse.

Under the linear voltage and thermal security constraints whose derivation was explained in Sections 4.9.1 and 4.9.2, congestion management can be seen as the solution of the following optimization problem:

$$\min_{\Delta P_i^+, \Delta P_i^-} \sum_{i=1}^{m} (\Delta P_i^+ + \Delta P_i^-) \tag{5.3}$$

$$subject\ to: \sum_{i=1}^{m} n_{ri}(\Delta P_i^+ - \Delta P_i^-) \leq C_r \qquad r = 1, \ldots, c \tag{5.4}$$

$$I_{rj}^o + \sum_{i=1}^{m} \frac{\partial I_{rj}}{\partial P_i}(\Delta P_i^+ - \Delta P_i^-) \leq I_j^{max} \quad r = 1, \ldots, c \quad j = 1, \ldots, b \tag{5.5}$$

$$\sum_{i=1}^{m} (\Delta P_i^+ - \Delta P_i^-) = 0 \tag{5.6}$$

$$0 \leq \Delta P_i^+ \leq P_i^{max} - P_i^o \tag{5.7}$$

$$0 \leq \Delta P_i^- \leq P_i^o - P_i^{min} \tag{5.8}$$

The voltage security constraints (5.4) may be written for all contingencies, as explained in Section 4.9.2. However, we restrict the above formulation to the contingencies unstable at $\mathbf{P}^o$. The thermal security constraints (5.5) may be written for each branch in each post-contingency state, which leads to $c \times b$ constraints, as explained in Section 4.9.1. Nevertheless, in order to keep the problem tractable and because most thermal security constraints are not limiting, we derive them only for the overloaded branches or those close to be overloaded in the post-contingency states. The constraints (5.7, 5.8) stem from bounds on the control variables. Clearly, for a generator, P_i^o is the current production and P_i^{max} (resp. P_i^{min}) is the maximum (resp. minimum) active power allowed by the turbine. For a load, P_i^o is the current consumption and $P_i^{max} - P_i^o$ is the maximum amount of power which can be curtailed. Finally, (5.6) is the overall power balance equation, assuming that losses will not change significantly. If this is not deemed acceptable, a full OPF incorporating (5.4, 5.5, 5.7 and 5.8) can be used (in which losses are taken into account through load flow equality constraints).

In the above formulation, controls are of active power nature, but reactive aspects can be taken into account in the computation of the sensitivities n_{ri}. More precisely, if a change in active power ΔP_i at the i-th bus is accompanied by a change $\Delta Q_i = a_i \Delta P_i$ of the corresponding reactive power injection, the effective sensitivity is taken as:

$$n_{ri} = n_{riP} + a_i\, n_{riQ} \tag{5.9}$$

where n_{riP} and n_{riQ} are the active and reactive sensitivities. This formula is applied in the following two cases:

- load curtailment: when load is cut, both active and reactive powers vary. In the absence of a more precise information, loads are assumed to be decreased under constant power factor, in which case $a_i = \tan \varphi_i^o = Q_i^o / P_i^o$;

- generation rescheduling: it is well known from the capability curves that increasing the active production of a generator decreases its reactive reserve. To account for this effect a_i is taken as the (negative) slope of the $Q(P)$ curve. This applies only to generators under reactive power limit at the point where the sensitivities are computed. Note that if the last term in (5.9) is large enough, when decreasing active power generation, the benefit of an increased reactive reserve may outweight the detrimental effect of importing active power from remote generators.

A formula similar to (5.9) is used for the sensitivities $\partial I_{rj}/\partial P_i$, when considering load curtailment, in which case a_i has the same meaning.

The relationships (5.3-5.8) make up a linear programming problem which may be solved through the standard simplex method. Let $\Delta\mathbf{P}^*$ be its solution. Since constraints (5.4) and (5.5) are only linear approximations of the complex boundaries $\mathcal{B}_V$ and $\mathcal{B}_T$, the "corrected" operating point $\mathbf{P}^* = \mathbf{P}^o + \Delta\mathbf{P}^*$ may be located (hopefully slightly) outside the overall secure region $\mathcal{S}_T$, or conservatively inside. Moreover, one cannot exclude the case where a contingency would create both voltage and thermal problems. A contingency which triggers voltage instability at $\mathbf{P}^o$ is labelled voltage harmful in the filtering phase but, as the system does not reach an operating point where branch overloads can be checked, the latter problem is hidden.

We propose a two-step procedure to deal with such situations:

1. *voltage security restoration*. First, $\mathbf{P}^o$ is brought inside $\mathcal{S}_V$. To this purpose, the voltage security constrained optimization problem (5.3, 5.4, 5.6, 5.7, 5.8) is solved;

2. *thermal security restoration*. When all contingencies are voltage stabilized, thermal overloads are checked; if any branch is overloaded, the corresponding constraint (5.5) is added and a new optimization is performed, in order to bring $\mathbf{P}^o$ inside $\mathcal{S}_T$.

A flow chart of this approach is presented in Fig. 5.1.

Alternatively, one can first "partially" restore voltage and thermal security by solving the problem (5.3-5.8) except of the thermal constraints corresponding to voltage unstable scenarios. The latter constraints are checked at the solution of this problem and, if any of them is active, it is added to the previous set and the problem is solved again.

Note that after solving the voltage security constrained optimization problem, it is possible that new contingencies become unstable at $\mathbf{P}^o + \Delta\mathbf{P}_V^\star$, where $\Delta\mathbf{P}_V^\star$ is the solution of this problem. For each such contingency, a new voltage security constraint is derived and added to the already existing set, before the so enlarged optimization problem is solved. The procedure can be repeated until all contingencies are voltage stable at $\mathbf{P}^o + \Delta\mathbf{P}_V^\star$. The same procedure can be performed after the thermal security correction.

The L_1-norm objective (5.3) tends to put the effort on controls with the highest sensitivities, even if the gap with respect to other controls is small. This may be considered discriminatory by the involved market players, since sensitivities are not perfectly exact.

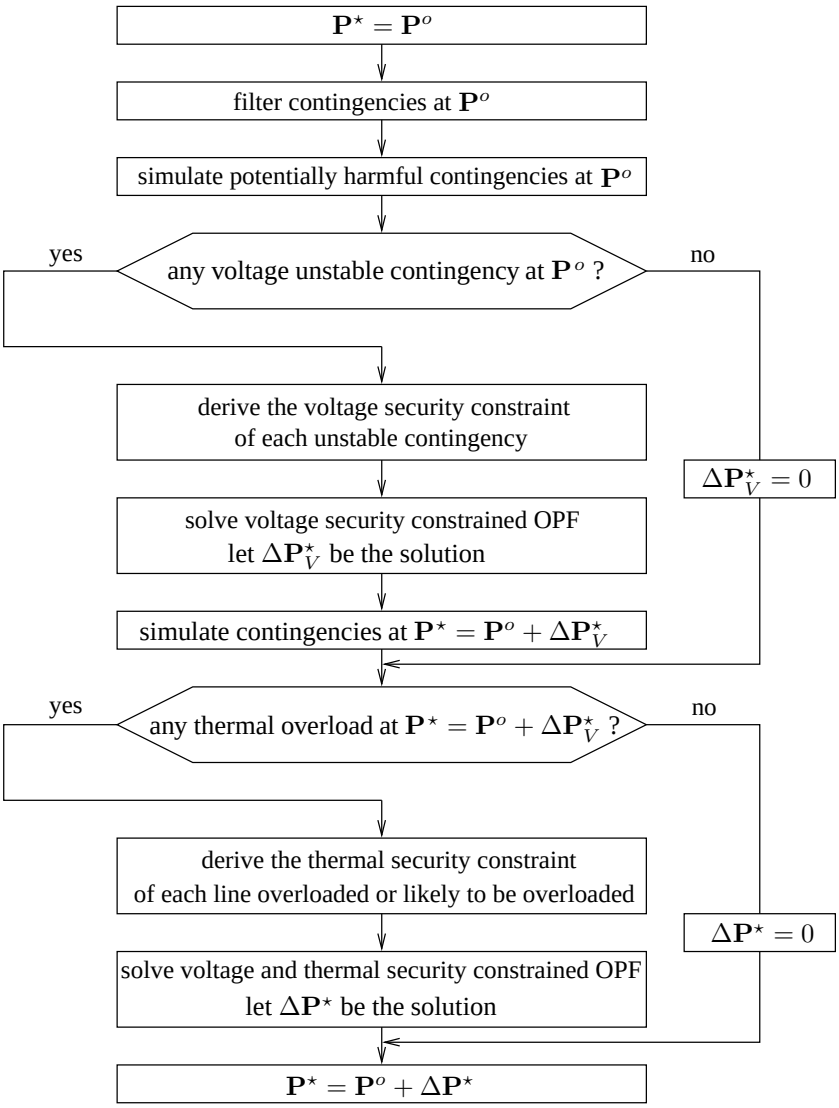

Figure 5.1: Algorithm of injection control for security restoration

This drawback can be attenuated by limiting the amplitude of the control changes. An alternative is to use the L_2-norm objective:

$$\min_{\Delta P_i^+, \Delta P_i^-} \sum_{i=1}^{m} (\Delta P_i^+)^2 + (\Delta P_i^-)^2 \tag{5.10}$$

On the other hand, this objective generally leads to a larger number of injection changes, which may be considered impractical by the TSO. This disadvantage could be mitigated by performing a second optimization, after removing from the candidate controls, those with small contributions ΔP_i.

The optimization problem (5.10, 5.4-5.8) can be solved using quadratic programming procedures [IMS97].

Note finally that future or current operating points $\mathbf{P}^o$ can be slightly modified in order to ensure that the system preserves a desired security margin [CVC02a].

5.2.3 Heuristic handling of nonlinearities

In the previous chapter we have derived linear voltage and thermal security constraints. We present now a heuristic technique to handle the nonlinearity of constraints (especially those related to voltage).

For the r-th unstable contingency, we consider that in (5.4) the *relative* values of the various n_{ri} sensitivities are correct while the C_r term may be affected by some error. We seek therefore at determining an improved value of this term. To this purpose we replace (5.4) by:

$$\sum_{i=1}^{m} n_{ri}\Delta P_i \leq f_r\, C_r \tag{5.11}$$

and we solve the optimization problem (5.3, 5.11, 5.6, 5.7, 5.8) adjusting f_r iteratively to obtain the best objective function together with a voltage secure point $\mathbf{P}^*$. A binary search is used to this purpose; it consists in building a smaller and smaller interval $[f_u\, f_a]$, such that the solution $\Delta\mathbf{P}^*$ of the linearized optimization problem (5.3, 5.11, 5.6, 5.7, 5.8) yields a voltage secure point $\mathbf{P}^*$ for $f_r = f_a$ and an insecure one for $f_r = f_u$. This is checked through the QSS simulation of the r-th harmful contingency. At each step, the interval is divided into two equal parts; if the midpoint leads to a secure (resp. insecure) optimum, it is taken as the new upper (resp. lower) bound. The procedure is repeated until the absolute difference between two successive objectives (5.3) becomes smaller than a tolerance, in which case f_r is set to f_a. Observe that for $f_r = 0$ the solution of the above optimization problem is $\Delta\mathbf{P}^* = \mathbf{0}$ and hence it corresponds to an insecure point because $\mathbf{P}^* = \mathbf{P}^o$. The search starts with $f_u = 0, f_a = 1$ if the very first optimization yields a secure operating point $\mathbf{P}^*$, and with $f_u = 1, f_a = 2$ if it yields an insecure one. Clearly, the iterative search of f_r consists in moving $\mathcal{H}_r$ parallel to itself, thus expanding or contracting the linear approximation of the voltage secure region (see Fig. 4.2).

This technique is applied to each constraint (5.4) (i.e. to each unstable contingency) separately. As a by-product, we obtain the control change required to make the system secure with respect to each contingency separately. Alternatively, one could use a single value f to correct all constraints, since not all of them are active at the optimum. This would significantly speed up the computations.

In principle, the same iterative procedure can be also used to find more accurate thermal constraints. However, a simpler technique exploiting the more linear nature of this problem can be used instead. Thus, once the post-contingency current I_{rj}^{real} has been obtained by QSS simulation, all sensitivities $\dfrac{\partial I_{rj}}{\partial P_i}$ are multiplied by:

$$\frac{I_{rj}^{real} - I_{rj}^{o}}{\displaystyle\sum_{i=1}^{m} \frac{\partial I_{rj}}{\partial P_i}\Delta P_i^*} \tag{5.12}$$

where the numerator is the real change in branch current between the optimum and the base case, and the denominator is the corresponding linear prediction. A single update of the sensitivities is usually enough.

5.2.4 Security margin restoration

In this section we require to operate the system so that none of the specified contingencies has a voltage or thermal security margin smaller than some threshold M_d.

As for security restoration, congestion management is stated as an optimization problem as follows:

$$\min_{\Delta P_i^+, \Delta P_i^-} \sum_{i=1}^{m} (\Delta P_i^+ + \Delta P_i^-) \tag{5.13}$$

$$subject\ to: \quad M_r^V(\mathbf{P}^o) + \sum_{i=1}^{m} S_{ri}^V\ (\Delta P_i^+ - \Delta P_i^-) \geq M_d \quad r = 1, \ldots, c \tag{5.14}$$

$$M_r^T(\mathbf{P}^o) + \sum_{i=1}^{m} S_{ri}^T\ (\Delta P_i^+ - \Delta P_i^-) \geq M_d \quad r = 1, \ldots, c \tag{5.15}$$

$$\sum_{i=1}^{m} (\Delta P_i^+ - \Delta P_i^-) = 0 \tag{5.16}$$

$$0 \leq \Delta P_i^+ \leq P_i^{max} - P_i^o \tag{5.17}$$

$$0 \leq \Delta P_i^- \leq P_i^o - P_i^{min} \tag{5.18}$$

The main difference with respect to the previous optimization problem (5.3-5.8) lies in the voltage and thermal security constraints (5.14 and 5.15), which are now derived as indicated in Section 4.9.3. Clearly, security restoration is a particular case of security margin restoration, corresponding to $M_d = 0$. Nevertheless, it makes sense to keep the two formulations separate since in a voltage unstable case, no margin, and hence no sensitivities, can be computed. In this case, the constraint (5.4) must be used instead of (5.14) until a security margin $M_r^V(\mathbf{P}^o + \Delta\mathbf{P}_V^\star)$ can be computed.

As for security restoration, we take into account reactive aspects in the computation of the sensitivities S_{ri}^V, through formula (5.9), in which S_{riP}^V (resp. S_{riQ}^V) is the sensitivity of security margin with respect to active (resp. reactive) injection. This formula is applied for both generation rescheduling or load curtailment.

As in the previous problem, there are situations where one cannot solve the above linear programming problem in a single step. For instance, if for a contingency, voltage instability is more constraining than thermal overload, its thermal security margin cannot be computed because one cannot check post-contingency currents in a voltage unstable scenario (for all stress levels beyond M^V). In such a case, we restore voltage and thermal margins in two steps:

1. *voltage security margin restoration.* The voltage security constrained optimization problem (5.13, 5.14, 5.16, 5.17, 5.18) is first solved. Let $\Delta\mathbf{P}_V^\star$ be the corresponding solution;

2. *thermal security margin restoration*. Once all voltage margins are restored, thermal overloads are checked at the point $\mathbf{P}^o + \Delta\mathbf{P}_V^\star$. If a contingency causes thermal

overload implies that its corresponding margin is smaller than M_d. In this case thermal margins are computed at $\mathbf{P}^o + \Delta\mathbf{P}^\star_V$, their corresponding constraints (5.15) are added to the previous set, and the so enlarged optimization problem is solved.

Let $M^V_r(\mathbf{P}^o + \Delta\mathbf{P}^\star_V)$ $(r = 1, \ldots, c)$ be the new voltage security margins obtained at the end of the first step. We expect to have $M^V_r(\mathbf{P}^o + \Delta\mathbf{P}^\star_V) \geq M_d$ $(r = 1, \ldots, c)$ with at least one inequality constraint of the type (5.14) binding at the solution, i.e.

$$\exists r : \; M^V_r(\mathbf{P}^o + \Delta\mathbf{P}^\star_V) = M_d$$

or in practice:

$$|M^V_r(\mathbf{P}^o + \Delta\mathbf{P}^\star_V) - M_d| \leq \epsilon$$

where ϵ is a tolerance. The r-th contingency is the most dangerous in the post-control situation, with a margin just equal to M_d.

Two situations, however, may prevent us from directly reaching this objective:

1. Under- or over-correction of margins. We have emphasized that the inequalities (5.14) are somewhat approximate with respect to the true nonlinear constraints. As a consequence, it can happen that some new margins are still smaller than M_d or, on the contrary, all of them are significantly larger than M_d. In such cases, we compute improved sensitivities and determine the new correction to apply to $\mathbf{P}^o$. Let us emphasize that this new correction is not added to the previous $\Delta\mathbf{P}^\star_V$, but rather replaces the latter. Now, we only have c new margins to improve $c\,m \gg c$ sensitivities. To face this lack of information, we correct all the sensitivities S^V_{ri} $(i = 1, \ldots, m)$ relative to the r-th contingency by the scaling factor:

$$\frac{M^V_r(\mathbf{P}^o + \Delta\mathbf{P}^\star_V) - M^V_r(\mathbf{P}^o)}{\sum_{i=1}^m S^V_{ri}\Delta P^\star_{Vi}} \tag{5.19}$$

in which the numerator represents the real change in the r-th margin and the denominator the one expected from linearization. As in the security restoration procedure, the above heuristics is equivalent to assuming that, for a given contingency, the relative values of the various sensitivities S^V_{ri} are correct. In principle, the procedure has to be repeated until the margins are distributed as indicated above.

2. Antagonistic controls. It can happen that changing $\mathbf{P}^o$ to meet the harmful contingency inequality constraints (5.14) causes harmless contingencies to become harmful. A first solution consists in extending the set of inequalities (5.14) to contingencies having a margin in an interval $[M_d \; M'_d]$, where we assume that margins larger than M'_d (i.e. much larger than M_d) will not fall below M_d. Note that incorporating to the optimization problem more inequalities (5.14) than necessary has no consequence; the latter will merely remain non-binding. Alternatively, we may stick with the M_d threshold and, if some new margins fall below M_d, add the corresponding inequalities to the former set and perform a new optimization.

The above two situations may also arise when treating thermal margins. Although the thermal security constraints (5.15) are much more linear, a similar scaling technique can be used if needed.

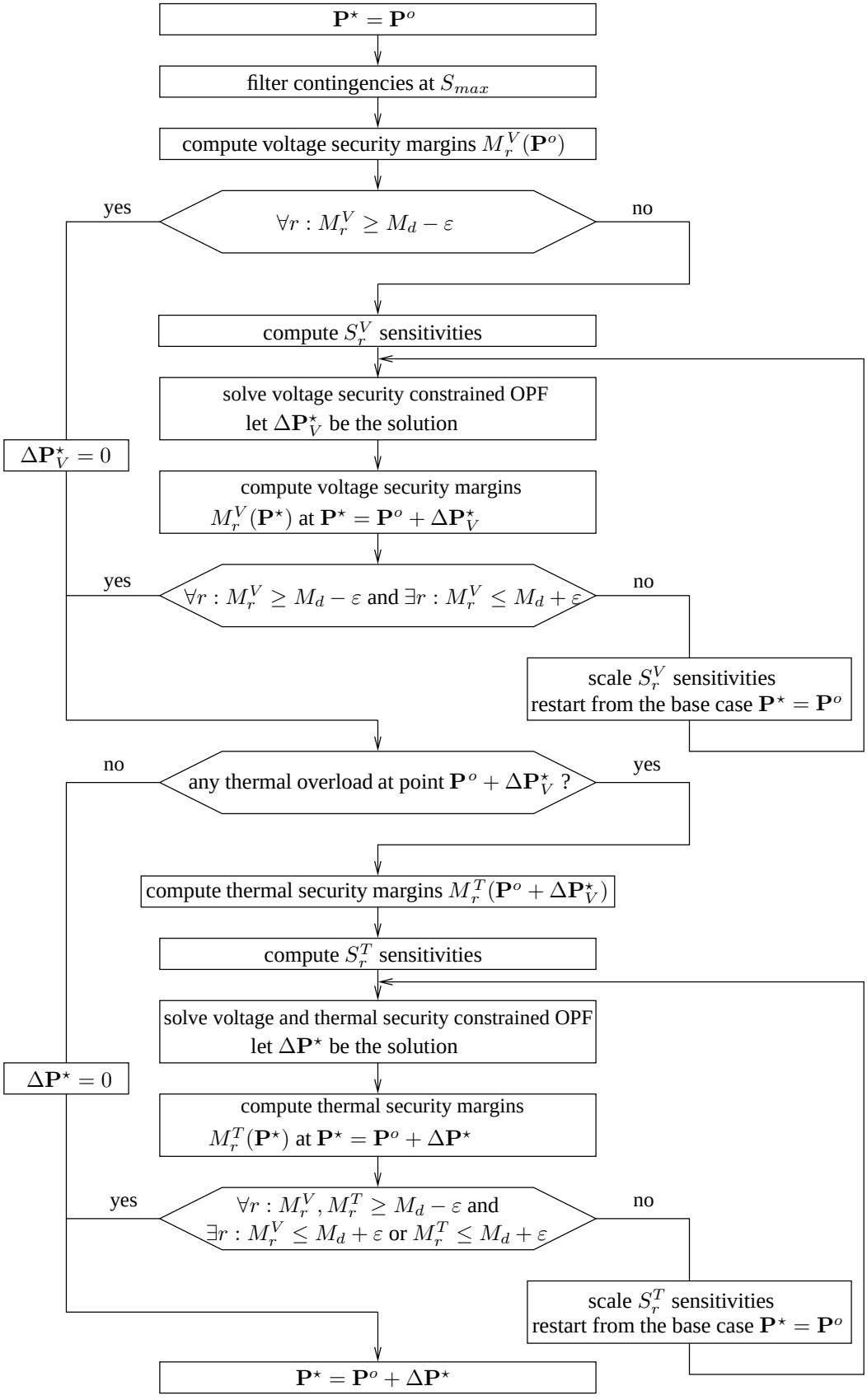

Figure 5.2: Algorithm of injection control for security margin restoration

The whole computational procedure is sketched in Fig. 5.2.

We finally mention a variant that saves the voltage security margin computation at the first iteration of the algorithm of Fig. 5.2. It consists in checking the contingencies after stressing the system at $\mathbf{P}^d = \mathbf{P}^o + M_d\mathbf{d}$. For the contingencies causing instability, (5.4) is used instead of (5.14), since $M(\mathbf{P}^o)$ is not known. For the subsequent iterations the original algorithm steps are followed. Note that after changing the system operating point into $\mathbf{P}^d = \mathbf{P}^o + M_d\mathbf{d}$, the problem reduces to security restoration, and the approach of Section 5.2 can be applied. This technique also applies to thermal security margin restoration.

5.3 Transaction control approach

As already mentioned, in a liberalized electricity market under bilateral contract model, suppliers and consumers arrange power transactions to their own financial interest. These simultaneous trades are then submitted to the TSO whose role is to check that they do not threaten system security. If they make the system insecure, the TSO has the possibility to curtail transactions in some optimal (and transparent) manner. This also holds true in real-time operation, as soon as a congestion appears.

The curtailment of a transaction implies in turn a modification of power injections at both sending and receiving buses involved in transaction. More precisely, a transaction is a linear combination of power injections and, hence, the security constraints derived with respect to transactions (4.50 and 4.47) are a particular case of the constraints determined with respect to power injections (5.4 and 5.5). This applies to both IC and TC approaches.

5.3.1 Security restoration

As discussed in Section 5.1 many objectives can be thought of, ranging from the least overall trade curtailment given by the L_1 norm to the (weighted) L_2 norm or the TLR formula.

In this work we use a L_2-norm objective, as originally proposed in [GI98], which consists in minimizing the sum of squared transaction deviations (from the base case values):

$$\sum_{k=1}^{t} \Delta T_k^2$$

This objective yields a compromise between market forces and system capability. All trades are weighted in terms of MW instead of money, which is non-discriminatory. This objective is fairer than a L_1 norm in as much as it reschedules trades according to their relative impact on the violated constraints, instead of focusing only on the trades with the highest impact.

The formulation is thus:

$$\min_{\Delta T_k} \sum_{k=1}^{t} \Delta T_k^2 \tag{5.20}$$

$$subject\ to: \quad \sum_{k=1}^{t} \tilde{n}_{rk} \Delta T_k \leq C_r \quad r = 1, \ldots, c \tag{5.21}$$

$$I_{rj}^o + \sum_{k=1}^{t} \frac{\partial I_{rj}}{\partial T_k} \Delta T_k \leq I_j^{max} \quad r = 1, \ldots, c \;\; j = 1, \ldots, b \tag{5.22}$$

$$-T_k \leq \Delta T_k \leq 0 \tag{5.23}$$

Note that, unlike the previous formulations (5.6 or 5.16), this one does not require an explicit power balance equation, since each transaction (4.45) is balanced by itself.

The solution $\Delta \mathbf{T}^*$ of this quadratic programming problem provides the closest distance of the proposed set of transactions $\mathbf{T}^o$ to the secure region defined by inequalities (5.21 and 5.22).

The algorithm of Fig. 5.1 can be used in this case as well, with the specification that the base case $\mathbf{P}^o$ must be replaced by $\mathbf{T}^o$.

The curtailment of a transaction can be performed in two ways:

1. decreasing source generator output as well as sink load consumption (or generator output);
2. preserving the load level and decreasing only the output of generators involved in trades to be curtailed. In this case the overall generation deficit can be compensated through an increase in the cheapest generators. This is a particular case of the IC approach where the ΔP_i^-'s are known and only the ΔP_i^+'s have to be determined.

5.3.2 Security margin restoration

The equations (5.20-5.23) can be straightforwardly extended to security margin restoration. The algorithm (see Fig. 5.2) still applies in this case.

In some systems it is possible that transactions are submitted to the TSO together with a minimal price at which they are willing to be curtailed [WS00]. This leads to consider a mixed objective function of the type (5.1) where the control variables are now the generator outputs, the load consumptions and the transactions.

5.3.3 Relationship with coordinated auctioning

Congestion management by coordinated auctioning [ESO01, ACT02, PCH02] consists in maximizing the *value* of the allocated capacity, i.e. the sum over all requested transactions

of their bid price multiplied by their bid quantity:

$$\sum_{k=1}^{t} b_k \, T_k \tag{5.24}$$

under security constraints, where b_k is the bid price of the k-th transaction and T_k the corresponding allocated power. The above objective can be easily transformed as follows:

$$\max_{T_k} \sum_{k=1}^{t} b_k \, T_k \;\Leftrightarrow\; \min_{T_k} \sum_{k=1}^{t} -b_k \, T_k \;\Leftrightarrow\; \min_{T_k} \sum_{k=1}^{t} b_k (T_k^o - T_k) \;\Leftrightarrow\; \min_{\Delta T_k} \sum_{k=1}^{t} b_k \, \Delta T_k \tag{5.25}$$

where T_k^o is the requested power of the k-th transaction ($0 \leq T_k \leq T_k^o$) and $\Delta T_k = T_k^o - T_k$ is the deviation between the requested and allocated values. The last objective is nothing but the one mentioned in Section 5.1.

As a particular case, if all transactions bid the same price, e.g. $b_k = 1, \forall k$, the coordinated auctioning objective (5.24) coincides with the least overall trade curtailment objective:

$$\min_{\Delta T_k} \sum_{k=1}^{t} \Delta T_k$$

Replacing (5.20) by the objective (5.24) and considering the same set of linear constraints (5.21- 5.23) leads to a linear programming problem, to which the procedure of Fig. 5.1 can be applied.

5.4 Numerical results from the Nordic 32 test system

This section presents congestion management results obtained with the Nordic 32 test system introduced in previous chapters.

5.4.1 Security restoration through IC

We analyze the voltage and thermal security of a given operating point with respect to a set of 49 contingencies. At the first step of the procedure (see Fig. 5.1) 37 harmless contingencies are filtered out using the method described in Section 3.6.2. The remaining 12 potentially harmful contingencies are analyzed in greater detail by QSS simulation. Among them, 4 false alarms are discarded, the corresponding contingencies being voltage stable. The 41 thrown out contingencies cause no thermal overload nor branches likely to be overloaded as a result of a possible voltage security restoration.

The remaining 8 harmful contingencies are listed in the first column of Table 5.1 [4]. Most of these contingencies are outages of southern generators. The explanation is that voltage

[4] the other columns will be used in the sequel

security is strongly related to the power transfer from the "North" to the "South" area of the system (see Fig. A.1). Since only the northern generators participate in frequency regulation, the active power lost in the South part adds to this transfer and prompts instability.

Table 5.1: Nordic 32 system : individual control of contingencies

contingency :	generation changes (MW)						objective
loss of	g4	g5	g6	g7	g16	g17b	(MW)
line A		-41		41			82
g8	-42			42			84
g14	-81		39	42			162
g15	-45			42	3		90
g16	-30			30			60
g17	-90			42		48	180
g17b	-25			25			50
g18	-7			7			14

We consider hereafter four combinations of controls and objectives, whose results are detailed in Table 5.2, where column V (resp. V+T) contains the voltage (resp. the overall voltage and thermal) insecurity correction.

Table 5.2: Nordic 32 system : changes in generation or load (MW)

	case							
generator	A		B		C		D	
or load	V	V+T	V	V+T	V	V+T	V	V+T
g2					-22	-39		
g3		-66		-75	-23	-40	-25	-53
g4	-90	-90	-78	-78	-25	-42	-28	-56
g5					-24	-39	-27	-51
g6					18	29		
g7	42	42			22	34	17	39
g14		66				11		
g15					17	28		
g16					17	28		
g17b	48	48			20	30		
1044							-16	-28
1045			-78	-78			-17	-28
4042								-12
4043				-75			-14	-26
4046								-12
4051							-16	-26
$\sum_{i=1}^{m}(\Delta P_i^+ + \Delta P_i^-)$	180	312	156	306	188	320	160	320

Case A: L_1 norm, generation rescheduling

For each of the 8 harmful contingencies, the voltage security constraint is identified iteratively, as described in Section 5.2.3. On the average, this procedure requires 6 iterations (and hence 6 post-control QSS simulations) to meet a 2 MW tolerance (the difference between the objective functions obtained for the marginally stable and unstable values of the

multiplier f_r, respectively). The shift in generation needed to restore voltage security for each harmful contingency, analyzed separately, is shown in Table 5.1. Broadly speaking, any decrease in generation in the "North" area, covered by an increase in generation in "South" area, diminishes the "North" to "South" power transfer, and hence enhances voltage security. In this respect the southern generator g7 appears as the "panacea" against all harmful contingencies. On the other hand, among the northern generators, g4 is the one with the greatest impact on voltage security.

Coming back to Table 5.2, one can see that the combination of controls that stabilizes the most dangerous contingency (loss of g17) alone is also the one that stabilizes all harmful contingencies simultaneously. Based on this observation [Mil03] presents a method which focuses on the iterative stabilization of the worst contingency only. Thus, at each iteration, one identifies the most dangerous contingency and adjusts the controls for ensuring the desired security level of the system with respect to this contingency. The latter may change from one iteration to another. Note that stabilizing the worst contingency does not always lead to the stabilization of all harmful contingencies. Indeed, "conflicting" controls may also exist from one contingency to another, as will be shown in Section 5.5.

The optimal solution to restore voltage security consists of increasing the production of g7 and g17b by 42 MW and 48 MW, respectively, and decreasing the one of g4 by 90 MW. The so obtained voltage secure operating point is next checked with respect to thermal overloads. It is found that the loss of line A causes the current in the line 4031-4032 to reach 107 % of its admissible value, while the trip of one circuit of the line 4022-4031 causes the current in the other circuit to reach 87 % of its limit value. The thermal constraints relative to these two branches are thus incorporated to the optimization problem. One can observe that the solution of the overall optimization problem includes the voltage insecurity correction. We hence deduce that the shift of 66 MW between g14 and g3 is necessary to remove the overload. Let us remark that, in this particular case, the overall optimal solution consists in merely adding the voltage and thermal insecurity correction.

Case B: L_1 norm, load curtailment

In this example, both generation rescheduling and load curtailment are allowed to restore voltage security. The maximum interruptible fraction of each load is limited to 20 % and power factors are preserved. The obtained correction consists in shedding 78 MW (and the corresponding 28 Mvar) at bus 1045, located in the voltage sensitive area, and compensating on the remote generator g4. With respect to Case A, the objective function (5.3) reaches a lower value (156 MW) thanks to the larger number of controls offered.

Case C: L_2 norm, generation rescheduling

This case is the same as Case A, except for the objective, which is taken as (5.10). This yields a larger number of changes, each of smaller magnitude: 22 non limited generators participate. The total rescheduling needed to restore voltage security is of 208 MW, greater than the one provided by the L_1-norm objective.

In the solution shown in Table 5.2, however, the changes have been limited to 9 generators, selected on the basis of their sensitivities. The total power rescheduling is 188 MW, i.e. somewhat larger than with the L_1 norm. Among the various participating generators, the

rescheduled powers are quite close, which is the consequence of close values of their sensitivities. A comparison with Case A shows that with the L_2-norm the effort is shared by more generators, which is less discriminatory. Indeed, in Case A, generator g4 takes on the whole effort because of somewhat higher sensitivities; the latter, however, are not perfectly accurate values and a slight change in the computational procedure could have led another generator to take the whole effort.

After adding thermal overload constraints, one more generator with a rather high sensitivity (g14) is rescheduled.

Case D: L_2 norm, load curtailment

Again, when all controls are allowed to vary, the total change in power injections to stabilize the system is 182 MW, a greater value than in Case B. When only the most sensitive generators are allowed to vary, a smaller variation (160 MW) is obtained, involving 4 generators and 4 loads.

After including thermal security constraints to the optimization problem, two more loads are allowed to be curtailed (4042 and 4046) because of their relatively high sensitivities.

5.4.2 Security margin restoration through IC

We start from the previous example and consider the operating point obtained after restoring voltage and thermal security as in Case A in Table 5.2. At this operating point, no contingency causes voltage instability or thermal overloads. We now consider the problem of bringing voltage and thermal security margins (for all 49 contingencies) to at least a desired level, i.e. greater or equal to a threshold M_d, which we take as 250 MW.

With respect to this target, 10 contingencies are harmful, i.e. have a margin smaller than M_d, as shown in the second column of Table 5.3. To anticipate for possible antagonistic effects, we follow the procedure of Section 5.2.4 and choose $M_d^{'} = 300$ MW. This leads to monitoring $c = 12$ contingencies.

We consider hereafter four combinations of controls and objectives, whose results are detailed in Tables 5.3 and 5.4.

Case A: L_1 norm, generation rescheduling

The optimization problem (5.13-5.18) leads to reschedule 241 MW (objective function (5.13) $= 241 \times 2 = 482$ MW). It consists of increasing the production of generators g6, g17b and g17 which are located in the voltage sensitive area, while decreasing the generation of g4 and g3, located far away in the North. This decreases the North to South power transfer. After this generation shift, all margins are above 250 MW and one of them (loss of g14) approaches this threshold by less than $\epsilon = 10$ MW; there is thus no need for another correction. One can observe that the margin relative to the loss of generator g6 increases significantly less (167 MW) than the others (from 210 to 302 MW). This is due to the fact that the rescheduling raises the production of g6 by 65 MW, and hence the loss of this increased generation causes the North to South transfer to increase correspondingly

Table 5.3: Nordic 32 system : voltage security margins before and after control

contingency: loss of	base case	voltage margins (MW) A	B	C	D
g14	42	252	248	253	248
g15	107	338	314	279	330
line A	132	377	350	369	348
g8	134	353	340	343	340
g16	134	352	340	296	341
g17	156	458	339	382	364
g18	164	401	384	383	380
g19	168	403	389	390	383
g20	168	403	389	390	383
g17b	176	398	393	398	389
line B	266	495	478	485	475
g6	282	449	497	462	489

Table 5.4: Nordic 32 system : changes in generation or load (MW)

generator or load	A	B	C	D
g2			-74	-68
g3	-54	-20	-75	-68
g4	-187	-187	-76	-69
g6	65		47	
g15			43	
g16			45	
g17	63		45	
g17b	113		45	
1044		-141		-54
1045		-66		-51
4042				-50
4043				-50
$\sum_{i=1}^{m}(\Delta P_i^+ + \Delta P_i^-)$	482	414	450	410

(due to already mentioned frequency control effects). An opposite example is provided by the loss of the southern generator g17. Despite the fact that the tripping of g7 increases the North to South transfer, the security margin of this contingency shows the greatest increase (302 MW) owing to the increased production of its neighbouring generator g17b.

After the controls are applied, all thermal security margins are above $M_d = 250$ MW and the procedure stops.

Case B: L_1 norm, load curtailment

In this example, both generation rescheduling and load curtailment are allowed to restore security margins. Interruptible fractions and power factors are handled as in the previous section. The solution consists of shedding 207 MW in the voltage sensitive area, and again compensating on the remote generators g4 and g3. With respect to Case A, the objective function (5.2) reaches a lower value (414 MW) thanks to the larger number of controls offered.

Case C: L_2 norm, generation rescheduling

This case is the same as Case A, except for the objective, which is taken as (5.10). Paradoxically, when controls are limited to 8 generators (selected on the basis of their sensitivities), the total rescheduling (225 MW) is less than with the L_1 norm (241 MW), while the margin of the severest contingency has been increased to almost the same value (252 vs. 253 MW). This unexpected result is attributed to the nonlinear effects being well known that sensitivities may become inaccurate for large injections variations. We exemplify this outcome for the most dangerous contingency (loss of g14). Table 5.5 shows the sensitivities of the voltage security margin with respect to the most influencing generations, in the base case (denoted by BC) as well as in 4 operating points (denoted by OP1 to OP4). Starting from the base case, the latter are obtained by progressively imposing the controls provided by the L_1-norm optimization (column A in Table 5.4). Namely, OP1 is obtained after increasing g6 by 50 MW and decreasing g4 by the same amount. OP2 is obtained after increasing g6 and g17b by 65 MW and 35 MW respectively, while decreasing g4 by 100 MW, etc.

In the base case, the production of g4 appears as the best to be decreased (owing to its small sensitivity). However, at the other four operating points, its sensitivity changes due to nonlinear effects, and it becomes less efficient than g3 and g2. One can also observe that generators g15 and g16 become more efficient than g6 as the operating point changes from OP1 to OP4. Moreover, g15 and g16 become even more efficient than g17 and g17b for OP3 and OP4.

The paradox of obtaining a better L_1-norm objective when optimizing the L_2 norm has been seldom observed. This is likely to occur when the best controls have very close values of their sensitivities, as shown for the base case in Table 5.5.

Table 5.5: Nordic 32 system : generators sensitivities for different operating points (pu)

generator	BC	OP1	OP2	OP3	OP4
g2	-0.009	-0.012	-0.013	-0.014	-0.016
g3	-0.010	-0.013	-0.014	-0.016	-0.016
g4	-0.017	0.004	0.023	0.041	0.053
g6	0.816	0.796	0.785	0.785	0.786
g15	0.799	0.797	0.792	0.793	0.796
g16	0.799	0.797	0.793	0.793	0.796
g17	0.807	0.804	0.796	0.790	0.786
g17b	0.807	0.804	0.796	0.789	0.785

Incidentally, note that in Case C, a second optimization is needed to make the smallest margin approach 250 MW by less than ϵ.

Case D: L_2 norm, load curtailment

Expectedly, the control effort is shared by a larger number of injections than in Case B. Once more, we find that minimizing the L_2 norm provides a slightly better objective than minimizing the L_1 one (410 vs. 414 MW).

To summarize, the L_1 optimization yields a smaller number of changes and (usually) a

smaller total power change. On the other hand, the L_2 optimization is more robust with respect to inaccuracies on the sensitivities that could lead to shifting the control effort from one generator (or load) to another.

5.4.3 Security restoration through TC

We now consider transactions as control variables. For the sake of comparison, we consider the same (voltage and thermal) insecure operating point as in Section 5.4.1 but we assume now that this base case situation stems from the request of 10 transactions, as detailed in Table 5.6).

Table 5.6: Description of the requested transactions

transaction	source(s)	sink(s)	$T_{desired}(MW)$
T_1	g21	g18	40
T_2	g1,g2,g3	g15,g16	50
T_3	g4,g5	g17,g17b	40
T_4	g9,g10	1041,1045	50
T_5	g1,g2,g3	1011,1012,1013,1014	30
T_6	g8	2031	10
T_7	g19,g20	4045	20
T_8	g12	4044	10
T_9	g14	g8	20
T_{10}	g18	g11	20

For comparison purposes, we first use an L_1 norm to restore voltage security. The solution of the corresponding optimization problem consists in merely reducing transactions T_2 and T_4, which have the greatest impact on voltage security (see column A in Table 5.7). Adding thermal security constraints to the optimization problem requires to curtail two more transactions (T_1, and T_3) as shown in column B of the same table.

The L_1 norm is "unfair" because it leads to curtailing transactions by decreasing order of their impact on security: after voltage and thermal security have been restored, transactions T_4, T_3 and T_2 are completely removed from the market.

Expectedly, this effect is attenuated when using the L_2 norm, as shown by columns C and D of Table 5.7, which correspond to columns A and B, respectively. The quadratic objective leads to cutting down some more power (-178.3 MW vs. -161.1 MW for the L_1 norm) but the effort is distributed over the transactions in a fairer way.

One can observe that acting on transactions instead of power injections is less efficient. For instance, when acting on power injections to restore voltage security (with norm L_1), one needs to curtail either 78 MW load, if loads are considered as control variable, or to reschedule 90 MW of generation, if only generators are taken as control variables (see Table 5.2) by comparing with 93.5 MW of transactions curtailment. The same applies for the L_2 norm: 80 MW load curtailment or 94 MW generation rescheduling vs. 110.1 MW transactions curtailment. The inefficiency of using power transactions as control variables

Table 5.7: Curtailment of transactions for voltage and thermal security restoration

transaction	A	B	C	D
ΔT_1		-21.1	-24.4	-38.2
ΔT_2	-43.5	-50	-25.3	-41.4
ΔT_3		-40	-15.4	-30.8
ΔT_4	-50	-50	-26.8	-42.8
ΔT_5			-0.1	-0.2
ΔT_6			-5.2	-7.5
ΔT_7			-2.9	-5.3
ΔT_8			-10	-10
ΔT_9				
ΔT_{10}				-2.1
$\sum_k \Delta T_k$	-93.5	-161.1	-110.1	-178.3

is due to the fact that each transaction is a linear combination of power injections which may contain less efficient injections.

5.5 Numerical results from the Hydro-Québec system

We briefly present here an example of antagonistic controls observed on the Hydro-Québec (HQ) system. Fig. 5.3 sketches the structure of the 735-kV transmission system.

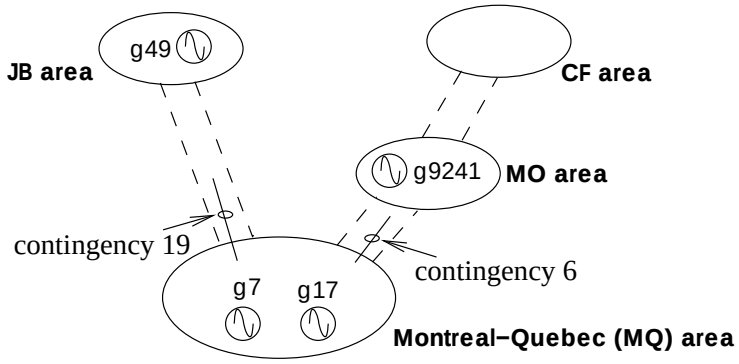

Figure 5.3: Simplified Hydro-Québec system

The stress consists of increasing the demand in the Montréal-Québec (MQ) area, where most of the load is concentrated, and the generation in the JB, CF and MO areas. Security margins are computed for a set of 37 contingencies, with $S_{max} = 1000$ MW. Two contingencies have limits lower than S_{max} (see Table 5.8). They are located in the MO-MQ and JB-MQ corridors, respectively.

We consider the minimal generation rescheduling in the L_1 sense, corresponding to four values of M_d. The computed controls are shown in Table 5.9. Three successive optimizations are required on the average, in order to bring (at least one) of the post-control margins close to M_d, as explained in Section 5.2.4. This is attributed to the fact that

Table 5.8: Hydro-Québec system : pre- and post-control margins

contingency	margins (MW)				
	base	after rescheduling, for $M_d =$			
	case	300	400	425	525 and 400
6	264	299	398	428	529
19	398	480	469	428	399

Table 5.9: Hydro-Québec system : generation rescheduling (MW)

gener	$M_d = 300$	$M_d = 400$	$M_d = 425$	$M_d = 525$ and 400
g9241	-35	-48	-67	-137
g7	27	27	27	27
g17	8	13	13	13
g49		8	27	97

margins change more abruptly with controls, under the effect of the shunt reactor tripping devices.

For $M_d = 300$ MW, contingency 6 is harmful. Expectedly, the minimal generation rescheduling consists in decreasing the power flow in the MO-MQ corridor, shifting 35 MW from g9241 (MO area) to g7 and g17 (MQ area). Both margins are increased. However, after this preventive control, almost no active power reserve is left to the MQ area. Therefore, when M_d is set to 400 MW, the minimal generation rescheduling slightly increases the production of g49, located in the JB area. This is accompanied by a slight decrease in the margin of contingency 19 (which, however, remains above M_d). If M_d is set to 500 MW, for instance, the problem is infeasible. Indeed, at this level, bringing both margins above M_d would require to decrease both corridor flows. The largest value of M_d for which a solution exists is 425 MW. The corresponding results are given in Tables 5.8 and 5.9; both margins have been raised at the 425 MW threshold. By setting (for checking purposes) M_d to 525 MW for contingency 6 and 400 MW for contingency 19, the problem is feasible again, with the solution shown in the last column of each table.

5.6 Final discussion

Before deregulation, power systems have been naturally operated with comfortable security margins relative to the "N-1" plausible contingencies. At the same time, system operators have relied on preventive rather than on corrective control in order to ensure suitable security.

Some recent publications (e.g. [SAK98, UPK98, Weh99, CMP01, CCS02]) question this deterministic security criterion applied by most transmission companies, as being too conservative. It is first argued that it often results in unnecessary high operation costs. A second quoted limitation is that it does not take into account the likelihood of the various contingencies, but rather treats them all as equiprobable. Finally, in the deregulated context, the N-1 criteria is felt as an obstacle rather than an incentive to competition. On the other hand, during severe weather conditions likely to affect transmission lines or in view

of the non negligible probability of having protection failures, even the N-1 criterion may not provide enough security.

Admittedly, there is an increasing need for more flexible security criteria especially due to the higher pressure exerted by market players. There are incentives to rely less on preventive actions and more on corrective countermeasures. In this context the security margin restoration considered in this work might be considered too severe. Indeed, on one hand, security margin computation depends on the assumed stress direction, whose choice may be detrimental to some market players. On the other hand, depending on the choice of the M_d threshold, requesting some security margin may hamper competition to a greater extent than requesting the survival of the system.

The future is most probably in a careful tradeoff between preventive and corrective controls [SAK98, UPK98, Weh99, CMP01]. The objective will be to minimize the overall cost of both preventive and corrective actions. However, while the cost of preventive actions is rather easy to calculate, getting a reliable estimate of the corrective costs is a challenging problem for voltage unstable scenarios as well as for severe post-contingency thermal overloads. Indeed, if the system is not equipped with an undervoltage load shedding protection [Tay92, Moo02] it is very difficult to foresee how system operators will react during a voltage unstable scenario (in such cases it would be suitable to ensure adequate voltage security margins). On the other hand, if the system is equipped with such an automatic protection [5] the interruption costs could be better estimated. The same holds true for mild thermal overload situations. However automatic or human corrective countermeasures may fail to remove a congestion and therefore the interruption costs may be greater than foreseen. Finally, the results of this "combined" optimization strongly rely on the probabilities of disturbance occurrence for which enough accurate values may not be available.

The above suggested "take-risk" strategies are more appropriate when dealing with thermal overloads than with voltage instabilities. The former are softer than the latter in the sense that operators generally have more time to counteract them. Moreover, an overloaded branch may be disconnected without necessarily redirecting the overload to other elements, thereby allowing system operation to continue in the $N-1$ configuration until operators take appropriate actions to restore the system integrity. In this respect, it could be less acceptable to refuse power transactions because some thermal margins are (positive but) lower than the desired threshold M_d.

Finally, if power generations are the only controls available, it is possible that no method succeeds in managing a congestion. Such a situation may become even more plausible under the pressure of market laws which tend to fully use cheaper generators and exhaust reserves (except those needed for ancillary services). Besides the inclusion of load curtailment among the control variables, starting-up of out-of-merit generators (and possibly shutting-down of in-merit generators) can be conceived. Our congestion management formulations (5.3-5.8 or 5.13-5.18) should be modified in order to take switching units into account [LRN00, LRG02, Mil03]. This new problem could be tackled by mixed

[5] so far such protections focus rather on saving the system with, hopefully, the least load shedding (especially if the system may become unstable very quickly) than on performing the cheapest load curtailment. Protections should be improved to take into account load compensation prices.

linear-integer programming.

Chapter 6

Computation of Simultaneous Available Transfer Capabilities

This chapter deals with the evaluation of Available Transfer Capabilities (ATC) in the presence of multiple transactions. It thus extends the notions and techniques which were presented in Chapter 3 in the case of a single system stress.

We first explain the motivation for computing simultaneous ATCs. We then propose an optimization-based formulation to obtain the latter. We finally present application results, including a comparison between simultaneous and non-simultaneous ATCs.

At the level of computation techniques this issue offers some similarities with the one of congestion management, although the objectives are totally different.

As in previous chapters, our approach encompasses voltage instability and thermal overload aspects.

6.1 Introduction

6.1.1 ATC definition

In a deregulated system under bilateral contract model the determination of ATCs relative to all foreseen trade paths is a crucial information [ATC96, Sau97]. The ATC values may be posted on a Website so that each market player can use them in order to make reservation. ATC is a measure of the transfer capability remaining in the physical transmission network for further commercial activity over and above already committed uses [ATC96]. Note that the ATC terminology does not apply to bilateral contracts exclusively; more generally, an ATC refers to the trade capability between two regions of the same country (as in USA) or between two countries (as in Europe [ESO99]).

Most publications up to now rely on the following ATC definition given by NERC[1] [ATC96]:

$$ATC = TTC - ETC - TRM - CBM$$

where TTC is the Total Transfer Capability, ETC represents the Existing Transmission Commitments, TRM is the Transmission Reliability Margin and CBM the Capacity Benefit Margin.

TTC is defined as the amount of electric power that can be transferred over the interconnected transmission network in a reliable manner, i.e. while meeting all predefined pre- and post-contingency system conditions. The latter may involve steady-state security, voltage stability and angle stability constraints.

TRM is defined as the amount of transmission transfer capability necessary to ensure that the interconnected transmission network is secure under a reasonable range of uncertainties in system conditions. So basically TRM accounts for uncertainties in the model as well as simultaneous trades. Admittedly, very few TRM evaluation methods have been proposed [Sau97, GN99, GDA02]. These approaches range from probabilistic computations to simple rules such as taking TRM as a fixed percentage (e.g. 5 %) of TTC [Sau97].

CBM is defined as the amount of transmission transfer capability reserved by load serving entities to ensure access to generation from interconnected systems to meet generation reliability requirements. As TRM, CBM is also seldom mentioned in papers dealing with ATC calculations. Both probabilistic and deterministic methods may be used in reliability evaluation [OS02].

Thus, the computation of an ATC requires the computation of the corresponding TTC as well as the TRM and CBM margins. In this work, the latter are neglected. In this case, as far as the existing transmission commitments are known, the TTC and ATC computations are equivalent.

Most ATC computation methods proposed up to now focus on thermal constraints [GN99, Ham00a, CWW00, MK01], and are based on the DC load flow model. Voltage stability constrained ATCs have received comparatively less attention. The methods proposed for their computation rely on continuation power flow [ETW98], repeated power flow [GN99], security constrained OPF [MBG02] or QSS simulation [CCM00].

Note that, soon after implementing the ATC protocol in USA many congestions appeared due to the fact that market players reserved transmission capacity on a contractual basis whereas a significant fraction of the physical power flows was taking place on other paths (parallel flows) [CWW00]. Clearly, the above type of reservation can only work in a radial system (where the ATC of a chain of paths is the smallest ATC among all paths belonging to that chain), but not in a meshed one. Nowadays, the trend is to use correctly the posted ATCs, that is to reserve the real physical power paths.

[1] North American Electric Reliability Council

6.1.2 Non-simultaneous ATCs

Chapter 3 has presented efficient methods for the computation of secure operation limits in a given direction of stress. Basically, an ATC is nothing but the security margin obtained from such a computation, when the direction of stress is adjusted to match the sources and sinks involved in the transaction. Simultaneous Binary Search (see Section 3.5.2) is well suited to this type of computation since the ATC value is dictated by the most constraining contingency of the specified set. Examples of SBS method have been presented in Section 3.7.

When several transactions have to be taken into account, the first method to come to mind consists in repeating the above computations for the direction of stress corresponding to each transaction separately. This leads to computing *non-simultaneous ATCs*.

On the basis of non-simultaneous ATC values, the allocation of transmission capacity must be made in two steps. First, the non-simultaneous ATCs are computed for all foreseen paths. This establishes the maximum amount of power that can be reserved by each trader. Then, traders send to the TSO the quantity of power they wish to reserve; each quantity is below the ATC of the path. The TSO checks if all trades can be accommodated. If no security constraint is violated, all requested transactions are allowed; otherwise, the system is congested and transactions must be curtailed. This can be done using methods described in Chapter 5.

6.1.3 Simultaneous ATCs

A drawback of the non-simultaneous ATC computation is that each transaction is considered separately whereas the various transactions take place simultaneously. Therefore, the volume of one trade will to some extent affect the ATC of the other trades.

One could think of accounting for this effect through the value of TRM but, to our knowledge, no systematic method has been proposed to this purpose. One solution consists in computing the sensitivities of ATCs with respect to simultaneous transfers. Such sensitivities can be computed analytically [GDA02], by finite differences [GN99] or as a by-product of an OPF aimed at computing the TTC [MBG02]. In the latter case, the TTC sensitivity to the thermal limit of the congested lines are the Lagrange multipliers of the constraints active at the solution point. Such sensitivities can be useful to quickly update the ATCs when other transactions or operating conditions change.

Alternatively, one can consider several transactions simultaneously in the ATC computation. In fact, the latter problem is not completely new. The pioneering paper [LA73] focuses on the determination of the simultaneous maximal interchange between several companies under thermal security constraints. Besides, probabilistic approaches (relying mainly on Monte Carlo simulations) are proposed in [XM96, MMG97] to assess the simultaneous transfer capability of a power system.

A first approach to this problem in the very context of ATC computation is presented in [MK01]. It consists in maximizing, in the L_1 sense, the sum of all possible transactions

under linearized operating constraints corresponding to circuit loading, bus voltage magnitude and generator reactive power. More recently, reference [LL02] proposes to maximize the product of transactions over a security region bounded by linearized operating constraints based on load flow equations.

The above publications have inspired the work presented hereafter and published [CVC02c].

6.2 Simultaneous ATCs as the solution of an optimization problem

6.2.1 Problem statement

We have defined in Section 3.3 voltage and thermal security regions in the power injection space. These concepts can be straightforwardly extended to the transaction space. Let us consider the t-dimensional space of transactions, each point of which corresponds to a particular value of the pre-contingency transactions.

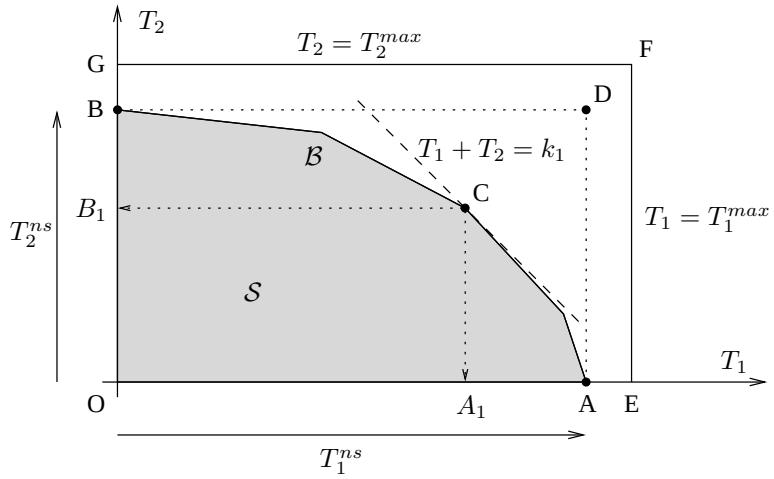

Figure 6.1: Secure region and ATC's in 2-D transaction space

We define the *transaction security region* $\mathcal{S}$ as the set of points of the transaction space such that no contingency of a specified list causes thermal overload nor voltage instability. ATCs are associated with points lying on the boundary $\mathcal{B}$ of this secure region $\mathcal{S}$.

The concept of simultaneous ATC is best illustrated on the following two-dimensional example. Let us consider the space of two transactions T_1 and T_2 as depicted in Fig. 6.1. Lower and upper bounds restrict the transaction space to the interior of rectangle OEFG, where O corresponds to the base case $\mathbf{T}^o$. Moreover, let us assume for simplicity that the secure transaction region $\mathcal{S}$ is piece-wise linear.

If each transaction is considered separately, the ATC for T_1 (resp. T_2) corresponds to point A (resp. B). Now, if both transactions were accepted at these maximal values the system would operate at point D, outside the secure region. It is thus necessary to compute ATCs

by maximizing a function of T_1 and T_2 while taking into account the boundary $\mathcal{B}$, which expresses the influence between the two transactions.

The first function to come to mind for the simultaneous ATC computation is the sum of transactions [MK01], i.e. the L_1 norm:

$$\max_{T_1,T_2 \in \mathcal{S}} (T_1 + T_2)$$

This objective is directly related to the maximum use of the network. In the simple example of Fig. 6.1, the optimum corresponds to point C and its projection on the two axes (points A_1 and B_1) provides the ATC of the two simultaneous trades T_1 and T_2.

Consider, however, the simpler form of secure region shown in Fig. 6.2. This situation may appear in a system where one constraint is more restrictive than all others. In this simple example, the solution of the L_1 norm optimization problem is point A, where transaction T_2 is zero ! In other words, maximizing the L_1 norm tends to allocate network capacity to the transaction with the least effect on security. This situation may be considered discriminatory, especially when both transactions have almost equal effects, which corresponds in Fig. 6.2 to a boundary $\mathcal{B}$ almost parallel to the equi-($T_1 + T_2$) lines. In this case, a mere change in slope from -44 to -46 degrees, for instance, causes the optimum to jump from A to B !

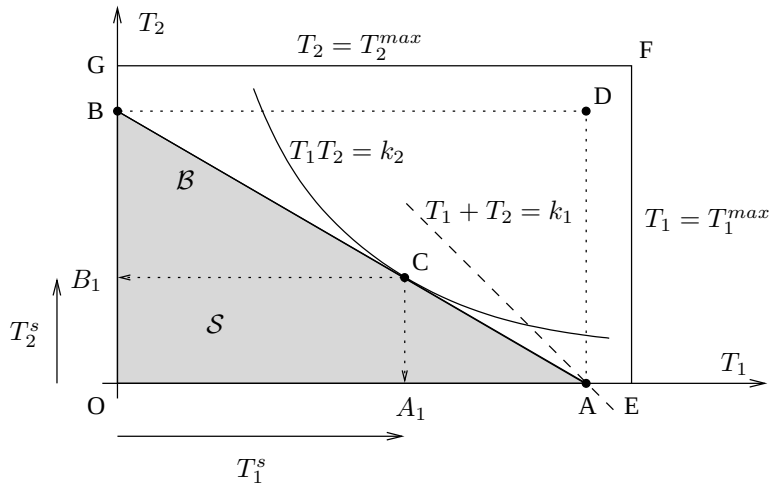

Figure 6.2: Secure region and ATC's in 2-D transaction space

Admittedly, this effect is less pronounced when the boundary is piece-wise linear (as in the example of Fig. 6.1) or when the bound constraints are more limiting (point E lying in between O and A in Fig. 6.2): T_2 is then nonzero at the optimum.

An alternative, however, is to maximize the product of transactions [LL02], namely:

$$\max_{T_1,T_2 \in \mathcal{S}} T_1 T_2$$

In Fig. 6.2, the optimum now corresponds to point C, where an hyperbola $T_1 T_2 = k_2$ is tangent to the boundary $\mathcal{B}$. The ATC values correspond to the projections of point C on the axes (points A_1 and B_1). As can be seen, this objective is less discriminatory and,

more importantly, allocates capacity to the transactions in proportion with their respective impact on security.

This objective aims at maximizing the area of rectangle $\mathrm{O}A_1\mathrm{C}B_1$ inside the secure region. The larger the area of this rectangle, the more flexibly transactions can be dispatched. Indeed, a trade is not obliged to use its entire ATC, which makes it necessary for the TSO to provide flexible solutions when transactions do effectively not reserve the whole computed capacity. In the case of Fig. 6.1 the two objectives will yield very close, if not identical, optimal point.

Note finally that the ATC computation requires the base case to belong to the secure region ($\mathbf{T}^o \in \mathcal{S}$). Otherwise the system is congested and any technique discussed in the previous chapter can be used to relieve the congestion.

6.2.2 Formulation of the optimization problem

We derived in Section 4.9.5 voltage and thermal security constraints in terms of transactions, given by formulae (4.50) and (4.47). Under these linear approximations, the ATC of the t simultaneous transactions, taking into account c contingencies, can be obtained as the solution of the following optimization problem:

$$\max L_1 = \sum_{k=1}^{t} T_k \tag{6.1}$$

$$\text{or} \qquad \max L_\pi = \prod_{k=1}^{t} T_k \tag{6.2}$$

$$subject\ to: \qquad \sum_{k=1}^{t} \tilde{n}_{rk}\, T_k \leq C_r \quad r = 1, \ldots, c \tag{6.3}$$

$$I^o_{rj} + \sum_{k=1}^{t} \frac{\partial I_{rj}}{\partial T_k}\, T_k \leq I^{max}_j \quad r = 1, \ldots, c \;\; j = 1, \ldots, b \tag{6.4}$$

$$0 \leq T_k \leq T^{max}_k \tag{6.5}$$

The voltage security constraints (6.3) may be derived for each of the c contingencies, as explained in Section 4.9.2. Thermal security constraints (6.4) may be derived for each post-contingency state and each branch j. The number of these constraints can, however, be limited to only the branches likely to be overloaded, following a transaction increase, in any of the post-contingency states. Finally, the inequalities (6.5) relate to physical bounds on source and sink powers. For instance, for a given transaction k, T^{max}_k represents the minimum between the sum of all available source powers and the sum of all available sink powers.

The L_1 objective (6.1) leads to a simple linear programming problem, whereas the product objective (6.2), leads to a geometric programming problem, for which we use a successive quadratic programming solver [IMS97].

Whereas the constraints (6.3, 6.4) are only linear approximations of the boundary $\mathcal{B}$, the solution $\mathbf{T}^\star$ of the above optimization problem may be located (hopefully slightly) inside the secure region $\mathcal{S}$ or outside. In the latter case, for contingencies which create voltage instability, branch overloads cannot be checked as the system does not have a post-contingency equilibrium point. To face such situations we first solve the voltage-constrained optimization problem (6.1 or 6.2, 6.3, 6.5). Then, when all contingencies are stabilized, we check thermal overloads, add the corresponding constraints (6.4) and perform a new optimization.

A flow chart of the whole procedure is presented in Fig. 6.3.

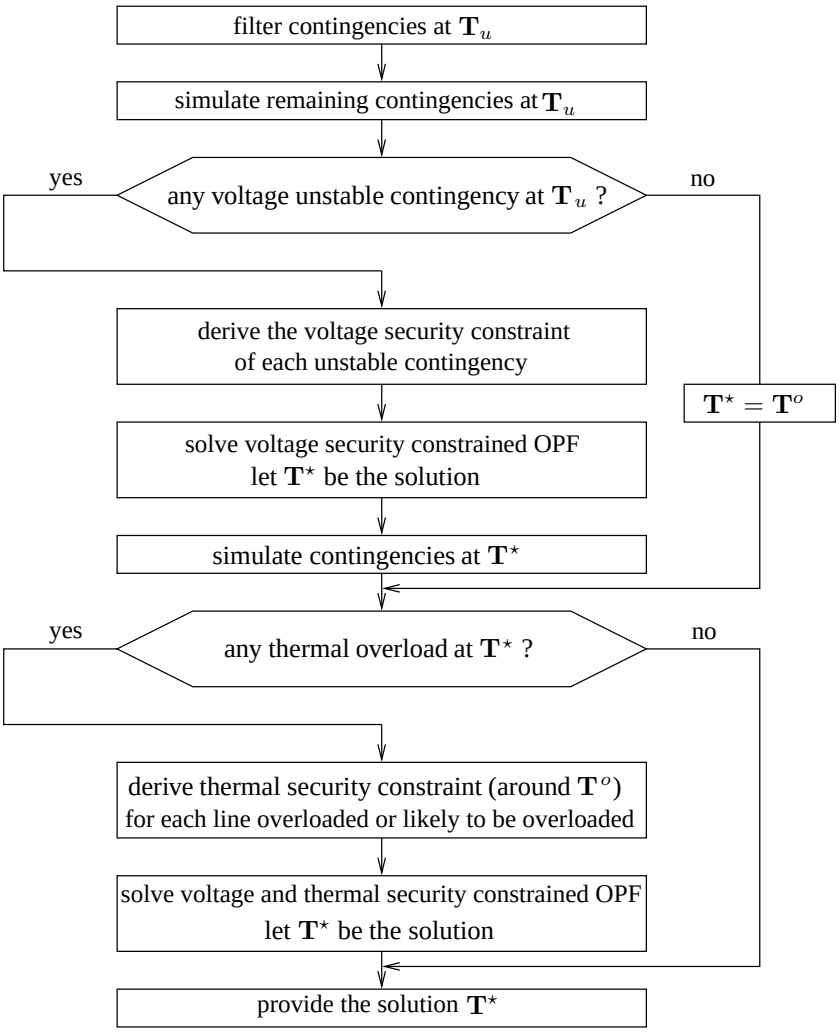

Figure 6.3: Algorithm for simultaneous ATC computation

6.2.3 Heuristic handling of nonlinearities

In order to obtain the voltage security constraints (6.3) the system must be set to an operating point $\mathbf{T}_u$ where it responds to some contingencies in an unstable way. $\mathbf{T}_u$ does not appear explicitly in the linear approximation (4.50 or 6.3); it is merely used to bring the

system to instability. On the other hand, the choice of $\mathbf{T}_u$ influences the point at which the system linearization is performed and, consequently, the relative values of the $\tilde{n}_{rk}$ coefficients. The voltage security constraints (6.3) may be limited to only those contingencies unstable at $\mathbf{T}_u$.

In practice, $\mathbf{T}_u$ is chosen so that all participating transactions are increased *beyond the expected ATC values* (so that this point falls outside the voltage secure region) and *equitably* (to avoid distortions). Admittedly, such a choice requires some knowledge of the system under concern. We usually chose $\mathbf{T}_u$ as about 80-90 $\%$ of the so obtained security limit of the system without contingency.

Incidentally, note that in congestion management, the problem of choosing $\mathbf{T}_u$ does not exist: this point is simply the operating point resulting from the various *requested* transactions.

We presented in Section 5.2.3 a technique to handle the nonlinear nature of voltage security constraints in the context of congestion management. This technique can be re-used in the context of the present problem. Thus, we replace (6.3) by:

$$\sum_{k=1}^{t} \tilde{n}_{rk}\, T_k \leq f_r\, C_r \tag{6.6}$$

and solve the voltage security constrained optimization problem (6.1 or 6.2, 6.6, 6.5), while adjusting f_r iteratively in order to obtain the largest, but secure, objective function.

Note that, whereas not all constraints are active at the optimum, a single value of f could be used to correct all of them and hence to significantly speed up the computation.

If the derivation of security constraints starting from the arbitrary point $\mathbf{T}_u$ is deemed unacceptable, the following alternative procedure can be used to obtain improved values of the coefficients $\tilde{n}_{rk}$:

1. Initialize $\mathbf{T}_s = \mathbf{T}^o$.
2. Simulate contingencies at $\mathbf{T}_u$. Derive voltage security constraints for each unstable contingency.
3. Solve the optimization problem (6.1 or 6.2, 6.3, 6.5). Let $\mathbf{T}^\star$ be the solution.
4. Simulate contingencies at $\mathbf{T}^\star$.
5. If $\mathbf{T}_u - \mathbf{T}_s \leq \epsilon$ then $\mathbf{T}^\star = \mathbf{T}_s$, stop.
6. If any contingency is unstable, derive voltage security constraints. $\mathbf{T}_u = \mathbf{T}^\star$. Go to 3. Otherwise: $\mathbf{T}_s = \mathbf{T}^\star$, $\mathbf{T}^\star = (\mathbf{T}_s + \mathbf{T}_u)/2$. Go to 4.

This procedure is illustrated graphically in Fig. 6.4 for a two-transaction case. The sought maximum (e.g. objective (6.1)) corresponds to point C. The sequence of points generated by this procedure is: $\mathbf{T}_u$, $\mathbf{T}_1$, $\mathbf{T}_2$, $\mathbf{T}_3$, $\mathbf{T}_4$, $\mathbf{T}_5$, $\mathbf{T}_6$. When the voltage security

constraints are derived for pre-contingency transactions set to $\mathbf{T}_u$, the solution of the optimization problem is $\mathbf{T}_1$. The next level of transactions considered is thus $\mathbf{T}_2$, the mid-point between $\mathbf{T}_u$ and $\mathbf{T}_1$. New voltage security constraints are derived for pre-contingency transactions set to $\mathbf{T}_2$. The solution of the new optimization problem is $\mathbf{T}_3$, and so on, etc. The procedure stops when a secure and an insecure point, namely $\mathbf{T}_5$ and $\mathbf{T}_6$ in Fig. 6.4, approach each other by less than ϵ.

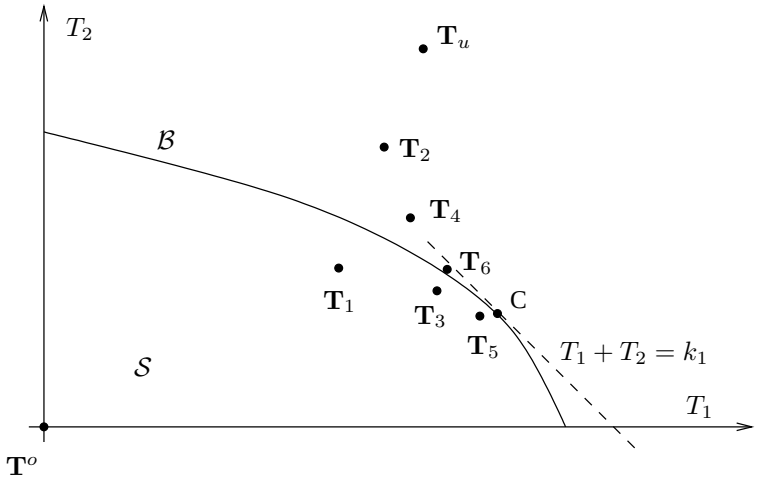

Figure 6.4: Heuristic handling of nonlinearities

In the above procedure, the final system linearization is performed at a slightly insecure point (very close to the solution $\mathbf{T}^\star$) which yields the best possible values of the coefficients $\tilde{n}_{rk}$.

A technique similar to that described in Section 5.2.3 can be used in order to improve the sensitivities (5.12) of branch currents to transactions. A single update of the sensitivities is usually enough.

Let us emphasize that this procedure allows to filter contingencies using the same technique as for a single transaction (or stress). It consists in simulating contingencies at $\mathbf{T}_u$. The idea is that a contingency found stable at $\mathbf{T}_u$ is harmless since this point is located outside the secure region (determined by more constraining contingencies). The remaining, harmful contingencies are kept and incorporated into the simultaneous ATC computation.

6.3 Numerical results

We consider again the Nordic 32 system. A list of 49 contingencies is specified, including single line or generator trippings.

We consider a set of 10 different transactions. The source(s) and sink(s) as well as the upper bound of each transaction are given in Table 6.1.

Table 6.1: Description of the involved transactions

transaction	source(s)	sink(s)	T^{max} (MW)
T_1	g21	4062	60
T_2	g22	4046	123
T_3	g4,g5	4051	99
T_4	g9,g10	1041,1045	115
T_5	g1,g2,g3	1011,1012,1013,1014	30
T_6	g8	2031	20
T_7	g19,g20	4047	17
T_8	g12	4043	30
T_9	g16	2032	40
T_{10}	g18	4042	70

6.3.1 Non-simultaneous ATC computation

For comparison purposes, we first present the results of non-simultaneous ATC computations. They are given in the column labelled "V" of Table 6.2. Note that most transactions, except T_2, T_3 and T_4, do not violate any security constraint at their upper bound. However, in order to obtain the corresponding security limit, we relaxed the bounds on the power exchanges by source(s) and sink(s).

Most of the chosen transactions are limited by voltage instability. Expectedly, transactions between northern source(s) and southern sink(s) (e.g. T_1 to T_4 and T_8) endanger voltage security significantly more than the others. Using standard 400-kV line thermal ratings, no contingency causes thermal overloads, when transactions are set to their maximum T^{max} or to the voltage stability limit, whichever is smaller. Hence, for the sake of testing the proposed procedure, the thermal limits of the 400-kV lines have been artificially decreased by 7 %. This causes the ATCs of most transactions, except T_9, to decrease drastically, as can be seen from the column labeled "T" in Table 6.2. Again, this is even more true for the transactions between northern source(s) and southern sink(s). Indeed, even in the absence of transactions, the post-contingency current in line 4031-4032 approaches its limit value after the tripping of line 4011-4021. The 4031-4032 branch current is the most limiting for almost all contingencies. This overload is partly due to a voltage drop at bus 4032 caused by the field current limitation of generator g11. In such a case, which could not be handled under the DC load flow approximation, the correction (5.12) proves useful.

6.3.2 Simultaneous ATC computation

We present now examples of transmission capacity allocation to these 10 transactions taking place simultaneously.

$\mathbf{T}_u$ is taken as corresponding to a total transaction increase of 450 MW (with respect to the base case), equally shared by all transactions. The initial set of contingencies is simulated at this operating point. Ten contingencies lead to voltage instability (which confirms that $\mathbf{T}_u$ is outside the security region) but no thermal overload is revealed. The

Table 6.2: Non-simultaneous ATC results

transaction	V	T
T_1	109	7
T_2	112	6
T_3	88	5
T_4	95	6
T_5	> 1000	> 1000
T_6	239	45
T_7	455	56
T_8	111	10
T_9	307	307
T_{10}	250	50

linear constraints (6.3) are derived for each of the 10 contingencies.

Case A

The L_1 objective is maximized over the secure region. Thus the optimization problem (6.1, 6.3, 6.5) is solved, yielding an objective value of 239 MW. At this point, the system is stable with respect to all contingencies. Hence a larger ATC value is sought, using the technique of Section 6.2.3. This leads to increasing the objective function to 279 MW.

The results are presented in the second column of Table 6.3. At the solution, most transactions are allowed to go up to their upper bound, except T_3 and T_4 (left at zero) and T_2 (for which no bound constraint (6.5) is active).

Case B

The L_π objective (6.2) is now maximized over the secure region. Obviously, the harmful contingencies are the same and the system is voltage stability limited as in Case A.

The solution of the optimization procedure is shown in the third column of Table 6.3. As can be seen, this objective leads to allocate a nonzero power to all trades.

Table 6.3: Simultaneous ATC results

transaction	case A	case B	case C	case D
T_1	60	18	0	6
T_2	12	17	0	5
T_3	0	16	0	5
T_4	0	17	0	5
T_5	30	30	30	30
T_6	20	20	20	20
T_7	17	17	17	17
T_8	30	30	24	7
T_9	40	40	40	40
T_{10}	70	70	70	24
$\sum_k T_k$	279	275	201	159

The solutions obtained with the two objectives differ by the first four transactions. In fact, the $\tilde{n}_{rk}$ sensitivities of the latter are only slightly different (whatever the contingency) but the small differences are "amplified" by the L_1 objective, which favours the T_1 trade to the detriment of T_2, T_3 and T_4. The L_π objective, on the other hand, yields a fairer capacity allocation while keeping the total power transfer at almost the same value (only 4 MW less than with the L_1 objective). This confirms that the allocation is in proportion with the impact on security.

Case C

In this case, and in the next one, the thermal limits of the 400-kV lines have been artificially decreased by 7 % to create thermal congestions, as explained previously.

Again, the L_1 objective is considered first. In this case, the system is thermal limited, the ATC being constrained by the loss of line 4011-4021. The solution of the optimization problem is shown in the fourth column of Table 6.3. The first four transactions are refused because the current in line 4031-4032 is most sensitive to these transactions. Transactions with the lowest sensitivities are accepted at their maximum.

Case D

The solution corresponding to the L_π objective is shown in the last column of Table 6.3. With respect to the previous case, transmission capacity is now allocated to the first four transactions, although to a little extent. Conversely, T_9, the only trade which can produce a counterflow in line 4031-4032, is accepted at its maximum. The same holds true for other trades which have less impact on that branch current.

A comparison of Cases C and D shows that significantly more (42 MW) network capacity is allocated with the L_1 objective. This is due to the fact that the current in branch 4031-4032 is almost equally sensitive to T_1, T_2, T_3, T_4 and T_8.

6.4 Final remarks

With reference to Fig. 6.1, let the non-simultaneous ATCs of the transactions T_1, T_2 be T_1^{ns} and T_2^{ns}, respectively. As suggested by the figure, even if $T_1 < T_1^{ns}$ and $T_2 < T_2^{ns}$, there is some probability that the system is insecure if the transactions approach their allowed limits. This is due to their interaction.

A simultaneous ATC computation attempts to take into account these interactions while still exploiting as much as possible the available transmission resources. In the case of Fig. 6.2, if $T_1 < T_1^s$ and $T_2 < T_2^s$, where T_1^s and T_2^s are the simultaneous ATCs, the system will be secure.

This property, however, is not guaranteed in all cases. A typical counterexample is provided by trades producing counterflows in the "limiting" elements of the system. The higher the counterflow in a congested line, the higher the allowed value for the other transactions which contribute to increasing the flow in that line. However, if the coun-

terflow transaction eventually does not use the whole maximum allocated capacity, while the harmful transactions use their maximum allocated capacity, the system is likely to be congested.

Such a situation is sketched in Fig. 6.5, which shows that transaction T_1 can reach a higher value if T_2 increases. The figure also shows the simultaneous and non-simultaneous ATCs. In this case:

- if $T_1 < T_1^{ns}$ and $T_2 < T_2^{ns}$, the system is secure but the ATC values are very conservative;
- even if $T_1 < T_1^s$ and $T_2 < T_2^s$, there is a probability that the system is insecure.

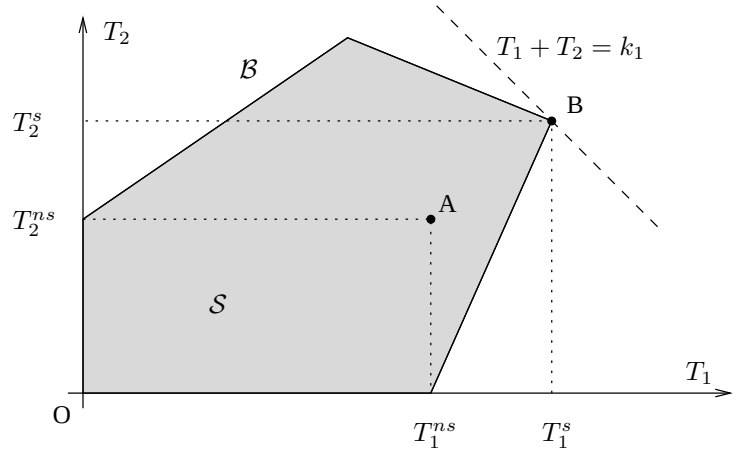

Figure 6.5: Secure regions illustrating the limitation of ATCs

Clearly, the simultaneous ATC relates to a single point of the secure region of the transaction space, i.e. to a particular loading scenario. A single point cannot take into account for the complex shape of practical security regions.

Allocation of ATCs on a simultaneous basis seems to be suitable in "longitudinal" systems where several transactions tend to use the same corridor, whose capacity must be fairly allocated between the traders. This was the case in the Nordic 32 test system. On the other hand, non-simultaneous allocation of transmission capacity may be used in highly meshed networks, where the counterflow transactions may lead to an overestimation of ATCs.

Incidentally, the problem of counterflow transactions not using the full allocated capacity does not occur in the implicit auctioning system [ESO01, ACT02, PCH02] because the corresponding traders have to pay if they do not use all what they requested. Our approach can be easily extended to the transmission capacity allocation through implicit auctioning, by taking as objective function the sum of transactions, each weighted by its bid price (see objective function 5.24).

Chapter 7

Computing security margin intervals under power transfer uncertainty

We presented in Chapter 3 methods aimed at computing voltage and thermal security margins for a given stress direction. In this chapter we deal with the uncertainty which may affect the stress direction. More precisely, we propose computational methods to determine minimal and maximal (voltage and/or thermal) security margins for specified intervals of variations of power injections. Special attention is paid to the sensitivity of the margins to the bounds imposed on power injections variations. Numerical examples of these approaches are given for a test as well as for a real system.

7.1 Motivation and previous works

As shown in Chapter 3, there are mature techniques to compute voltage and thermal security margins for a given source-sink pattern, defined by the participations of the various bus injections. In practice, however, the system evolution may be somewhat different from the one assumed in the above calculation. For instance, there is some uncertainty concerning the load increase pattern. Similarly, there is some uncertainty in how generators from external systems will participate to a power transfer. This is the case when market rules (still) do not require to disclose all transaction details. Even when the transaction amount and the participating countries (in case of UCTE for instance) will be disclosed, there will be most probably no information about the participations of the various sources and sinks. As security margin computations are reliant on the choice of the source-sink pattern, they are to some extent sensitive to uncertainty on the underlying bus participations.

Therefore, it may be of interest in both operational planning and real time to provide not only the security margin with respect to a contingency but also, as a complementary information, the (lower and upper) values on this margin for specified ranges of bus injection values. The lower value of the margin represents the minimum increment of power transfer above base case that can be safely achieved by any source-sink pattern. Thus it yields a conservative estimate of the transfer capability. The upper value of a margin conveys

less information when dealing with the above uncertainties in as much as usual security analyses are somewhat conservative. On the other hand, it becomes of interest within the context of markets, where actors try to maximize source-sink power transfers in order to gain more profit [Bet00, WL00, GLB01].

In this chapter we present methods to compute security margins relative to the worst and the best source-sink pattern, for the contingency(ies) of concern.

Several works have been devoted to determining the minimum distance to the boundary of a feasible space. One of the first method to calculate the closest infeasibility to a given operating point was proposed in the early reference [JG81]. The feasible region of the injection space was defined as the set of all injections for which the load flow has a solution. A minimum margin was defined and computed using the constrained Fletcher-Powell minimization.

Reference [DL93] proposes an iterative and a direct method to compute the locally closest saddle-node bifurcation to the current operating point in the load power parameter space. The L_2-norm (Euclidian distance) is used to compute the worst-case load increase causing the system to lose equilibrium. More extensive tests with the iterative method are reported in [ADH94], where a Monte-Carlo technique allowed to identify multiple closest bifurcations in some of the test systems. A drawback of the formulation is the independent and unbounded behaviour of the bus active and reactive powers. Incidentally, insight into the geometry of the bifurcation surface may be found in the above references as well as in [Dob92, VKM01, WL00].

The dual problem of maximizing the power transfer between generators and loads was presented in [WL00], taking into account either voltage stability or voltage quality. Under the assumption that individual loads evolve along a specified direction, the active power generations are varied so as to maximize the power transferred to loads. This L_1-norm maximization problem was solved using a gradient search algorithm.

We tackled this problem in [Cap00], for voltage stability constraints only. Our goal was to maximize a power transfer between two systems while keeping voltage security margins with respect to several contingencies above some threshold.

Reference [Bet00] focuses on determining the generation pattern which maximizes the power transfer between sources and sinks, under transient stability constraints.

The case where the feasible region is bounded by inequality constraints (instead of bifurcations as for voltage instability) was considered in [WL00], for minimum voltage constraints. More recently, [GLB01] proposed a method to find the thermal-constrained interface maximum transfer capability under the worst scenario in generation-load space. The min-max interface transfer is obtained as a bi-level optimization problem whose constrains are derived from the DC load flow equations.

Some of the ideas presented hereafter can also be found in our publication [CVC02b].

7.2 Statement of the problem

7.2.1 "Conventional" limits and margins

In the margin calculations considered so far, the source and sink participation factors α_i's and β_i's are chosen in accordance to (3.9) and the margin is obtained as the maximum value of the pre-contingency stress S such that the system responds to the contingency in an acceptable way (see Section 3.4.4). An intuitive view of a voltage and thermal security limit and margin was given in Fig. 3.2.

Let us now denote by $\mathcal{B}$ any of the surfaces $\mathcal{B}_V$ or $\mathcal{B}_T$, defined in Section 3.3.3. We formally describe the boundary $\mathcal{B}$ by:

$$h(\Delta P_1^+, \ldots, \Delta P_i^+, \Delta P_i^-, \ldots, \Delta P_m^-) = 0 \tag{7.1}$$

At this point, it is convenient to reformulate the margin computation problem (3.14-3.20) as follows. Let us first eliminate the S variable and work with the ΔP_i^+ and ΔP_i^- variables only. Summing (3.5) or (3.8) over all buses and taking (3.9) into account yields:

$$\sum_{i \in L \, or \, G^-} \Delta P_i^- = S \tag{7.2}$$

which shows that it is equivalent to maximize S or the sum of ΔP_i^-'s. Doing the same with (3.4, 3.7, 3.9) yields:

$$\sum_{i \in G^+} \Delta P_i^+ = (1+\delta)\, S \tag{7.3}$$

and the above two equations can be combined into:

$$\sum_{i \in G^+} \Delta P_i^+ = (1+\delta) \sum_{i \in L \, or \, G^-} \Delta P_i^- \quad (= S) \tag{7.4}$$

Let us consider that the sinks are loads only, although all what follow remains valid when the sinks comprise generators as well.

The "conventional" security margin corresponds to the point of surface $\mathcal{B}$ which maximizes the sum of ΔP_i^-'s while satisfying (7.4). This leads to the optimization problem:

$$\max_{\Delta P_i^+, \Delta P_i^-} \quad \sum_{i \in L} \Delta P_i^- \tag{7.5}$$

$$subject\ to: \quad h(\Delta P_1^+, \ldots, \Delta P_i^+, \Delta P_i^-, \ldots, \Delta P_m^-) = 0 \tag{7.6}$$

$$\sum_{i \in G^+} \Delta P_i^+ = (1+\delta) \sum_{i \in L} \Delta P_i^- \tag{7.7}$$

$$0 \le \Delta P_i^+ \le B_i^+ \quad i \in G^+ \tag{7.8}$$

$$0 \le \Delta P_i^- \le B_i^- \quad i \in L \tag{7.9}$$

$$\frac{\Delta P_i^-}{\beta_i} = \frac{\Delta P_i^+}{\alpha_i} \quad (= S) \quad \forall i \in G^+ \cup L \quad \text{and} \quad \alpha_i, \beta_i \neq 0 \tag{7.10}$$

$$where: \quad \sum_{i \in L} \beta_i = 1 \quad \sum_{i \in G^+} \alpha_i = 1 + \delta \tag{7.11}$$

Note that the "box" constraints (7.8, 7.9) have been added to avoid reaching unrealistic load patterns or generation schemes. For loads, the bound B_i^- may be taken as a fraction of the base case power P_{li}^o. For generators, B_i^- and B_i^+ relate to the generation capacity. The last two equations restrict the variation of ΔP_i^+'s and ΔP_i^-'s to the stress direction defined by the specified α_i's and β_i's.

Let M be the maximum stress, corresponding to the conventional margin. We now consider the problem of minimizing (resp. maximizing) M with respect to the α_i's and β_i's.

7.2.2 Minimum and maximum margins

The minimum (resp. maximum) margin corresponds to the point of surface $\mathcal{B}$ which minimizes (resp. maximizes) the sum of ΔP_i^-'s while satisfying (7.4). This leads to the optimization problem:

$$\min_{\Delta P_i^+, \Delta P_i^-} \sum_{i \in L} \Delta P_i^- \quad \text{or} \quad \max_{\Delta P_i^+, \Delta P_i^-} \sum_{i \in L} \Delta P_i^- \tag{7.12}$$

$$subject\ to: \quad h(\Delta P_1^+, \ldots, \Delta P_i^+, \Delta P_i^-, \ldots, \Delta P_m^-) = 0 \tag{7.13}$$

$$\sum_{i \in G^+} \Delta P_i^+ = (1+\delta) \sum_{i \in L} \Delta P_i^- \tag{7.14}$$

$$0 \leq \Delta P_i^+ \leq B_i^+ \quad i \in G^+ \tag{7.15}$$

$$0 \leq \Delta P_i^- \leq B_i^- \quad i \in L \tag{7.16}$$

7.3 Computing thermal security margin intervals

7.3.1 Thermal security region

When dealing with thermal overloads, the formal equation (7.1) can be replaced by a piece-wise linear approximation of $\mathcal{B}_T$, each linear part corresponding to one branch current being at its maximum. This is depicted for a two-dimensional example in Fig. 7.1. The box constraints (7.8, 7.9) are shown with thin lines and the boundary $\mathcal{B}_T$ with heavy lines. The thermal security region $\mathcal{S}_T$ is tinted in grey.

With reference to (7.2), we assume that the objective function is $\Delta P_1 + \Delta P_2$ (shown with dashed lines). Considering that the optimum must lie on $\mathcal{B}$ while obeying the box constraints, the solution to the min and max problems are the two points shown in the figure.

7.3.2 Minimum margins

As already mentioned, $\mathcal{B}_T$ is the union of several linear parts, each relative to a different branch. Denoting one of them by $\mathcal{B}_j$, the minimum of the objective function (7.2) over

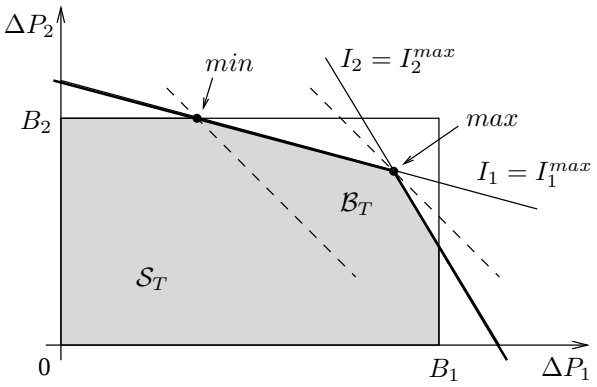

Figure 7.1: Secure sub-space in the linear case

the set $\mathcal{B}_T$ is the smallest among the minima obtained over each subset $\mathcal{B}_j$ separately. The latter is the solution of:

$$\min_{\Delta P_i^+, \Delta P_i^-} \sum_{i \in L} \Delta P_i^- \tag{7.17}$$

$$subject\ to: \quad I_j^o + \sum_i \frac{\partial I_j}{\partial P_i}(\Delta P_i^+ - \Delta P_i^-) = I_j^{max} \tag{7.18}$$

$$\sum_{i \in G^+} \Delta P_i^+ = (1+\delta) \sum_{i \in L} \Delta P_i^- \tag{7.19}$$

$$0 \leq \Delta P_i^+ \leq B_i^+ \quad i \in G^+ \tag{7.20}$$

$$0 \leq \Delta P_i^- \leq B_i^- \quad i \in L \tag{7.21}$$

where constraint (7.18) refers to post-contingency currents.

The procedure is thus the following: for each branch j, solve the above problem to find the minimum margin over the subset $\mathcal{B}_j$, and finally take the smallest among all so found minima.

Note that the above LP problem is very simple (in fact it can be solved without resorting to an LP program, as explained in Section 7.4.2. For some branches, it may be infeasible; this would correspond, in Fig. 7.1, to a branch constraint not intersecting the box relative to the B_1 and B_2 bounds. Such a branch can be merely ignored and the branch enumeration can proceed. Finally, branches with $I_j^o \ll I_j^{max}$ may be also skipped.

7.3.3 Maximum margins

As suggested by Fig. 7.1, the maximum margin is obtained by replacing (7.1) by the set of inequalities (4.41) that define the secure region. By so doing, (7.12-7.16) becomes:

$$\max_{\Delta P_i^+, \Delta P_i^-} \sum_{i \in L} \Delta P_i^- \tag{7.22}$$

$$subject\ to: \quad I_j^o + \sum_i \frac{\partial I_j^o}{\partial P_i}(\Delta P_i^+ - \Delta P_i^-) \leq I_j^{max} \quad j = 1, \ldots, b \tag{7.23}$$

$$\sum_{i \in G^+} \Delta P_i^+ = (1+\delta) \sum_{i \in L} \Delta P_i^- \tag{7.24}$$

$$0 \leq \Delta P_i^+ \leq B_i^+ \quad i \in G^+ \tag{7.25}$$

$$0 \leq \Delta P_i^- \leq B_i^- \quad i \in L \tag{7.26}$$

Note that (7.23) involves b inequalities while (7.18) involved a *single equality*.

The maximum margin is thus obtained by solving a single Linear Programming (LP) problem. As usual, sparsity programming techniques must be used to preserve computational efficiency. In this respect, small sensitivities may be set to zero.

7.3.4 Handling of multiple contingencies

The thermal secure region $\mathcal{S}_T$ can be defined with respect to a set of contingencies and minimum (resp. maximum) margins can be computed over this sub-space.

For the minimum margin computation, the size of the minimization problem (7.17-7.21) remains unchanged but a different equality (7.18) has to be considered for all branches and all contingencies, successively.

For the maximum margin computation, the set of inequalities (7.23) is extended to all contingencies, which increases the size of the optimization problem.

7.3.5 Accounting for nonlinear effects

If the min and max points computed from the linear approximations are checked with a more accurate model, it is possible that some branches are overloaded due to the neglected nonlinearities. The latter often result from the voltage drops caused by the increased power transfer.

In such a situation, the sensitivities used in (7.23) or (7.18) can be corrected. For the j-th branch, the sensitivities are multiplied by $\dfrac{I_j^{real} - I_j^o}{I_j^{max} - I_j^o}$ where I_j^{real} is the current obtained from the AC load flow calculation. A single new optimization based on the corrected sensitivities is usually enough.

7.4 Computing voltage security margin intervals

It was shown in Section 4.5 that the voltage security boundary $\mathcal{B}_V$ can be linearly approximated by its tangent hyperplane $\mathcal{H}$. The latter is obtained by : (i) stressing the system to a point where it responds in an unstable way to the contingency of concern, (ii) identifying the critical point of the system, and (iii) computing the normal vector $\mathbf{n}$. It will be shown in the sequel that, in order to compute the minimal and maximal voltage security margins, the information taken from this hyperplane is basically a ranking of buses, as for the identification of the most effective controls to increase voltage security. To this purpose, the sensitivities $\dfrac{\partial V_\ell}{\partial \mathbf{P}}$ can be used instead of the normal vector, since it has been shown that both provide essentially the same information. In the remaining of this chapter, the methods will be presented using the normal vector, for simplicity and clarity.

In practice the boundary $\mathcal{B}_V$ is nonlinear. We thus propose hereafter two techniques to handle such nonlinearities.

Unless otherwise mentioned, we concentrate on the minimum margin computation, to avoid repetitions, but the extension to the maximal margin determination is straightforward.

7.4.1 First approach

Using the linearized relationship (4.42) as an approximation of the boundary $\mathcal{B}_V$, the problem of determining the minimal voltage security margin with respect to a contingency takes on the form:

$$\min_{\Delta P_i^+, \Delta P_i^-} \quad \sum_{i \in L} \Delta P_i^- \tag{7.27}$$

$$subject\ to: \quad \sum_{i=1}^{m} n_i (\Delta P_i^+ - \Delta P_i^-) = f\, C \tag{7.28}$$

$$\sum_{i \in G^+} \Delta P_i^+ = (1+\delta) \sum_{i \in L} \Delta P_i^- \tag{7.29}$$

$$0 \le \Delta P_i^+ \le B_i^+ \quad i \in G^+ \tag{7.30}$$

$$0 \le \Delta P_i^- \le B_i^- \quad i \in L \tag{7.31}$$

Because (7.28) represents a linear approximation of the exact boundary $\mathcal{B}_V$, we resort to the procedure explained in Section 5.2.3, i.e. we adjust the value of f iteratively.

In order to obtain a first estimate of the boundary $\mathcal{B}_V$ we stress the system at a point located outside the voltage security region $\mathcal{S}_V$. One possibility is to set the system at the maximum stress S_{max} used to compute conventional margin; alternatively the ΔP_i's can be set to their upper bounds B_i.

A possible weakness of this approach is that the sensitivities n_i are derived once for all and are not updated. This may lead to a "near" minimal margin. An efficient sensitivity update can be performed using the approach described hereafter.

7.4.2 Second Approach

Let us first consider the simple problem, illustrated in Fig. 7.2, of finding the minimum of $\Delta P_1 + \Delta P_2$ over a single linear boundary $\mathcal{B}_V$, taking into account the box constraints. Let n_1 and n_2 be the components of the vector normal to $\mathcal{B}_V$.

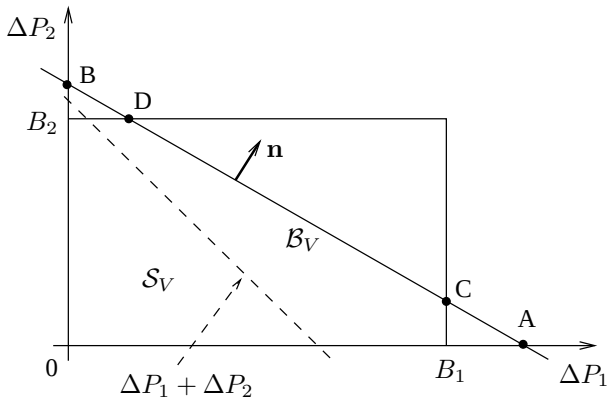

Figure 7.2: Optimum in the case of linear $\mathcal{B}_V$ surface

If the only constraints were $\Delta P_1, \Delta P_2 \geq 0$, the solution would be at point B if $|n_2| > |n_1|$, at point A if $|n_1| > |n_2|$ and at any point of $\mathcal{B}_V$ is $|n_2| = |n_1|$. In the sequel, we ignore this last case.

If we further impose $\Delta P_1 \leq B_1$ and $\Delta P_2 \leq B_2$, the solution is either C or D, depending again on the relative magnitude of n_1 and n_2.

In the general, n-dimensional case, it can be easily shown that the minimum is such that:
• $\Delta P_i = B_i$ for k variables corresponding to the largest (absolute) components of $\mathbf{n}$
• $\Delta P_i = 0$ for $n - k - 1$ variables corresponding to the smallest components of $\mathbf{n}$. In other words, the ΔP_i's corresponding to the largest components of $\mathbf{n}$ are the first to be changed. k may vary from 0 to $n - 1$ [1].

We described in Section 3.5.1 the simple binary search used to determine the voltage security margin for a given stress direction. Based on the above observations, we now present a method using the information provided by normal vectors $\mathbf{n}$ to "redirect the stress" in the course of the binary search, with the objective of converging towards the minimum margin. The procedure will be illustrated step-by-step on the simple example of Fig. 7.3, in which the minimum margin corresponds to point M.

We start by choosing a direction and a maximum stress S_{max}. The corresponding point must fall outside $\mathcal{S}_V$, in order the system to be unstable and a first normal vector $\mathbf{n}$ to be obtained from the analysis of the unstable evolution. Figure 7.3 illustrates the case where all ΔP_i's are set to their upper bounds B_i.

[1] clearly, a similar reasoning applies to the maximum margin. Assuming $|n_2| > |n_1|$, the latter corresponds to point A if the constraints are $\Delta P_1, \Delta P_2 \geq 0$ and to point C if one further imposes $\Delta P_1 \leq B_1$ and $\Delta P_2 \leq B_2$. In the general case, the ΔP_i's corresponding to the smallest components of $\mathbf{n}$ are the first to be changed.

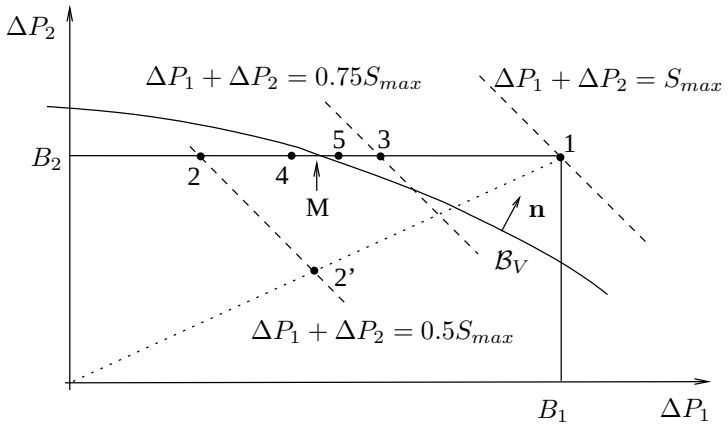

Figure 7.3: Search of the minimum voltage margin

In a standard binary search the next point to be tested would be 2', corresponding to half stress along the same direction. However, in order to converge to the minimum margin, we change the direction of stress. To this purpose, we approximate $\mathcal{B}_V$ by a linear surface and apply the property stressed at the beginning of this section (see Fig. 7.2). Thus, we first sort the various ΔP_i's by decreasing order of their corresponding components of $\mathbf{n}$. Then, following this order, we set the successive ΔP_i's to their bound B_i until their sum exceeds the current level of stress $S_{max}/2$. We adjust the last ΔP_i so that the sum matches $S_{max}/2$ exactly. This leads to point 2 in Fig. 7.3. At this point we simulate the contingency. The system is stable. No new normal vector is obtained.

We proceed with the $0.75 S_{max}$ stress. In the absence of a new normal vector, we keep the previous ranking of the ΔP_i's. Again, we successively set the ranked ΔP_i's to their bounds B_i and adjust the last one so that the sum equals $0.75 S_{max}$. This leads to point 3. At this point, the system is unstable. A new normal vector is obtained, corresponding to a new linear approximation of $\mathcal{B}_V$ and providing a new ranking of the ΔP_i's.

The procedure continues in the same way, passing through points 4 and 5 in Fig. 7.3, until the difference between two successive stresses falls below a tolerance. Note that the fact that points 2, 3, 4 and 5 lie on the same line is a limitation of the two-dimensional example used.

7.4.3 Remarks common to both approaches

The two above approaches call for the following comments:

1. it must be stressed that in both cases the computational effort is exactly that of a conventional margin computation (i.e. for a fixed direction of stress);

2. all what matters in these procedures is the *ranking* of the ΔP_i's. In some systems (for instance in the RTE one), we have obtained very good results by simply ranking buses according to the values of post-contingency voltages. The latter are picked up from one point of the unstable evolution provided by QSS simulation;

3. since the first (resp. second) method implicitly relies on one (resp. successive) linearization of the $\mathcal{B}_V$ surface, the latter should be "smooth enough". On the other hand, changes in $\mathbf{n}$ have no impact as long as the ranking of its components is unchanged. Moreover, only the optimum set of buses matter for the minimal and maximal margins. This "robustness" is an advantage of the L_1 norm over the L_2 one used in previous works on the subject;

4. as already mentioned, loads are changed under constant power factor. Thus, for each change in active power, there is a change in reactive power. The corresponding components of the $\mathbf{n}$ vectors are combined into a single number, used for ranking. Similarly, we correct the component relative to active power generation to take into account the resulting change in reactive power capability.

7.4.4 Handling of multiple contingencies

The minimum margin with respect to several contingencies can be obtained by treating each contingency separately and taking the lowest among the so found minima. Let us remark that this procedure is similar to that used for computing the minimal thermal margin with respect to one or several contingencies. Indeed, in both cases, the overall voltage (resp. thermal) security boundary is approximated by linear pieces. For the voltage security margin each piece corresponds to a contingency.

The problem of determining a maximum margin with respect to several contingencies is somewhat more complex.

Within the context of the first approach, one can compute the maximum margin relative to each of contingency separately using the procedure described in Section 7.4.1. The latter yields the corresponding value of the f factor in Eq. (7.28). Then, the maximum margin can be obtained as the solution of an overall optimization problem incorporating the equality constraints (7.28) of all contingencies together:

$$\max_{\Delta P_i^+, \Delta P_i^-} \quad \sum_{i \in L} \Delta P_i^- \tag{7.32}$$

$$subject\ to: \quad \sum_{i=1}^{m} n_{ri}(\Delta P_i^+ - \Delta P_i^-) \leq C_r \qquad r = 1, \ldots, c \tag{7.33}$$

$$\sum_{i \in G^+} \Delta P_i^+ = (1+\delta) \sum_{i \in L} \Delta P_i^- \tag{7.34}$$

$$0 \leq \Delta P_i^+ \leq B_i^+ \quad i \in G^+ \tag{7.35}$$

$$0 \leq \Delta P_i^- \leq B_i^- \quad i \in L \tag{7.36}$$

The extension of the second approach to multiple contingencies seems more delicate, since it requires to combine the bus rankings relative to several contingencies.

This approach can be extended to include thermal security constraints (7.23). The so obtained problem can be solved by a two-step procedure, as explained in Section 6.2.2.

7.5 Numerical examples

In this section, the above procedures are illustrated on the Nordic 32 system. The next section will focus on the influence of the bounds B_i^+, B_i^- and will report on results obtained with the RTE system.

7.5.1 Power transfers

The results reported hereafter involve two different power transfers:

1. *Generation to Load* (denoted GL in the sequel): a load increase in the South area ($S_{max} = 600$ MW/ 180 MVAr) is covered by a generation increase in the North one ($S_{max} = 630$ MW, accounting for losses). The initial direction of stress is such that each of the 22 loads has the same participation factor (both for active and reactive power) and each Northern generator participates according to speed droop;

2. *Generation to Generation* (denoted GG in the sequel): active power generation is shifted from the North ($S_{max} = 630$ MW) to the South area ($S_{max} = -600$ MW), all loads remaining unchanged. The initial direction of stress is such that Northern generators participate according to speed droop while all Southern generators have the same participation factor.

Not all α_i's and β_i's need to be treated as variables. Table 7.1 lists the six possible variants. For instance, in variants (a) and (c) a load power margin is determined. In variant (a), the generator individual participations are fixed, while in variant (b) the load individual participations are fixed. In variant (c) both are allowed to vary. Obviously, the choice depends on the particular application. In this paper, all combinations are considered, except (a) and (c) when maximizing margins, as these variants seem less meaningful.

Table 7.1: Margin variants

variant	transfer	α_i	$\beta_i \;\; i \in L$	$\beta_i \;\; i \in G^-$
(a)	GL	fixed	variable	= 0
(b)	GL	variable	fixed	= 0
(c)	GL	variable	variable	= 0
(d)	GG	fixed	= 0	variable
(e)	GG	variable	= 0	fixed
(f)	GG	variable	= 0	variable

The bounds B_i^- on load power increase have been set to 10 % of the base case load. For generators, B_i^+ and B_i^- correspond to the turbine capacity.

The results shown hereafter deal with the loss of the line between buses 4011 and 4021. For a large enough North-South power transfer, this contingency causes voltage instability. If the transfer is somewhat decreased the system survives but with an overloaded line. These two aspects are treated successively.

Thermal and voltage problems are thus strongly coupled in this example. For instance, at the thermal overload limit, some voltages are as low as 0.9 pu.

7.5.2 Voltage security margins

GL power transfer

For the initial direction of stress, the margin with respect to the selected contingency is 461 MW.

The results when optimizing the α_i's and β_i's are given in Table 7.2.

Table 7.2: Intervals (MW) of voltage stability margin (GL power transfer)

variant	(a)	(b)	(c)
min margin	304	373	248
max margin	-	643	-

In variant (c), the load consumption concentrates on buses 1043, 1041, 1045, 1044 and 4051 which have the highest components of the normal vector. This load increase is covered by generators g4 and g3, whose electrical distance to the load center is higher. This corresponds to the worst direction of stress.

If only loads are varied, the generator participations being set as indicated in the previous section, a larger minimum margin is found, as expected. The same loads as for variant (c) participate in the load increase. If only generators are varied, the load increase is covered by g4, g3 and g2.

Let us emphasize that, for voltage security analysis purposes, *the identification of buses participating to the minimum load power margin brings as much information as the value of the margin itself*. It points out the weak area for the contingency of concern, more precisely *the smallest area in which a bounded load increase would make the system insecure with respect to the contingency*.

Table 7.3 illustrates the iterative procedure of Section 7.4.2. It shows the ranking of load buses at 4 unstable steps of the binary search. The components of the normal vector have been scaled so that the largest one is equal to 1.

The lower the stress of an unstable scenario, the more accurate the bus ranking. In this respect, the rows of the table have been ordered according to the normal vector obtained in the marginally unstable scenario, i.e. at 305 MW of stress (for a margin of 304 MW), while the stars point out changes with respect to this ranking. As can be seen, the normal vector does not change significantly from one iteration to the next. Only permutations of two or three successive buses are observed. Since the first ranked buses are loaded at their upper bounds B_i^- and the last ranked are not loaded at all, these permutations lead, at most, to loading one bus instead of another. Moreover the values relative to

permuted buses are very close and, therefore, the margin is little affected. Note that it is quite acceptable to use the very first vector throughout the whole procedure, which further saves computing time.

Table 7.3: Load bus ranking at various steps of the binary search

buses	600 MW	375 MW	337 MW	305 MW
1045	0.996*	1.0	0.998*	1.0
1043	1.0*	0.993	1.0*	0.996
1041	0.998*	0.979*	0.996	0.988
1044	0.986	0.990*	0.986	0.988
4051	0.977	0.988*	0.981	0.985
4043	0.974	0.983	0.973	0.977
4046	0.974	0.983	0.972	0.976
1042	0.970	0.974	0.964	0.969
4047	0.954*	0.967	0.953	0.966
4061	0.967*	0.964	0.952	0.959

Let us underline that a very good agreement between the load ranking according to the normal vector components and that according to a snapshot of an unstable post-contingency voltage profile has been observed in real-life systems, e.g. RTE. This is not the case in our test system because the voltage instability concerns middle points of the transmission system and not ending points.

The maximum margin is 643 MW, a significantly different value compared to the original margin (461 MW). This is due to the quite large active power reserve available on the most appropriate generators (by decreasing order : g11, g12, g8 and g5). The next ranked generator is g9. It has enough reserve but does not much contribute to margin increase.

GG power transfer

For the initial direction of stress, the margin with respect to the selected contingency is 320 MW. The computed margin intervals are given in Table 7.4.

Table 7.4: Intervals (MW) of voltage stability margins (GG power transfer)

variant	(d)	(e)	(f)
min margin	303	270	262
max margin	329	467	482

When generator participations can vary in both exporting and importing areas, the smallest (voltage stability constrained) transfer of 262 MW takes place between g4, g3 (North) and g7, g17 (South). This minimum is obtained by involving groups of generators electrically far away from each other.

The same Northern (resp. Southern) generators keep on participating when the Southern (resp. Northern) participations are fixed at their original values, which leads obviously to a larger minimal margin.

With all participations free to vary, the maximum transaction (of 482 MW) takes place between g11, g12, g8, g5, g9 (North) and g14 alone (South). Thus, the whole effort is put on the electrically closest generators.

The maximum margins obtained when letting a single group of generators vary indicate that the generators of the importing area have less influence than those of the exporting area. This is confirmed by the margin sensitivities to injections: all Southern generators have almost the same sensitivities, while significantly larger differences are observed among the various Northern generators.

7.5.3 Thermal security margins

GL power transfer

For the initial direction of stress and taking into account thermal overloads, the margin is 408 MW. This value corresponds to the overload of line 4031-4032 after the tripping of line 4011-4021. The computed margin intervals are given in Table 7.5.

Table 7.5: Intervals (MW) of thermal overload margin (GL power transfer)

variant	(a)	(b)	(c)
min margin	254	338	231
max margin	-	579	-

For the minimum margin of 231 MW, the load increase concentrates on buses 4042, 4043, 4046, 4047 and 1044 and is covered by g4 and g2. This load increase location causes a larger post-contingency current in line 4031-4032.

The lower margin value of 338 MW involves g4 and g2, while the upper margin value of 579 MW involves g11, g12, g8, g5, and g9.

The lower margin value of 254 MW involves one more load at bus 1043 as when both generation and load participations are varied.

GG power transfer

For the initial direction of stress, the maximum power transfer increase is 272 MW. It is again limited by the overload of line 4031-4032 after the tripping of line 4011-4021. The computed margin intervals are given in Table 7.6.

Table 7.6: Intervals (MW) of thermal overload margin (GG power transfer)

variant	(d)	(e)	(f)
min margin	265	239	228
max margin	293	415	443

The smallest margin of 228 MW corresponds to an increase of g2 and g4 productions, compensated by a decrease of g14.

The largest margin of 443 MW is obtained by increasing the output of generators g11, g12, g5, g8 and g9 (located mainly in the left part of the network) and decreasing the output of g19. Indeed, by redirecting the pre-contingency power flow through the (double circuit) line 4031-4041, a higher transfer can take place from North to South, for the same post-contingency current in the constraining branch 4031-4032.

In this example, the limiting branch does not change when the direction of stress is modified, but the method can deal with cases where it changes.

7.5.4 Maximum voltage security margins with respect to multiple contingencies

Due to its structure and simplicity, the Nordic 32 system does not allow to illustrate a case where a maximum margin would correspond to a "compromize" between two contingencies. Rather, we have obtained the maximal power transfer with respect to several contingencies as being simply the smallest among the individual maxima computed for each contingency separately.

As already mentioned, all contingencies basically involve the same voltage instability mechanism (increase of power transfer from North to South). Among them, the loss of generator g14 is the most dangerous contingency. Even when it is maximized by adjusting the stress pattern, the margin of this contingency remains smaller than the margins of other contingencies.

For the power transfer between Northern generators and all loads, variant (b), the computed power transfer is of 467 MW. Loads are increased according to fixed participations, that load increase being covered by generators g11, g12, g8, g5 and g9 which are closest to the South area.

For the power transfer between the Northern and Southern generators, variant (f), we have obtained a maximal power transfer of 355 MW between g11, g12, g8, g5 and g9 from the North and g19 and g20 from the South.

Minimal voltage security margins with respect to several contingencies corresponds to the loss of g14 which has the smallest among the minimal margins. For instance, in the variant (c), the minimal power transfer is about 243 MW, loads involved are 1044, 1045, 4042, 4043, 1043 and 4046, their increase being compensated by g3 and g4.

7.6 Sensitivity of margins to bounds on injection variations

In this section, we investigate the sensitivity of minimal margins with respect to the bounds B_i^- or B_i^+ specified in the optimization problem (see Eq. (7.9)). For simplicity, we concentrate on a transfer between a fixed set of generators and a variable sets of loads, as considered in usual load power margin computations. Other transfers may be dealt with similarly.

7.6.1 Properties of minimal margins under homothetic load increases

With the L_1-norm formulation used in this chapter:

- if no bound B_i^- was specified on individual load increases, the whole effort would unrealistically concentrate on a single bus;
- when B_i^- bounds are specified, the optimum corresponds to setting some ΔP_i's at their bounds, and leaving $\Delta P_i = 0$ for all others, except one.

The lower the B_i^- bound, the wider the area in which loads are increased at the optimum. More precisely, if all B_i^- bounds are decreased by the same factor, the load increase takes place in larger and larger "concentric" areas including the area most affected by instability.

It makes sense to take B_i^- proportional to the size of the load[2]. Let p be the maximum fraction of power increase allowed for all loads. Thus, at the i-th bus, we assume:

$$B_i^- = p\, P_{li}^o$$

where P_{li}^o is the base case active load.

For a given p we can determine the minimal margin M_{min} as well as the area $\mathcal{L}$ of buses participating to the load increase. Under the above assumption, all loads inside $\mathcal{L}$, except one, are increased by a fraction p, while loads outside $\mathcal{L}$ are not increased at all.

Now, if one neglects the single load of $\mathcal{L}$ not increased at its upper bound, the load increase pattern of the minimal margin computation is identical to the load increase pattern of an "area-constrained" conventional margin computation, in which loads are homothetically increased *in area $\mathcal{L}$ only*[3]. Let BC the total active load power of area $\mathcal{L}$ in the base case, i.e.

$$BC = \sum_{i \in \mathcal{L}} P_{li}^o$$

[2] except for industrial loads which do not take part in the load increase

[3] of course, the area $\mathcal{L}$ is not known until the optimization problem is solved

Thus, for the minimal margin M_{min} and the area-constrained conventional margin M, we have:

$$M_{min} \cong M = \sum_{i \in \mathcal{L}} p\, P_{li}^{o} = p \sum_{i \in \mathcal{L}} P_{li}^{o} = p\, BC \tag{7.37}$$

7.6.2 Example from the Nordic 32 system

We come back to the example of Section 7.5.2, variant (a). Table 7.7 shows the minimum margin M_{min}, the base case load BC of area $\mathcal{L}$ and the number of loads in $\mathcal{L}$, for various values of p. As expected, when p decreases, M_{min} increases (since the minimum is more and more constrained) as well as BC (since area $\mathcal{L}$ grows).

As p decreases, M_{min} increases, first smoothly (for $p \geq 5$ %) then sharply (for $p \in [4.72; 5]$ %).

Another value of interest is the relative margin M_{min}/BC, which combines the maximum load increase and the size of the stressed area. The results show that when M_{min}/BC decreases with p, indicating that BC grows faster than M_{min}.

Table 7.7: Variation of M_{min}, BC, $\mathcal{L}$ and M_{min}/BC with p

$p(\%)$	25	20	15	10	5	4.72
M_{min} (MW)	283	288	292	304	311	468
BC (MW)	1277	1946	2614	3366	4968	9940
nb of loads	3	4	5	6	14	22
M_{min}/BC	0.221	0.147	0.111	0.09	0.062	0.047

7.6.3 Examples from the RTE system

We now turn to the RTE system, in which we consider a national load increase (512 candidate loads) covered by 145 French generators. The results relate to the same two contingencies of Section 3.8.7, denoted A and B, respectively. Each of them consists in tripping a double-circuit 400-kV line in the Western part of the system.

When a national, homothetic load increase is considered, the security margin with respect to the loss of line A (resp. B) is of 490 (resp. 4142) MW.

Results similar to those of Table 7.7 are shown in Table 7.8, for the loss of line B.

The left plot in Fig. 7.4 shows the variations of M_{min} and M_{min}/BC with p. The greatest minimal margin M_{min} is obtained for a relatively small value of p ($\cong 9.2$ %). In this system also we observe that, as p increases, M_{min} decreases first very sharply ($p \in [9.2; 10]$ %) then very mildly ($p \in [10; 20]$ %). For $p \geq 20$ % the minimal margin

Table 7.8: Variation of M_{min}, BC, $\mathcal{L}$ and M_{min}/BC with p

$p(\%)$	90	50	40	30	25	20	15	10	9.2
M_{min} (MW)	307	313	339	346	364	375	406	624	3242
BC (MW)	387	765	936	1217	1504	2121	2900	6246	35251
nb of loads	3	5	6	7	9	12	16	37	281
M_{min}/BC	0.793	0.409	0.362	0.284	0.242	0.176	0.140	0.099	0.091

remains almost constant. Note the large difference between the two extreme values of M obtained in this large system.

From Eq. (7.37), one can predict that $M_{min}/BC \cong p$. Indeed, the variation of M_{min}/BC in Fig. 7.4 is quite linear and very close to the first bisectrix. The nonlinearities are attributable to the load which is not increased at its maximum B_i^-. The lower the number of loads involved, the more pronounced the effect of this load. For the conventional area-constrained margin, M/BC is exactly equal to p, by definition.

The right plot in Fig. 7.4 shows the same results but with the base case load BC on the abscissa. The variation of the relative margin M_{min}/BC is hyperbolic. The smallest value of M_{min}/BC is obtained by increasing the load in the whole system. However, to the right of point A, the value does not change significantly (although both M_{min} and BC increase). As a consequence, from the value of M_{min} at point A, one can estimate with a good accuracy the value of M_{min} relative to any larger area. In some sense, point A is a compromize between the smallest relative margin and the identification of the area "at the heart of instability".

The variation of the M_{min} with BC is almost linear, owing to the relationship (7.37).

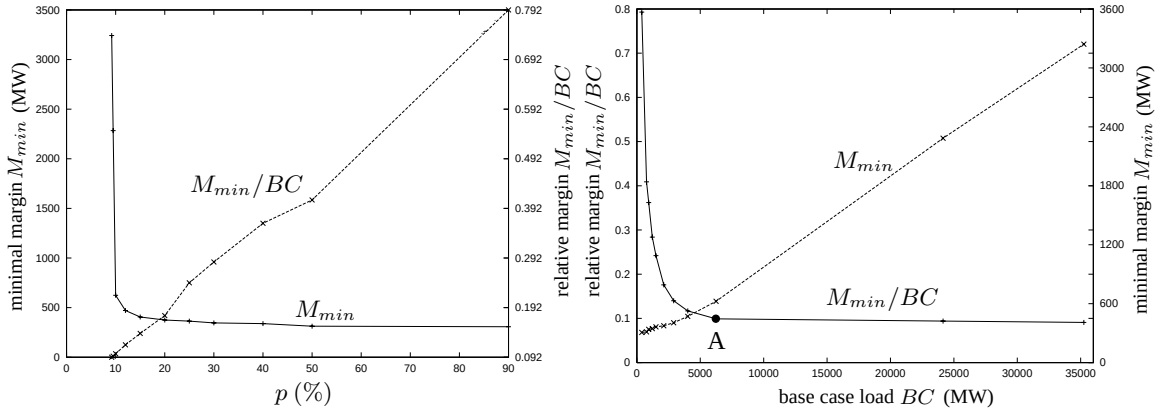

Figure 7.4: Minimal and relative margins for the loss of line B

Table 7.9 and Figure 7.5 present the results relative to the loss of line A which is the most dangerous contingency for a national homothetic load increase. Note that when p decreases below 4 %, the minimal margin remains constant albeit the number of involved

loads increases. The reason is that the three loads participating are quite equal sensitive.

Table 7.9: Minimal margin (MW) for different values of p

$p(\%)$	> 9	$5 < p < 9$	4	3	2	1.5	1
M_{min} (MW)	16	16	16	18	18	71	335
BC (MW)	169	340	416	703	1069	4968	33670
nb of loads	1	2	3	5	7	33	263
M_{min}/BC	0.094	0.047	0.038	0.025	0.016	0.014	0.099

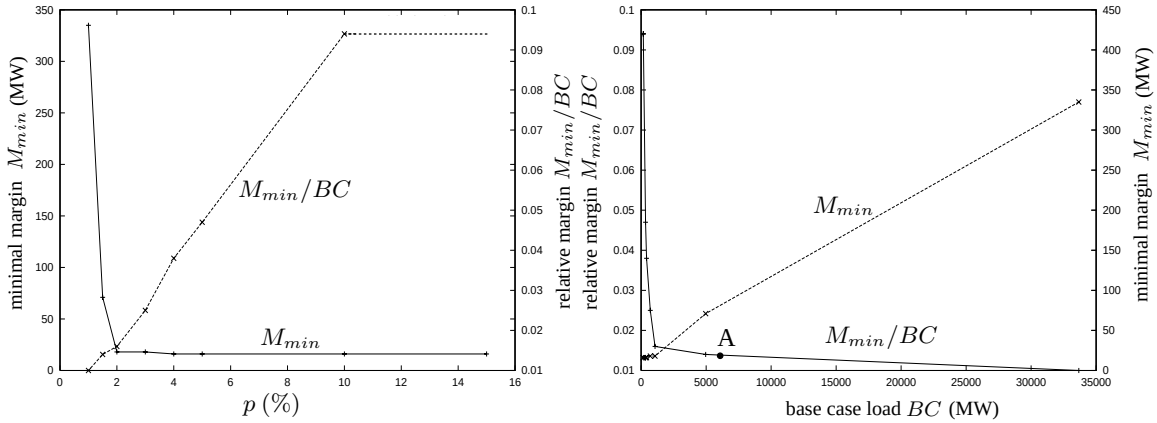

Figure 7.5: Minimal and relative margins for the loss of line A

In the left plot of Fig. 7.5, the "saturation" of the relative margin for $p > 10$ % comes from the fact that a single load is increased.

The value of p above which the minimal margin remains constant varies from one contingency to another. For the loss of line A, this value is 2 % while for the loss of line B it is 15 %.

Chapter 8

Conclusion and future work

8.1 Main contributions of the thesis

This thesis was devoted to the preventive assessment and enhancement of voltage stability and security in electric power systems.

Although the approaches proposed in this work have been derived within the context of a deregulated environment (whatever its type: pool, bilateral contract or combination of both), they apply equally well to a classical, vertically integrated system.

In the course of deriving all the proposed methods we have paid attention to keeping them compatible with the (more traditional) handling of thermal overloads, thereby providing a *unified treatment of voltage and thermal security*.

The heart of most proposed procedures is the derivation of sensitivities indicating the relative efficiency of the various bus injections to restore voltage stability or increase an insufficient voltage security margin. In this respect, we started from the work previously performed at the University of Liège within the context of corrective (emergency) control. *The information obtained from the unstable post-contingency system evolution can be re-used to identify the best pre-contingency controls*. To this purpose, we have first re-used the normal ($\mathbf{n}$) vector technique which had been found effective to identify the best load shedding locations in a post-disturbance situation. Next, we have *proposed and successfully tested an alternative criterion to rank the power injections, namely the* $\frac{\partial V_\ell}{\partial \mathbf{P}}$ *sensitivities*. With respect to the previous $\mathbf{n}$-based criterion, these sensitivities offer advantages in terms of efficiency, reliability and extension to low but stable voltage problems, while exhibiting equally good ranking capabilities.

Based on the above information, we propose to *handle voltage security through a set of linear equality constraints* that can be incorporated to various optimization problems. These constraints can be combined with those stemming from the thermal overload aspect. Nevertheless, as voltage security constraints are less linear by nature, we have devised *techniques which allow to compensate for the nonlinearities while keeping the*

computational effort at a tractable level.

From there on, the so derived sensitivities and inequality constraints have been used to deal with *three different problems* of interest in preventive security analysis:

1. *Congestion management*. We have proposed two optimization-based approaches to manage congestions due to voltage instability and/or thermal overload within the day-ahead or the real-time environment. The first one relies on power injections (generator outputs and load consumptions) while the second one uses power transactions as controls. In parallel, we have considered the problem of "simply" restoring stability with respect to a set of contingencies or, additionally, restoring security margins.

   To this purpose, the inequality constraints could be incorporated to an optimal power flow, although we have considered simpler optimization problems to test our methods. A salient feature of our approach is the simultaneous treatment of all harmful contingencies and the handling of conflicting controls. This may require to incorporate the inequality constraints of some harmless contingencies.

   The optimization aims at removing the congestion while disturbing the market equilibrium to the least extent. As regards the minimal control change objective, we considered the relative merits of the L_1 and L_2 norms in terms of fairness and effectiveness of congestion management. The L_1 norm yields the minimum deviation from the market equilibrium but may be deemed discriminatory. On the other hand, the L_2 norm is less discriminatory, allows to account for sensitivity inaccuracies but leads to larger changes of the control variables.

2. *Computation of simultaneous Available Transfer Capabilities (ATCs)*. Clearly, the non-simultaneous ATCs computation cannot properly take into account the fact that multiple transactions take place at the same time. The allocation of transmission capacity on non-simultaneous basis may have thus two negative consequences: the ATCs may be either overestimated, which may lead to congestions (see example of Fig. 6.2), or too conservative (see example of Fig. 6.5), which may unacceptably hamper trades.

   We have instead proposed a single optimization-based computation providing the simultaneous ATC of a set of transactions. Here too, two objective functions were considered. While the L_1 objective maximizes the use of the transmission capacity, the L_π one yields a fairer capacity allocation to the various transactions.

   A possible drawback of our approach is the overestimation of ATCs which occurs when "counterflowing" transactions eventually do not use the whole maximum allocated capacity, while the "harmful" transactions use their maximum allocated capacity. This situation can be partially mitigated by using the L_π objective which allows a very flexible dispatch of transactions.

   The simultaneous ATCs seem suitable rather in "longitudinal" systems where several transactions tend to use the same corridor, whose capacity must be fairly allocated between the traders. On the other hand, non-simultaneous allocation of transmission capacity remains of interest in systems having counterflow transactions (for instance in meshed networks).

3. *Evaluation of security margin intervals*. In view of the uncertainty that may affect the participation of loads and generators to the power transfer from one area to another, we propose to determine the range of possible values of (voltage and thermal) security margins. More precisely, we propose an optimization-based computation of the minimal and maximal margins under the assumption that individual injection changes remain within specified bounds. When dealing with a single contingency, the minimal margin is appealing because it yields the value of a power transfer which can be safely achieved by any source-sink pattern. With respect to multiple contingencies, the maximal margin may prove useful when looking for a maximal power transfer between two systems. Moreover, the result of such computations is not only the margin interval (which by itself is a sort of sensitivity information) but also the location of the corresponding load/generation increases, which pinpoints the weak area of the system with respect to the given contingency.

   As regards thermal overloads, the computation of a minimal (or maximal) margin is fast, the main effort being two or three contingency evaluations at some stress levels (depending upon whether one relies on linearization or perform some nonlinear correction). Minimal (or maximal) margin with respect to voltage instability is obtained by a combination of both linear and nonlinear techniques. The computational effort is the same as for a conventional margin.

   Finally, we have investigated how the minimal margin varies with the bounds imposed on power injection variations. We have observed that it is generally little sensitive to these bounds. However, for certain (narrow) range of variation of these bounds it appears to be highly sensitive. To overcome this shortcoming the *relative margin* can be alternatively used.

Besides the above leitmotiv, the thesis offers some additional contributions:

- *Filtering of contingency*. We proposed a simple and reliable technique to filter out harmless contingencies when computing the voltage security margins of a large set of contingencies. This step is essential in real-time applications to large systems. Attention has been paid to the compromize between missing harmful contingencies and producing false alarms for harmless ones.

- *Evaluation of reactive reserves with respect to a contingency*. The central concept proposed here is the *effective capability* of a generator with respect to a given contingency. The latter is taken as the reactive power produced by the generator in the marginally acceptable post-contingency situation. For many generators of a (large enough) system, the effective capability is smaller than the physical one, due to the impossibility of transmitting reactive power over long distances. The reactive reserves are obtained as a by-product of the binary search of a security margin, thus at no additional computational cost.

  Such reserves could be precious pieces of information within the context of a deregulated market where providing reactive reserves is an ancillary service which should be properly paid.

We also propose a dimensionless security index, looking from the generation side, as an alternative to the conventional security margin. Its linear decrease with the system stress is noteworthy.

Most of the methods proposed in this thesis were successfully tested on real-life systems. Additional results can be found in the publications listed in Section 1.5.

From a practical viewpoint all the above computations have been *coupled to the fast time-domain quasi steady-state simulation of ASTRE*, the voltage stability and security analysis software developed at the University of Liège.

Finally, several ideas developed in this work have been implemented within the context of the OMASES project [1][VMK03].

8.2 Future work

Among the possible extensions of this work, let us quote:

- the development of an approach combining preventive and corrective control, in order to find a trade-off between the cost of protecting the system against low-probability disturbances and the cost of emergency actions if the harmful disturbance occurs (see Section 5.6). Such a trade-off between preventive and corrective control is attractive but complex. Whether it is feasible and can be accepted by industry is still an open question;

- the extension of our congestion management formulation to take into account discrete controls, mainly the starting-up of "out-of-merit" generators (and possibly the shutting-down of in-merit ones) to guarantee system security. As it disturbs even more the market equilibrium, the decision to have "must run" generators must be taken by the TSO in a transparent and objective manner. This extension of the congestion management problem could be tackled by mixed linear-integer programming;

- the extension of the congestion management techniques to account for time aspects. The approach discussed in this work is static in the sense that it refers to a particular point in time. If some "periodicity" is observed in the power system behaviour, the use of a "blind" static method will repeatedly penalize the same generators and/or loads at the same time of the day, which may be deemed discriminatory. This drawback can be partially alleviated by using an L_2 norm objective, which makes more market participants share the congestion removal effort. However, an extension incorporating the time dimension could be an interesting alternative; it should be able to take into account all actions previously taken to relieve congestions;

[1] "Open Market Access and SEcurity assessment System", project funded by the European Union

- besides further technical improvements (for instance a less rigid criterion for including generators in the $\mathcal{E}$ set), the evaluation of reactive reserves with respect to a whole set of contingencies deserves attention, as well as their valuation as an ancillary service.

Appendix A

Overview of the tested systems

We provide hereafter a short overview of the three systems used through this work.

A.1 The Nordic 32 test system

This system is a slightly modified variant of a test system used by CIGRE Task Force 32.02.08 on Long-Term Dynamics (1995). It includes 80 buses, 23 generators and 22 loads, each one fed through a transformer with LTC. Its one-line diagram is shown in Fig. A.1.

The system has two main areas, denoted respectively “North” and “South” in Fig. A.1. The production is mainly of the hydro type in the North and thermal type in the South. Most of the load is located in the South area which leads to a rather heavy power transfer from North to South.

Loads are represented by an exponential model (see Fig. 2.2) with $\alpha = 1$ and $\beta = 2$.

The QSS long-term simulation reproduces the dynamics of LTCs and OELs, as explained in Section 2.2.

Note that there is no slack-bus in the QSS model; instead, generators respond to a disturbance according to governor effects [VCV98]. In this respect, it is assumed that only the generators of the North area participate to frequency control (i.e. the others have infinite speed droops). Thus, when a Southern generator is lost, the power deficit adds to the North to South transfer.

A.2 The RTE system

RTE is the Transmission System Operator of the French system (formerly EDF).

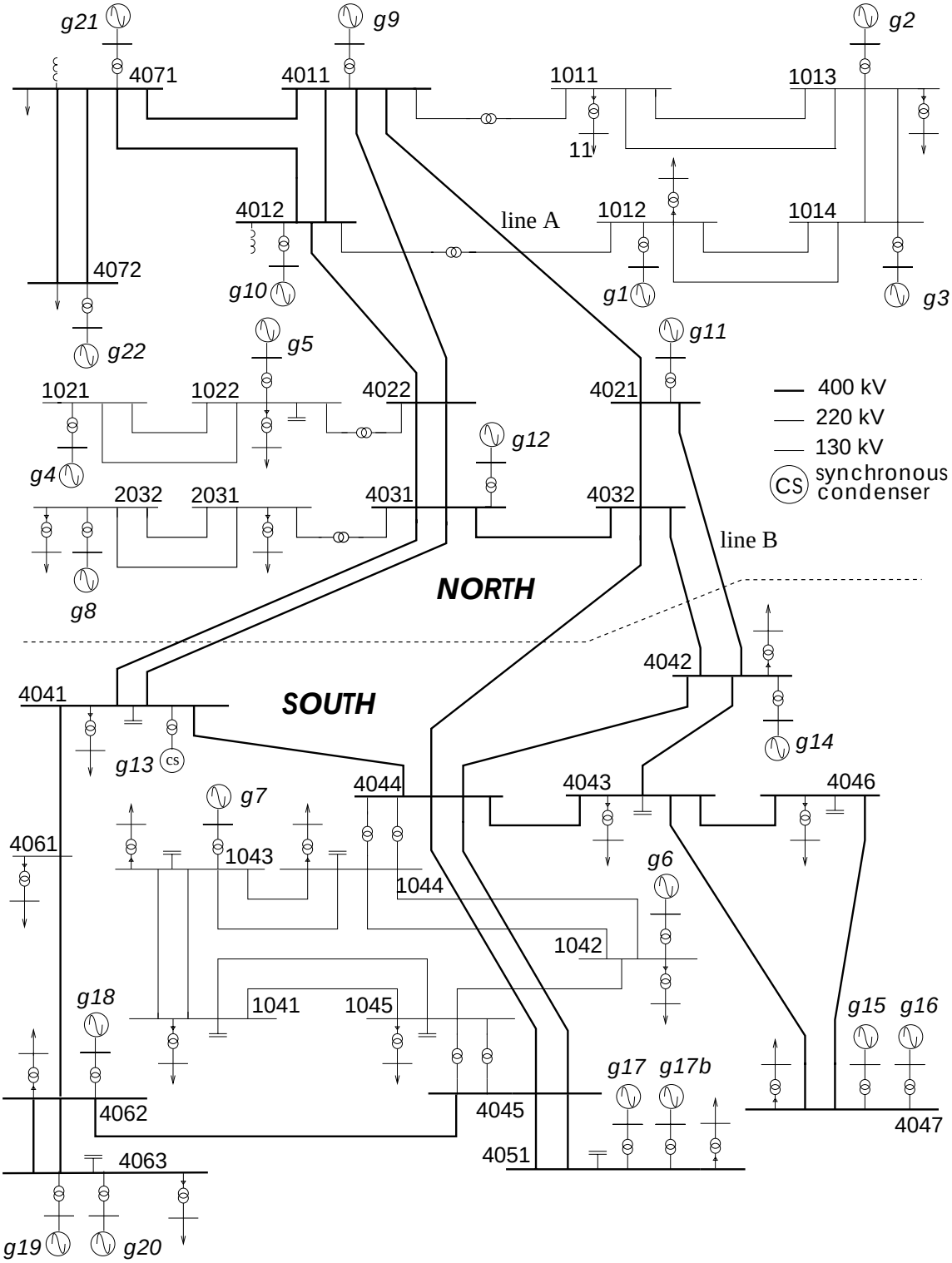

Figure A.1: The Nordic-32 system

With a peak load of about 75,000 MW, this large system is operated from 7 regional and one national control centers. As in many European countries, the network is rather dense and meshed. Much attention is paid to voltage security in the Western and South-East

regions where load centers are far away from generation.

A one-line diagram of the Western part of the transmission system is shown in Fig. A.2.

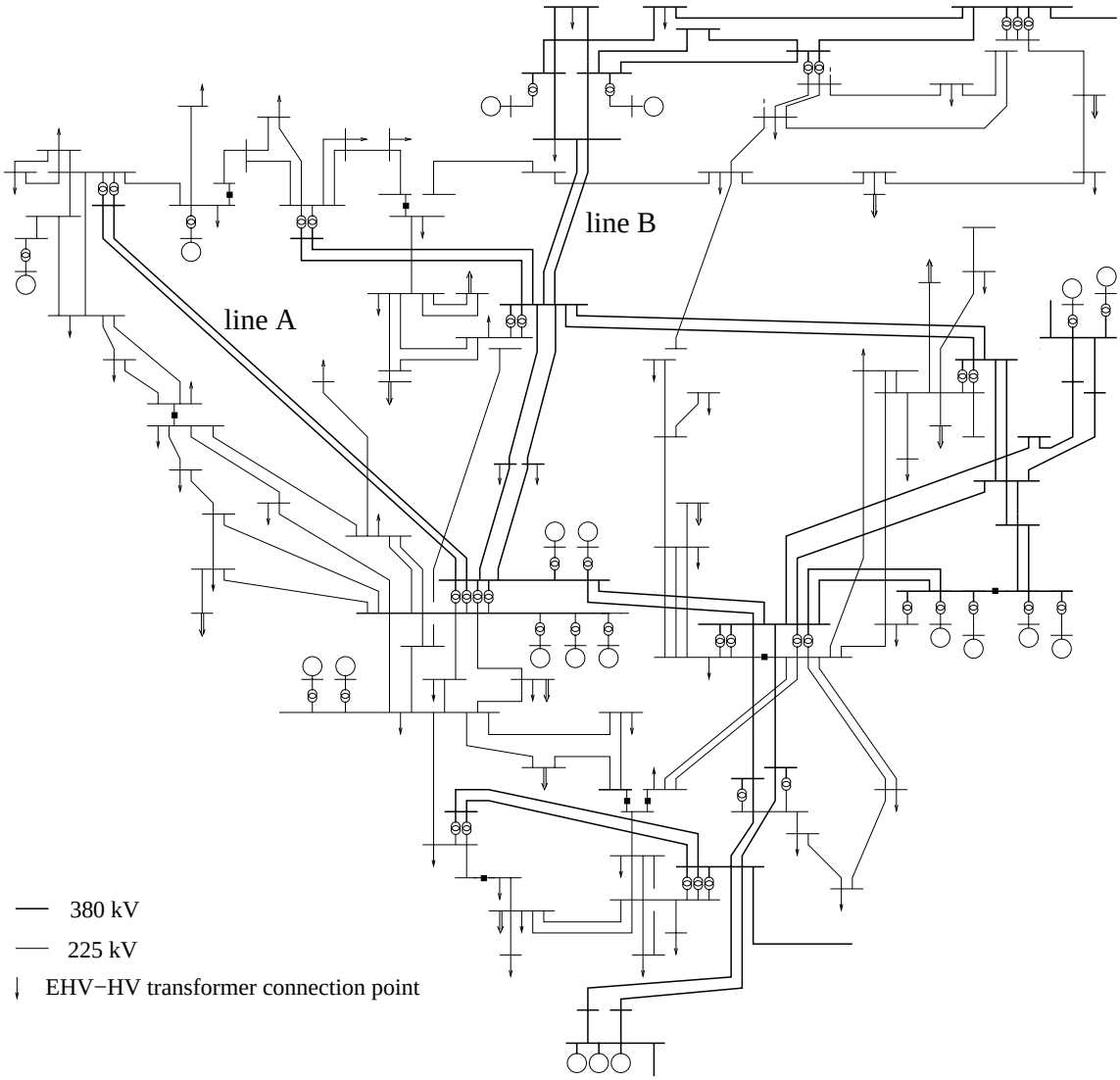

Figure A.2: Western part of the RTE system

The QSS simulation model includes 1203 buses at the 400 and 225-kV (EHV) levels. The subtransmission and distribution systems are represented in a simplified way through "cascades" of EHV-HV and HV-MV transformers. The former correspond to the real transformers feeding the (90 and 63-kV) subtransmission systems, while the latter are ideal transformers accounting for load restoration by many HV-MV distribution transformers. This load representation brings 512 additional HV buses in the model, as well as 1024 LTCs.

176 generators are represented in detail and equipped with OELs.

The QSS simulation also accounts for the presence of 15 secondary voltage controllers, represented in the Western and South-East regions [PLT87]. Each of them controls the

voltage setpoints of a set of generators so as to regulate the EHV voltage of a “pilot node”, while sharing the reactive power generation in accordance with the individual generator capabilities. Further information on the system modelling can be found in [CCM00, SMC98].

A.3 The Hydro-Québec system

The Hydro-Québec system is characterized by great distances (more than 1000 km) between the large hydro generation areas (James Bay, Churchill Falls and Manic-Outardes) and the main load center (around Montréal and Québec City). Accordingly, the company has developed an extensive 735-kV transmission system, whose lines are located along two main corridors. The system is angle stability limited in the North and voltage stability limited in the South (near the load center). Frequency stability is also a concern due to the system interconnection through DC links only, as well as the sensitivity of loads to voltage.

Figure 5.3 shows the structure of the 735-kV transmission system.

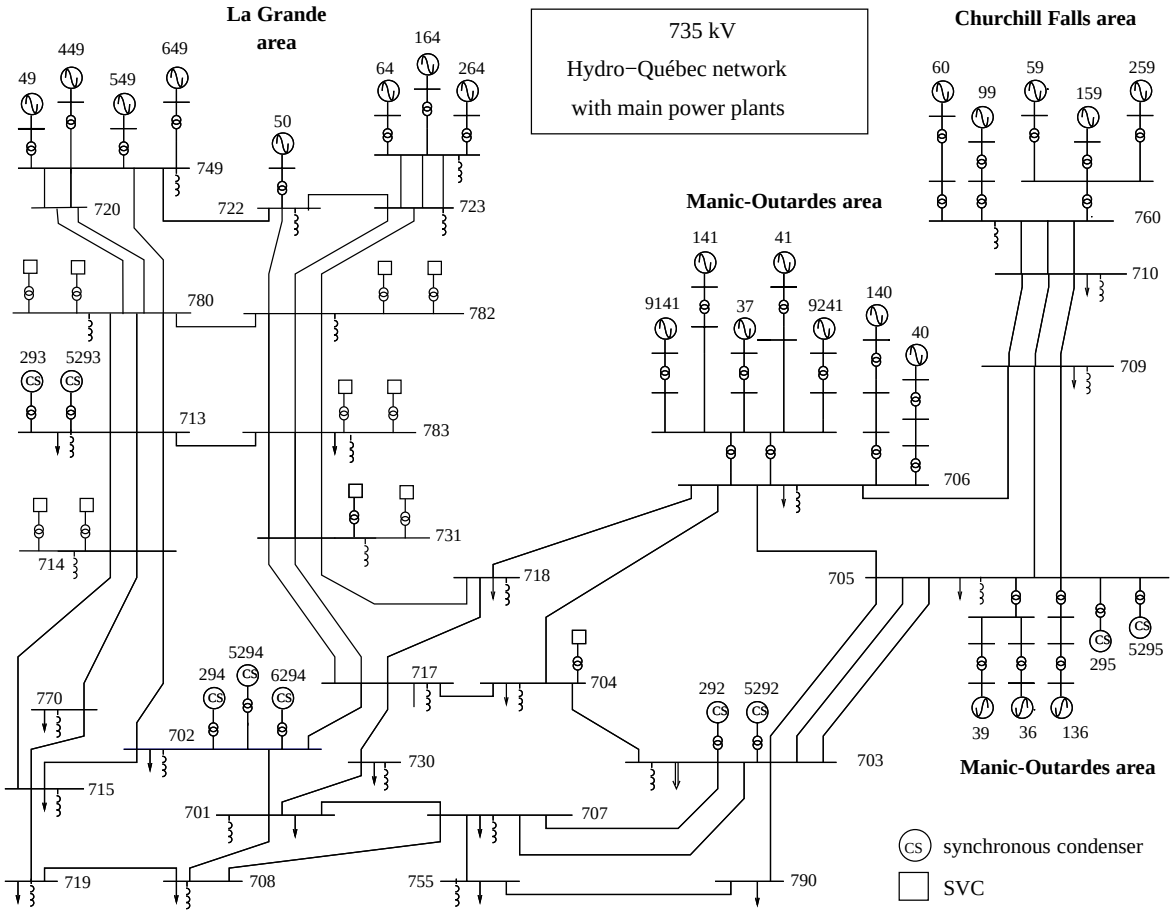

Figure A.3: One-line diagram of the Hydro-Québec system (735-kV grid)

Beside static var compensators and synchronous condensers, the automatic shunt reactor switching devices, named MAIS [1], play an important role in voltage control [BTS96]. These devices, in operation since early 1997, are now available in twenty-two 735-kV substations and control a large part of the total 25,500 Mvar shunt compensation. Simply stated, each MAIS monitors the EHV voltage of a 735-kV substation and if the latter stays below (resp. above) some threshold for some time, it trips (resp. connects) one shunt reactor. The coordination between substations is performed through the switching delays. While fast-acting MAIS can improve transient (angle) stability, slower MAIS significantly contribute to voltage stability.

The long-term evolution of voltages is thus very dynamic by nature, which has motivated the adoption of QSS simulation by HQ engineers for security limit computations.

The QSS simulation model includes around 550 buses, 100 generators, 11 SVCs. The discrete devices taken into account are the 230 LTCs, the OELs of several synchronous condensers, and the above mentioned MAIS devices, all with their own time delays. The total load is around 33,000 MW in the studied configuration.

[1] French acronym for “Manoeuvre Automatique d’Inductances Shunt”

Bibliography

[ABH82] F. Albuyeh, A. Bose, and B. Heath. Automatic contingency selection: ranking outages on the basis of real and reactive power equations. *IEEE Transactions on Power Apparatus and Systems*, PAS-101:107–112, January 1982.

[AC92] V. Ajjarapu and C. Christy. The continuation power flow: a tool for steady state voltage stability analysis. *IEEE Transactions on Power Systems*, 7:416–423, 1992.

[ACT02] R. Audouin, D. Chaniotis, P. Tsamasphyrou, and J-M. Coulondre. Coordinated auctioning of cross-border capacity: a comparison. In *Proc. of the 14th PSCC Conference*, Sevilla (Spain), June 2002.

[ADH94] F. Alvarado, I. Dobson, and Y. Hu. Computation of closest bifurcations in power systems. *IEEE Transactions on Power Systems*, 9:918–928, May 1994.

[AF92] B. Avramovic and L. H. Fink. Real-time reactive security monitoring. *IEEE Transactions on Power Systems*, Vol. 7:432–437, February 1992.

[AJ89] F.L. Alvarado and T.H. Jung. Direct detection of voltage collapse conditions. In *Proc. of Bulk Power System Voltage Phenomena - Voltage Stability and Security*, pages 5.23–5.38, EL-6183 EPRI, 1989.

[AST83] O. Alsac, B. Stott, and W.F. Tinney. Sparsity-oriented compensation methods for modified network solutions. *IEEE Transactions on Power Apparatus and Systems*, PAS-103:1050–1060, May 1983.

[ATC96] NERC document. Available transfer capability definitions and determination. Technical report, June 1996. Downloadable from http://www.nerc.com.

[BB00] S. Borenstein and J. Bushnell. Electricity restructuring: Deregulation or reregulation ? *Regulation*, 23 No. 2:46–52, 2000.

[Bet00] A.L. Bettiol. *Maximum power transfer in transient stability constrained power systems: Application to a Brazilian Power network*. PhD thesis, University of Liège, Belgium, 2000.

[BFD98] A. Berizzi, P. Finazzi, D. Dosi, P. Marannino, and S. Corsi. First and second order methods for voltage collapse assessment and security enhancement. *IEEE Transactions on Power Systems*, 13, No. 2:543–551, May 1998.

[BGC00] J.W. Bialek, A. Germond, and R. Cherkaoui. Improving NERC transmission loading relief procedure. *Electricity Journal*, pages 11–19, June 2000.

[Bia02] J.W. Bialek. Gaming the uniform-price spot market - quantitative analysis. *IEEE Transactions on Power Systems*, 17, No. 3:768–773, August 2002.

[BMZ00] A. Berizzi, M. Merlo, Y.G. Zeng, P. Marannino, and A. P.A. Scarpellini. Determination of N-1 security maximum transfer capability through power corridors. *IEEE PES Winter Meeting, Singapore*, pages 1739–1744, Janaury 2000.

[Bor01] P. Bornard. Congestion management and system security. Technical report, Opio, France, June 2001. 6-th International Workshop on Electric Power Control Centers.

[BP92] M. Begovic and A. Phadke. Control of voltage stability using sensitivity analysis. *IEEE Transactions on Power Systems*, 7:114–123, 1992.

[Bri69] J.P. Britton. Improved area interchange control for Newton's method load flows. *IEEE Transactions on Power Apparatus and Systems*, PAS-88:1577–1581, 1969.

[BS70] M. Baughman and F.C. Schweppe. Contingency evaluation: real power flows from a linear model. *IEEE Summer Power Meeting*, pages Paper CP 689–PWR, 1970.

[BTS96] S. Bernard, G. Trudel, and G. Scott. A 735-kv shunt reactors automatic switching system for hydro-québec network. *IEEE Transactions on Power Systems*, 11, No. 4:2024–2030, November 1996.

[Bul98] C. Bulac. *Contributions concerning the voltage stability of mixed AC-DC systems (in romanian)*. PhD thesis, University "Politehnica" of Bucharest, Romania, 1998.

[BZM00] A. Berizzi, Y.G. Zeng, P. Marannino, A. Vaccarini, and P.A. Scarpellini. A second order method for contingency severity assessment with respect to voltage collapse. *IEEE Transactions on Power Systems*, 15, No. 1:81–87, February 2000.

[Can98] C.A. Canizares. Calculating optimal system parameters to maximize the distance to saddle-node bifurcations. *IEEE Transactions on Circuits and Systems-I : Fundamental theory and Applications*, 45:225–237, 1998.

[Can02] C.A. Canizares. IEEE/PES voltage stability report. Technical report, August 2002. Downloadable from http://www.power.uwaterloo.ca/ claudio/claudio.html.

[Cap00] F. Capitanescu. Contributions à l'analyse et la commande préventive de la sécurité de tension. DEA thesis (in french), University of Liège, 2000.

[CCM00] T. Van Cutsem, F. Capitanescu, C. Moors, D. Lefebvre, and V. Sermanson. An advanced tool for preventive voltage security assessment. *Proc. of the VIIth SEPOPE conf.*, 2000. Paper IP-035.

[CCS02] H. Chen, C.A. Canizares, and A. Singh. Transaction security cost analysis by take-risk strategy. In *Proc. of the 14th PSCC Conference*, Sevilla (Spain), June 2002.

[CGA03] A.J. Conejo, F.D. Galiana, J.M. Arroyo, R. Garcia-Bertrand, C.W. Chua, and M. Huneault. Economic inefficiencies and cross-subsidies in an auction-based electricity pool. *IEEE Transactions on Power Systems*, 18, No. 1:221–228, February 2003.

[CGM98] J.W.M. Cheng, F.D. Galiana, and D.T. McGillis. Studies of bilateral contracts with respect to steady-state security in a deregulated environment. *IEEE Transactions on Power Systems*, 13, No. 3:1020–1025, August 1998.

[CGS84] J. Carpentier, R. Girard, and E. Scano. Voltage collapse proximity indicators computed from an optimal power flow. In *8-th PSCC Proceedings*, pages 671–678, Helsinki (Finland), 1984.

[CMM99] T. Van Cutsem, C. Moisse, and R. Mailhot. Determination of secure operating limits with respect to voltage collapse. *IEEE Transactions on Power Systems*, 14, No. 1:327–335, February 1999.

[CMP01] J. Carpentier, D. Menniti, A. Pinnarelli, N. Scordino, and N. Sorrentino. A model for the ISO Insecurity Costs Management in a Deregulated Market Scenario. In *Proc. of the IEEE Power Tech Conference*, Porto (Portugal), 2001. ISBN 0-7803-7140-2.

[CTF02] IEEE/CIGRE Joint Task Force on stability terms and definitions. Definition and classification of power system stability. Technical report, August 2002.

[CTF87] CIGRE Task Force 38-01-03. Planning against voltage collapse. Technical report, pp. 55-75, 1987. Electra No. 111.

[CTF94] N.D. Hatziargyriou and T. Van Cutsem editors. Indices predicting voltage collapse including dynamic phenomena. Technical report, 1994. Technical report CIGRE Task Force 38-02-11.

[Cut91] T. Van Cutsem. A method to compute reactive power margins with respect to voltage collapse. *IEEE Transactions on Power Systems*, 6, No. 1:145–156, February 1991.

[CVC01] F. Capitanescu and T. Van Cutsem. Evaluation of reactive power reserves with respect to contingencies. *Bulk Power System Dynamics and Control V, Onomichi, Japan*, pages 377–386, August 2001.

[CVC02a] F. Capitanescu and T. Van Cutsem. Preventive control of voltage security margins: a multicontingency sensitivity-based approach. *IEEE Transactions on Power Systems*, 17:358–364, 2002.

[CVC02b] F. Capitanescu and T. Van Cutsem. Evaluating bounds on voltage and thermal security margins under power transfer uncertainty. In *Proc. of the 14th PSCC Conference*, Sevilla (Spain), June 2002.

[CVC02c] F. Capitanescu and T. Van Cutsem. Computation of simultaneous available transfer capability under voltage and thermal security constraints. *Modern Electric Power Systems Conference, Wroclaw, Poland*, pages 204–210, September 2002.

[CW98a] R.D. Christie and I. Wangensteen. The energy market in Norway and Sweden: the spot and futures markets. *IEEE Power engineering review*, 18:55–56, March 1998.

[CW98b] R.D. Christie and I. Wangensteen. The energy market in Norway and Sweden: congestion management. *IEEE Power engineering review*, 18:61–63, May 1998.

[CWF97] H.D. Chiang, C.S. Wang, and A.J. Flueck. Look-ahead voltage and load margin contingency selection functions for large-scale power systems. *IEEE Transactions on Power Systems*, 12, No. 1:173–180, February 1997.

[CWW00] R.D. Christie, B.F. Wollenberg, and I. Wangensteen. Transmission management in the deregulated environment. *Proceedings of the IEEE*, 88:170–195, 2000.

[Dav98] A.K. David. Dispatch methodologies for open access transmission systems. *IEEE Transactions on Power Systems*, 13, No. 1:46–53, February 1998.

[DL92a] I. Dobson and L. Lu. Computing an optimum direction in control space to avoid saddle node bifurcation and voltage collapse in electric power systems. *IEEE Transactions on Automatic Control*, 37:1616–1620, 1992.

[DL92b] I. Dobson and L. Lu. Voltage collapse precipitated by the immediate change in stability when generator reactive power limits are encountered. *IEEE Transactions on Circuits and Systems-I: Fundamental Theory and Applications*, 45, No. 3:762–766, 1992.

[DL93] I. Dobson and L. Lu. New methods for computing a closest saddle node bifurcation and worst case load power margin for voltage collapse. *IEEE Transactions on Power Systems*, 8:905–911, 1993.

[DL74] T. E. Dy-Liacco. Real-time computer control of power systems. *Proceedings of the IEEE*, 62:884–891, 1974.

[Dob92] I. Dobson. Observations on the geometry of saddle node bifurcation and voltage collapse in electric power systems. *IEEE Transactions on Circuits and Systems – I*, 39(3):240–243, 1992.

[DS93] J. Deuse and M. Stubbe. Dynamic simulation of voltage collapses. *IEEE Transactions on Power Systems*, Vol. 8:894–904, August 1993.

[DT68] H.W. Dommel and W.F. Tinney. Optimal power flow solutions. *IEEE Transactions on Power Apparatus and Systems*, PAS-87, No. 10:1866–1876, October 1968.

[EDF00] T. Van Cutsem and G. Hassé. Security valuation on the EDF system. Technical report, November 2000. Contract No. R42/C29629 - ER424.

[EIM96] G.C. Ejebe, G.D. Irisarri, S. Mokhtari, O. Obadina, P. Ristanovic, and J. Tong. Methods for contingency screening and ranking for voltage stability analysis of power systems. *IEEE Transactions on Power Systems*, 11, No. 1:350–356, February 1996.

[ESO01] ETSO. Co-ordinated Auctioning a market-based method for transmission capacity allocation in meshed networks. Technical report, Final Report, April 2001. Downloadable from http://www.etso-net.org.

[ESO01b] ETSO. Definitions of Transfer Capacities in liberalised Electricity Markets. Technical report, Final Report, April 2001. Downloadable from http://www.etso-net.org.

[ESO99] ETSO. Evaluation of congestion management methods for cross-border transmission. Technical report, Florence Regulators Meeting, November 1999. Downloadable from http://www.etso-net.org.

[ETW98] G.C. Ejebe, J. Tong, J.G. Waight, J.G. Frame, X. Wang, and W.F. Tinney. Available transfer capability calculations. *IEEE Transactions on Power Systems*, Vol. 13, No. 4:1521–1527, November 1998.

[EW79] G.C. Ejebe and B.F. Wollenberg. Automatic contingency selection. *IEEE Transactions on Power Apparatus and Systems*, PAS-98:1521–1527, 1979.

[FAM00] Z. Feng, V. Ajjarapu, and D. J. Maratukulam. A comprehensive approach for preventive and corrective control to mitigate voltage collapse. *IEEE Transactions on Power Systems*, 15:791–797, 2000.

[FC78] L.H. Fink and K. Carlsen. Operating under stress and strain. *IEEE Spectrum*, pages 48–53, 1978.

[FGD02] A.J. Flueck, R. Gonella, and J.R. Dondeti. A new power sensitivity method of ranking branch outage contingencies for voltage collapse. *IEEE Transactions on Power Systems*, 17, No. 2:265–271, May 2002.

[FHR97] J.D. Finney, H.A.Othman, and W.L. Rutz. Evaluating transmission congestion constraints in system planning. *IEEE Transactions on Power Systems*, 12, No. 3:1143–1150, August 1997.

[FOC90] N. Flatabo, R. Ognedal, and T. Carlsen. Voltage stability condition in a power transmission system calculated by sensitivity methods. *IEEE Transactions on Power Systems*, 5:1286 –1293, November 1990.

[GDA99] S. Greene, I. Dobson, and F.L. Alvarado. Contingency ranking for voltage collapse via sensitivities from a single nose curve. *IEEE Transactions on Power Systems*, Vol. 14, No. 1:232–240, February 1999.

[GDA02] S. Greene, I. Dobson, and F.L. Alvarado. Sensitivity of transfer capability margins with a fast formula. *IEEE Transactions on Power Systems*, Vol. 17, No. 1:34–40, February 2002.

[GI98] F.D. Galiana and M. Ilic. A mathematical framework for the analysis and management of power transactions under power access. *IEEE Transactions on Power Systems*, 13, No. 2:681–687, May 1998.

[GLB01] D. Gan, X. Luo, D.V. Bourcier, and R.J. Thomas. Min-Max transfer capability: Preliminary results. *Power Engineering Society Winter Meeting*, 1:66–71, 2001.

[GMK92] B. Gao, G. K. Morison, and P. Kundur. Voltage stability evaluation using modal analysis. *IEEE Transactions on Power Systems*, 7:1529–1542, 1992.

[GMK96] B. Gao, G. K. Morison, and P. Kundur. Towards the development of a systematic approach for voltage stability assessment of large-scale power systems. *IEEE Transactions on Power Systems*, 11:1314–1324, 1996.

[GN99] M.H. Gravener and C. Nwankpa. Available transfer capability and first order sensitivity. *IEEE Transactions on Power Systems*, Vol. 14, No. 2:512–518, May 1999.

[Gre98] S. Greene. *Margin and sensitivity methods for security analysis of electric power systems*. PhD thesis, University of Wisconsin - Madison, USA, 1998.

[GS00] S. Grijalva and P.W. Sauer. Transmission loading relief and hour-ahead ATC. *Proceedings of the 33th Annual Hawaii International Conference on System Sciences*, 2000.

[Ham00a] G.A. Hamoud. Assessment of available transfer capability of transmission systems. *IEEE Transactions on Power Systems*, 15, No. 1:27–32, February 2000.

[Ham00b] G.A. Hamoud. Feasibility assessment of simultaneous bilateral transactions in a deregulated environment. *IEEE Transactions on Power Systems*, 15, No. 1:22–26, February 2000.

[HS96] S. Hunt and G. Shuttleworth. *Competition and choice in electricity*. John Wiley and Sons, New York, 1996.

[Hym98] L.S. Hyman. Setting the stage. *from the book Power systems restructuring Engineering and economics - edited by M. Ilic, F. Galiana and L. Fink*, pages 1–11, 1998.

[ILS79] G.D. Irisarri, D. Levner, and A.M. Sasson. Automatic contingency selection for on-line contingency analysis - real time tests. *IEEE Transactions on Power Apparatus and Systems*, PAS-98:1552–1559, September/October 1979.

[IMS97] IMSL Fortran Library. Technical report, 1997.

[IWT97] G.D. Irisarri, X. Wang, J. Tong, and S. Mokhtari. Maximum loadability of power systems using interior-point non-linear optimization method. *IEEE Transactions on Power Systems*, 12, No. 1:162–172, February 1997.

[JG81] J. Jarjis and F.D. Galiana. Quantitative analysis of steady state stability in power networks. *IEEE Transactions on Power Apparatus and Systems*, PAS-100:318–326, January 1981.

[KG86] P. Kessel and H. Glavitsch. Estimating the voltage stability of a power system. *IEEE Transactions on Power Delivery*, 1:346–354, 1986.

[Kun94] P. Kundur. *Power System Stability and Control*. EPRI Power system Engineering Series. McGraw Hill, 1994.

[KVE00] J. Kabouris, C.D. Vournas, S. Efstathiou, G.A. Manos, and G.C. Contaxis. Voltage security considerations in an open power market. *International Conference on Electric Utility Deregulation and Restructuring and Power Technologies*, pages 278–283, April 2000.

[LA73] G.L. Landgren and S.W. Anderson. Simultaneous power interchange capability analysis. *IEEE Transactions on Power Apparatus and Systems*, 92, No. 6:1973–1986, 1973.

[LL02] C.Y. Li and C.W. Liu. A new algorithm for available transfer capability computation. *Electrical Power and Energy Systems*, pages 159–166, 2002.

[LRG02] E. Lobato, L. Rouco, T. Gomez, F. Echavarren, M.I. Navarrete, R. Casanova, and G. Lopez. Solution of daily voltage constraints in Spanish electricity market. In *Proc. of the 14th PSCC Conference*, Sevilla (Spain), June 2002.

[LRN00] E. Lobato, L. Rouco, M.I. Navarrete, R. Casanova, J.C. Castillejo, and G. Lopez. An integrated tool for analysis of power system constraints in the Spanish electricity market security. *IEEE Summer Meeting, Seattle*, 3:1627–1632, July 2000.

[MBG02] P. Marannino, P. Bresesti, A. Garavaglia, F. Zanellini, and R. Vailati. Assessing the transmission transfer capability sensitivity to power transfer parameters. In *Proc. of the 14th PSCC Conference*, Sevilla (Spain), June 2002.

[MGC02] A.L. Motto, F.D. Galiana, A.J. Conejo, and J.M. Arroyo. Network-constrained multiperiod auction for a pool-based electricity market. *IEEE Transactions on Power Systems*, 17, No. 3:646–653, August 2002.

[Mil03] F. Milano. *Pricing system security in electricity market models with inclusion of voltage stability constraints*. PhD thesis, University of Genova, Italy, 2003.

[MK01] A.P.S. Meliopoulos and S.W. Kang. An improved model for the evaluation of actual transfer capability in a deregulated environment. *Bulk Power System Dynamics and Control V, Onomichi, Japan*, pages 203–209, August 2001.

[MMG97] J.C.O Mello, A.C.G. Melo, and S. Granville. Simultaneous transfer capability assessment by combining interior point methods and Monte Carlo simulation. *IEEE Transactions on Power Systems*, Vol. 12, No. 2:736–742, May 1997.

[Moo02] C. Moors. *On the design of load shedding schemes against voltage instability in electric power systems*. PhD thesis, University of Liège, Belgium, 2002.

[MVC99] C. Moors and T. Van Cutsem. Determination of optimal load shedding against voltage instability. In *Proc. of the 13th PSCC Conference*, pages 993–1000, Trondheim (Norway), 1999.

[NN02] T. Nakashima and T. Niimura. Market plurality and manipulation: performance comparison of independent system operators. *IEEE Transactions on Power Systems*, 17, No. 3:762–767, August 2002.

[OS02] Y. Ou and C. Singh. Assessment of available transfer capability and margins. *IEEE Transactions on Power Systems*, Vol. 17, No. 2:463–468, May 2002.

[Ove94] T. J. Overbye. A power flow measure for unsolvable cases. *IEEE Transactions on Power Systems*, 9:1359–1365, 1994.

[PCH02] K. Purchala, T. Van Craenenbroek, and J. Van Hecke. Co-ordinated auctioning algorithm for congestion management. *Modern Electric Power Systems Conference, Wroclaw, Poland*, pages 15–21, September 2002.

[PLT87] J.P. Paul, J.Y. Leost, and J.M. Tesseron. Survey of the secondary voltage control in France: present realization and investigations. *IEEE Transactions on Power Systems*, 2, No. 2:505–511, May 1987.

[RA98] R. Rajaraman and F.L. Alvarado. Inefficiencies of NERC's transmission loading relief procedure. *Electricity Journal*, pages 47–54, October 1998.

[RAU93] N.D. Reppen, R.R. Austria, J.A. Uhrin, M.C. Patel, and A. Galatic. Performance of methods for ranking and evaluation of voltage collapse contingencies applied to a large-scale network. In *Proc. of the IEEE Power Tech Conference*, pages 337–343, Athens (Greece), 1993.

[RCQ99] W. Rosehart, C.A. Canizares, and V.H. Quintana. Optimal power flow incorporating voltage collapse constraints. *Proc. of 1999 IEEE PES Summer Meeting, Edmonton*, pages 820–825, 1999.

[RV02] D. Ruiz-Vega. *Dynamic security assessment and control: transient and small signal stability*. PhD thesis, University of Liège, Belgium, 2002.

[RVC96] P. Rousseaux and T. Van Cutsem. Fast Small Disturbance Analysis of Long-Term Voltage Stability. In *Proc. of the 12th PSCC Conference*, pages 295–302, Dresden (Germany), 1996.

[SA74] B. Stott and O. Alsac. Fast decoupled load flow. *IEEE Transactions on Power Apparatus and Systems*, PAS-93:859–869, May/June 1974.

[SAK98] G. Strbac, S. Ahmed, D. Kirschen, and R. Allan. A method for computing the value of corrective security. *IEEE Transactions on Power Systems*, Vol. 13, No. 3:1096–1102, August 1998.

[SAM87] B. Stott, O. Alsac, and A.J. Monticelli. Security analysis and optimization (invited paper). *Proceedings of the IEEE*, 75, No. 12:1623–1644, 1987.

[Sau97] P.W. Sauer. Technical challenges of computing available transfer capability in electric power systems. *Proceedings of the 30th Annual Hawaii International Conference on System Sciences*, V:589–593, January 1997.

[SBD89] M. Stubbe, A. Bihain, J. Deuse, and J.-C. Baader. STAG - A new unified software program for the study of the dynamic behaviour of electrical power systems. *IEEE Transactions on Power Systems*, 4:129–138, 1989.

[Sch98] R.A. Schlueter. A voltage stability security assessment method. *IEEE Transactions on Power Systems*, Vol. 13, No. 4:1423–1438, November 1998.

[SCT88] F.C. Schweppe, M.C. Caraminis, R.D. Tabors, and R.E. Bohn. *Spot pricing of electricity*. Power electronics and power systems series. Kluwer Academic Publishers, 1988.

[SHC91] R. A. Schlueter, I. Hu, M.W. Chang, J.C. Lo, and A. Costi. Methods for determining proximity to voltage collapse. *IEEE Transactions on Power Systems*, Vol. 6, No. 1:285–292, February 1991.

[SHP98] H. Singh, S. Hao, and A. Papalexopoulos. Transmission congestion management in competitive electricity markets. *IEEE Transactions on Power Systems*, 13, No. 2:672–680, May 1998.

[SKL00] H. Song, S. Kim, B. Lee, S.H. Kwon, and V. Ajjarapu. Determination of interface flow margin for voltage stability analysis using the modified continuation power flow. *IEEE Summer Meeting, Seattle*, 1:32–37, July 2000.

[SLL02] H. Song, C.C. Liu, and J. Lawarrée. Nash equilibrium bidding strategies in a bilateral electricity market. *IEEE Transactions on Power Systems*, 17, No. 1:73–79, February 2002.

[SMC98] V. Sermanson, C. Moisse, T. Van Cutsem, and Y. Jacquemart. Voltage security assessment of systems with multiple instability modes. *Bulk Power System Dynamics and Control IV, Santorini, Greece*, pages 185–196, August 1998.

[STA71] A. Sasson, C. Trevino, and F. Aboytes. Improved Newton's load flow through a minimization technique. *IEEE Transactions on Power Apparatus and Systems*, PAS-90:1974–1981, 1971.

[Tay92] C. W. Taylor. Concepts of undervoltage load shedding for voltage stability. *IEEE Transactions on Power Delivery*, 7:480–488, 1992.

[Tay94] C. W. Taylor. *Power System Voltage Stability*. EPRI Power System Engineering Series. McGraw Hill, 1994.

[TB02] L.A. Tuan and K. Bhattacharya. Interruptible load services for transmission congestion relief. In *Proc. of the 14th PSCC Conference*, Sevilla (Spain), June 2002.

[TLR97] NERC document. Transmission Loading Relief procedure. Technical report, 1997. Downloadable from http://www.nerc.com.

[TMI83] Y. Tamura, H. Mory, and S. Iwamoto. Relationship between voltage instability and multiple load flow solutions. *IEEE Transactions on Power Apparatus and Systems*, PAS-102:1115–1125, 1983.

[TR98] C.W. Taylor and R. Ramanathan. BPA reactive power monitoring and control following the august 10, 1996 power failure. *Proc. of the VIth SEPOPE conf.*, 1998. Paper IP-003.

[UPK98] K. Uhlen, A. Petterteig, G.H. Kjolle, A.T. Holen, G.G. Lovas, and M. Meisingset. On-line security assessment and control - probabilistic versus deterministic operational criteria. *The European Safety and Reliability Conference, Trondheim*, June 1998.

[VC00] T. Van Cutsem. Voltage stability: phenomena, countermeasures, and analysis methods (invited paper). *Proceedings of the IEEE*, 88:208–227, 2000.

[VCJ95] T. Van Cutsem, Y. Jacquemart, J.-N. Marquet, and P. Pruvot. A comprehensive analysis of mid-term voltage instability. *IEEE Trans. on Power Systems*, 10:1173–1182, 1995.

[VCM97] T. Van Cutsem and R. Mailhot. Validation of a fast voltage stability analysis method on the Hydro-Québec system. *IEEE Transactions on Power Systems*, 12, No. 1:282–292, February 1997.

[VCV98] T. Van Cutsem and C. D. Vournas. *Voltage Stability of Electric Power Systems*. Kluwer Academic Publishers, 1998.

[VFX99] E. Vaahedi, C. Fuchs, W. Xu, Y. Mansour, H. Hamadanizadeh, and G.K. Morison. Voltage stability contingency screening and ranking. *IEEE Transactions on Power Systems*, 14, No. 1:256–265, February 1999.

[VKM01] C. Vournas, M. Karystianos, and N. Maratos. Exploring power system loadability surface with optimization methods. *Proceedings of 5th Bulk Power Systems Dynamics and Control workshop, Onomichi, Japan*, pages 457–469, August 2001.

[VMK03] C.D. Vournas, G.A. Manos, J. Kabouris, G. Christoforidis, G. Hassé, and T. Van Cutsem. On-line voltage security assessment of the Hellenic interconnected system. In *IEEE Power Tech Conference*, Bologna (Italy), 2003.

[Vou01] C.D. Vournas. Interruptible load as a competitor to local generation for preserving voltage security. *Power Engineering Society Winter Meeting*, 1:236–240, 2001.

[VPL96] H. Vu, P. Pruvot, C. Launay, and Y. Harmand. An improved voltage control on large-scale power system. *IEEE Transactions on Power Systems*, 11, No. 3:1295 –1303, August 1996.

[Weh99] L. Wehenkel. Emergency control and its strategies (invited paper). In *Proc. of the 13th PSCC Conference*, pages 35–48, Trondheim (Norway), 1999.

[WET98] X. Wang, G. C. Ejebe, J. Tong, and J. G. Waight. Preventive/corrective control for voltage stability using direct interior point method. *IEEE Transactions on Power Systems*, 13:878–883, 1998.

[WL00] R. Wang and R. H. Lasseter. Re-dispatching generation to increase power system security margin and support low voltage bus. *IEEE Transactions on Power Systems*, 15:496–501, 2000.

[WPH01] Q. Wu, D.H. Popovic, D.J. Hill, and C.J.Parker. Voltage security enhancement via coordinated control. *IEEE Transactions on Power Systems*, 16:127–135, 2001.

[WS00] X. Wang and Y.H. Song. Advanced real-time management through both pool balancing market and bilateral market. *IEEE Power engineering review*, 20:47–49, February 2000.

[WV99] F.F. Wu and P. Varaiya. Coordinated multilateral trades for electric power networks: theory an implementation. *Electrical Power and Energy Systems*, 21, No. 1:75–102, 1999.

[WW96] A. J. Wood and B. F. Wollenberg. *Power generation, operation and control*. John Wiley and Sons, New York, 1996.

[XM96] F. Xia and A.P.S. Meliopoulos. A methodology for probabilistic simultaneous transfer capability analysis. *IEEE Transactions on Power Systems*, Vol. 11, No. 3:1269–1278, August 1996.

[XZdS00] W. Xu, Y. Zhang, L.C.P. da Silva, and P. Kundur. Competitive procurement of dynamic reactive power support service for transmission access. *Proc. of 2000 IEEE PES Summer Meeting, Seattle*, 1:543–548, July 2000.

[YHC97] N. Yorino, S. Harada, and H. Cheng. A method to approximate a closest loadability limit using multiple load flow solutions. *IEEE Transactions on Power Systems*, Vol. 12, No. 1:424–429, February 1997.

[ZWP80] J. Zaborsky, K.W. Whang, and K. Prasad. Fast contingency evaluation using concentric relaxation. *IEEE Transactions on Power Apparatus and Systems*, PAS-99:28–36, January /February 1980.